GROWTH AND SHEAR LOSS CHARACTERISTICS OF AN AEROBIC BIOFILM

TIAM TENG SEE

1990

GROWTH AND SHEAR LOSS CHARACTERISTICS OF AN AEROBIC BIOFILM

A Thesis
submitted in partial fulfilment
of the requirements for the degree of
MASTER OF TECHNOLOGY in Biotechnology
at Massey University

by

Tiam Teng See

Department of Biotechnology
Massey University
Palmerston North
NEW ZEALAND

March, 1990

ABSTRACT

The application of biofilms in fermentation and waste treatment processes has been increasingly considered in recent years due to several inherent advantages over suspended growth systems. For example, they enable higher biomass hold-up providing larger quantity of cell per unit reactor volume which allows high loading rates. The biofilm systems , with fixed or immobilised cells, avoid washout conditions. The often difficult problems of sludge thickening, separation, recycle, and wasting associated with suspended growth systems are eliminated for biofilm systems. However, the major drawback lies in the control of film thickness in order to maintain high reactor productivities.

The attached film thickness depends on both the biological parameters such as growth rate, and physical parameters such as hydrodynamic shear. The understanding of the growth and shear loss characteristics is a prerequisite for effective film thickness control.

The main objective of this work therefore is to investigate the growth and shear loss characteristics of an aerobic biofilm utilizing phenol in a concentric cylindrical bioreactor. The growth and detachment of the

biofilm was studied at different shear stresses, and their relationships were established. Detachment by shear was studied under two different conditions. One was examined simultaneously with growth under a constant shear stress where the biofilm detachment and growth occurred at the same time in the bioreactor. The other was examined via a separate shear test performed on the biofilm initially grown at a shear stress lower than that applied during the test. A method for measuring the torque exerted on the biofilm surface was first developed to enable computation of the related shear stress necessary for the study.

The effect of film thickness on torque at film surface for a constant rotational speed was not significant. Shear stress can be conveniently determined from a quadratic relationship between torque and rotational speed for the range of film thickness studied.

The substrate consumption is directly proportional to film thickness up to about 0.050 to 0.100 mm only, and beyond that it becomes independent of film thickness.

The mass transfer resistance in the liquid phase appears to reach a minimum at shear stress greater than 3.44 N/m^2 coinciding with the maximum steady-state substrate removal rate.

The shear loss resistance of the biofilm increases with increasing shear stress during growth. The ultimate shear loss rate and shear stress relationship follows approximately:

$$R_S = (40.82 - 2.75\sigma + 0.15\sigma^2 - 31.83e^{-0.61\sigma}) \times 10^{-2}$$

The net growth rate varies with shear stress according to a parabolic function which predicts a shear stress of 19 N/m^2 is required to achieve zero net growth.

The biofilm-support adhesion must remain stronger than the film layer adhesion, otherwise, detachment will occur at the film-support interface rendering it impossible to control the film thickness.

ACKNOWLEDGEMENTS

I am greatly indebted to my supervisor, Dr S. M. Rao Bhamidimarri for his advice, guidance and inspiration during the course of this study, and to the Department of Biotechnology for providing the facilities to enable this research.

I also like to extend my appreciation and gratitude to the staff of Biotechnology Department and fellow students who had given me their help and support generously whenever required.

My special thanks to Mr John Algers for his technical assistance and expedious job in organizing the experimental equipment, without whom, the timely completion of this project will not be possible. Thanks also for his pleasant friendship and sense of humour that made my stay at Massey most comfortable and enjoyable.

The invaluable assistance of Mr Sridhar Susarla and Mr Wayne Mallet in the use of computers are gratefully acknowledged.

Last of all, my heartfelt thanks to my wife, Hong Kiow, for her love, patience, and cheerful endurance during the

many evenings and weekends when I have to work late on this project; and also to my parents for their never-ending support throughout the course of this graduate study.

TABLE OF CONTENTS

LIST OF FIGURES

LIST OF TABLES

CHAPTER 1

INTRODUCTION

In an aquatic environment, there is a tendency for the microorganisms to adsorb and colonize on submerged surfaces. The immobilized cells grow to form layer-like aggregates known as biofilm. Biofilms present in the natural environment consist of a complex community of primarily bacteria with other organisms such as fungi, algae and protozoa, and utilize the nutrients present in the bulk liquid medium for growth and reproduction. Such activity has its importance in the recycling of organic and inorganic substrates in the natural environment. These processes have been exploited to considerable industrial advantage in various fermentation and wastewater treatment systems e.g. trickling filters, rotating biological contactors and fluidized bed reactors.

Although biofilm or fixed-film biological processes found early application to wastewater treatment, their use declined with the development of suspended growth systems. The earliest application of biofilm system was that of trickling filter and later the rotating biological contactor was developed to achieve higher degree of treatment, eliminating some of the disadvantages of

trickling filters. The fluidized bed being the most recently introduced process, is essentially a hybrid of suspended growth and attached growth system. However, in recent years with the increasingly stringent discharge standard and high strength effluents from expanding manufacturing and processing industries, the application of biofilm or fixed-film has been increasingly considered due to certain inherent advantages over suspended growth systems. For example, they enable higher biomass hold-up, thus providing larger amount of cell per unit reactor volume, and thereby permitting high loading rates and treatment of inhabitory wastes and avoiding washout conditions. The often difficult problems of sludge thickening, separation, recycle, and wasting associated with suspended growth systems are eliminated for biofilm or fixed-film systems.

The major operational problem in fixed film systems is the control of film thickness. Biofilm thickness is thought to affect the performance of the system for a given loading rate and there is an optimum thickness beyond which substrate utilization rate will not increase any further. The mechanisms which act to remove the biomass such as decay, sloughing and attrition are still generally beyond operational control and in many cases they are not sufficient for removal of all excess

biomass. In the foregoing aerobic systems, the rapid consumption and stabilization of the organic substrate inevitably result in rapid cell growth. Thus problem of plugging or clogging of filter beds such as in trickling filters arises due to excessive growth and irregular dislodging/sloughing of thick films, whilst in other fixed-film systems periods of unsteady state system may arise resulting in fluctuating performance.

The accumulation or net attachment of biofilm on surfaces depends on both the biological parameters such as growth rate, and physical parameters such as hydrodynamic shear. The understanding of the growth and shear loss characteristics is a prerequisite for effective control of the film thickness. The existing knowledge of these is limited and no universal model has yet been developed for such control.

The objectives of this research are therefore to:

1. develop a reactor system in which biofilms of required thickness can be obtained under defined shear conditions,
2. develop a method for measuring shear stress in the reactor,
3. study the aerobic biofilm growth characteristic under different shear conditions,

4. study the aerobic biofilm loss characteristic due to hydrodynamic shear,
5. establish relationships between growth rate and shear stress, detachment or shear loss rate and shear stress.

CHAPTER 2

LITERATURE REVIEW

2.1 BIOFILM GROWTH AND DEVELOPMENT ON SURFACES

Before formation into a biofilm, microorganisms must first adhere to surfaces and continue to develop and multiply. During the initial stages, population growth and cell adhesion can occur simultaneously. Several physical, chemical and biological processes occur during the initial formation of biofilm including the following:

- Transport and adsorption of organic molecules to the wetted surface.
- Transport of microbial cells to the surface.
- Microbial adsorption.
- Microbial transformation at the surface resulting in the production of biofilm.
- Detachment (sloughing) of the biofilm.

During microbial cell growth, energy and nutrients are required for the synthesis of new cells and for the maintenance of the cell in its existing condition. Energy is supplied from the oxidation of the organic matter. The reaction takes place within the biofilm. The necessary

oxygen, organic matter and other nutrients are supplied to the reaction sites by diffusion.

The growth of the biofilm is a net result of transport of nutrients and microbial cells from the bulk liquid to the substratum and adsorption onto the surface by physio-chemical processes, attachment or consolidation of adsorbed microorganisms through biological effects and growth of the attached microorganisms which are attached to either the substratum or to other cells.

The distribution of the cells during initial stage of attachment may be relatively even but at times may be non-uniform. The growth can be explained in general terms according to Hoehn and Ray (1973) as follows:

Under suitable environmental condition (such as pH, nutrients concentration and temperature) the growth of the biofilm will continue until the whole surface is covered, and from then on growth will be outwards forming layers over the original layer. As the film grows thicker, diffusion of oxygen and organic matter/nutrients into the inner region becomes impeded giving rise to oxygen limited condition. A condition of oxygen limitation usually arises, unless there is very low initial substrate concentration, limiting the film thickness. The regions of the biofilm close to the solid surface and furthest

from the liquid film become anaerobic. In the anaerobic region, aerobes will die and lyse (due to insufficient oxygen supply). The dead aerobes thus act as organic matter for the remaining anaerobic and facultative bacteria. Eventually, when the food for maintenance of these cells becomes depleted, the anaerobic bacteria will die and lose adhesion with the solid surface and slough off. The process of film growth thus starts again. Figure 2.1 shows the main features of the biofilm process.

2.1.1 Environmental Factors Affecting Growth

pH of Bulk Liquid

Although the ability of organisms to survive at various pH levels varies, most preferred condition is close to pH 7 and few can tolerate pH levels above 9.5 or below 4 (Greenfield, 1987). The pH affects the growth rate by changing the enzymatic reactions since it is the enzyme that catalyses the metabolic reactions. Figure 2.2 shows the effect of pH on enzyme reaction velocity which gives similar effect on growth. In aerobic systems the optimum pH range is usually from 6.5 to 8.5. Efficiency of the process and therefore, the growth rate falls off both above and below this range (Eckenfelder, 1980).

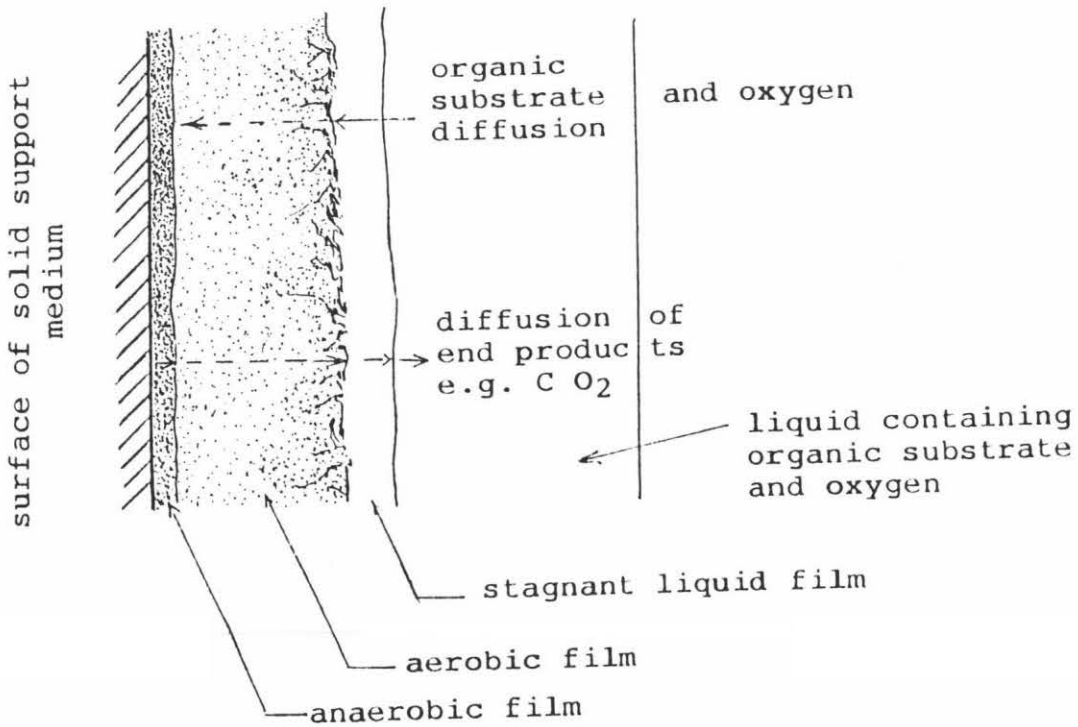

Figure 2.1 Diagram illustrating biofilm main features

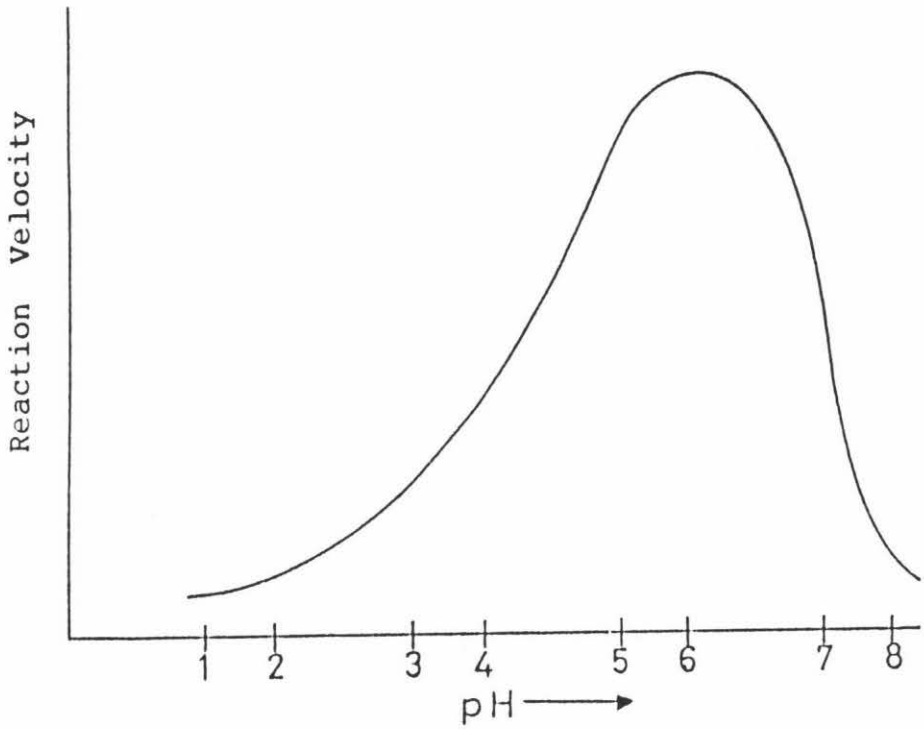

Figure 2.2 Effect of pH on enzyme reaction velocity (Greenfield, 1987)

Temperature

Temperature not only influences the metabolic activities of the microbial population, but also has a profound effect on such factors as gas-transfer rates (Metcalf & Eddy, 1979). The rate of biological reaction within the cell increases with increasing temperature and hence the growth until some limiting temperature is reached, beyond which the rates of reproduction and reaction fall. Table 2.1 shows the temperature ranges for the best functioning of different classes of microbial cells.

Table 2.1 Temperature ranges of microorganisms

Classification	Temperature, ^{o}C	
	Range	Optimum
Psychrophilic	-5 to 30	10 to 20
Mesophilic	20 to 45	30 to 40
Thermophilic	40 to 75	55 to 65

Source: Greenfield, 1987.

Substrate and Oxygen Concentrations

Substrate and oxygen concentrations in the bulk liquid besides other factors, affect their diffusion rate into

the biofilm. When the concentrations in the liquid are high, the concentration driving force causes their rapid diffusion into the biofilm so that they penetrate deeper into the film before being consumed. Atkinson and Fowler (1974) correlated the results of Tomlinson and Snaddon; Kornegay and Andrews; and others to show that the depth of penetration into the film is approximately proportional to the applied substrate concentration. Deeper penetration of the substrate into the film allows more biomass in contact with it at one time and therefore permit higher overall growth rate in the system provided oxygen is also adequate at the same depth. A condition can exist where the system is either substrate limited or oxygen limited, depending on their concentrations in the bulk liquid.

Hydrodynamic Conditions

The hydrodynamic conditions of the bulk liquid can severely affect the on-set and growth of the biofilm, not only because of their effects on the transportation of cells and nutrients to the substratum surface but also because of detachment caused by fluid shear (Rao, 1987).

2.1.2 Microbial Attachment to Surface

Microbial accumulation on solid surface can be divided into the following three stages:

- Adsorption or the immobilization of microorganism on the solid surface (also referred to as deposition).
- Attachment or consolidation of the interface between organism and the solid surface which may involve the formation of polymer bridging between organism and solid surface.
- Colonization or growth and reproduction of organism on the solid surface.

Although microbial attachment to solid surfaces is encountered in a large number of cell contact processes, the precise mechanisms are not yet clear.

Adsorption and Adhesion Process

The microbial adsorption onto surface may be effected by initial direct contact of suspended microorganisms onto solid surfaces as a result of their movement/migration within the bulk liquid. The microbial cell can move under the influence of electric field or as a result of agitation, convection or self-propulsion, or random diffusion. These movements can be further influenced by the attractive or repulsive forces of neighbouring

suspended particles and surfaces.

Initial attempts to explain the adhesion/adsorption phenomenon were made on the basis of colloid stability theory (DLVO theory) due to the small size, low density and net negative charge of bacteria similar to those of colloidal particles. An alternative approach involving the study of free energies employs analysis of the thermodynamic potential for cell adhesion on the basis of known interfacial tensions. Both the approaches did not take account of the biological reactions. However, Marshall (1976 & 1980) later incorporated the biological effect into the DLVO approach and proposed a two-phase theory of microbial adhesion.

The first phase involves cell deposition in which the bacterial cells are held on a small but finite distance from the solid surface, a situation maintained by the existence of an energy barrier which prevents firm adhesion. This phase is termed 'reversible sorption' because the bacteria, although electrically attracted to the surface, are easily removed by concentration differential or the application of a shear force, such as a jet of water. The second phase, 'irreversible attachment', occurs when the energy barrier is breached allowing intimate surface contact and permanent adhesion.

Three bridging mechanisms have been suggested. Firstly, short-range physico-chemical forces such as chemical bonds, dipole interactions or hydrophobic bonding (Tadros, 1980). Secondly, specialized bacterial holdfasts; or thirdly, 'polymer bridging' through the mediation of bacterial extracellular polymer (ECP). Since most bacteria have no obvious structures for attachment, it is widely believed that the existence of 'in-situ' synthesis of ECP is required for permanent adhesion. This requirement has been established for a number of situations, e.g the polymer occuring as an acidic polysaccharide (Fletcher and Floodgate, 1973).

Polymer bridging was the mechanism proposed by Marshall (1976) for the second phase in which irreversible sorption follows after polymer synthesis. However, it has been observed that some bacteria have the ability to bind rapidly to surfaces. This spontaneous binding suggests that bridging may depend on the compatibility of biopolymers with the solid surface rather than 'in-situ' synthesis as evidenced by studies in which the initial, rapid attachment of a marine pseudomonad was mediated by a compact acidic polysaccharide followed by synthesis of a 'secondary' fibrous polysaccharide responsible for biofilm consolidation (Fletcher and Floodgate, 1973).

However, no univeral mechanism prevails and that microbial adhesion is an extremely complex process with physical, chemical and biological components interacting to varying degrees in different organisms depending on the environmental conditions.

2.2 TRANSFER OF MATERIAL INTO BIOFILM

Mass transfer of substrate and oxygen from the bulk liquid to biofilm-liquid interface and then to within the biofilm occurs by means of pore diffusion. The significance of the effect of diffusivity on biofilm growth and hence the biodegradation of the organic content in wastewater has been recognised for sometime.

2.2.1 Diffusion in the Liquid Phase

There is evidence that the rate of transfer of materials from bulk liquid to the biofilm-liquid interface can be an important determinant of the performance of a biofilm process. The work of Chen and Bungay (1981) on biofilm from trickling filter demonstrated that oxygen concentration at the biofilm-liquid interface can be appreciably less than that in the bulk liquid which is shown in Figure 2.3 (and it follows that the concentration in the biofilm will be even lower as will be explained

in the next section).

The external mass transfer resistance can be simplified by linearising the concentration profile to represent a hypothetical stagnant liquid film or boundary layer between the biofilm-liquid interface and the bulk liquid phase as shown in Figure 2.4 (Rittman and McCarty, 1980; Chang and Rittman, 1987). Across this liquid film, diffusion of solute molecules follows Fick's First Law.

The work of LaMotta (1976(a)) provided an indirect evidence of the effect of fluid velocity on mass transfer in the liquid phase when he observed that the reaction rate in the biofilm increased with fluid velocity over the biofilm before reaching a constant rate at a velocity of around 0.8 m/s. His work also suggests that at higher velocities the transfer rate could have exceeded the maximum reaction rate and at lower velocities reaction rate was limited by the transfer rate. Trulear and Characklis (1982); Castaldi and Malina (1982) found similar effect in their experiment. Trulear and Characklis (1982) achieved a critical velocity of 0.935 m/s which is close to that of LaMotta (1976(a)). However, it should not be concluded that velocities beyond this range will always make external mass transfer effects insignificant, because reaction rate will also depend on

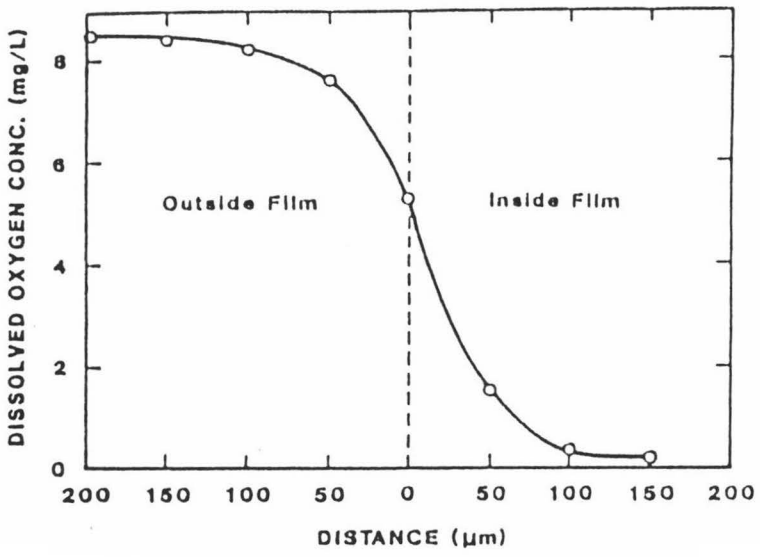

Figure 2.3 Oxygen concentration profile inside and outside a biofilm in bulk liquid (Chen and Bungay, 1981)

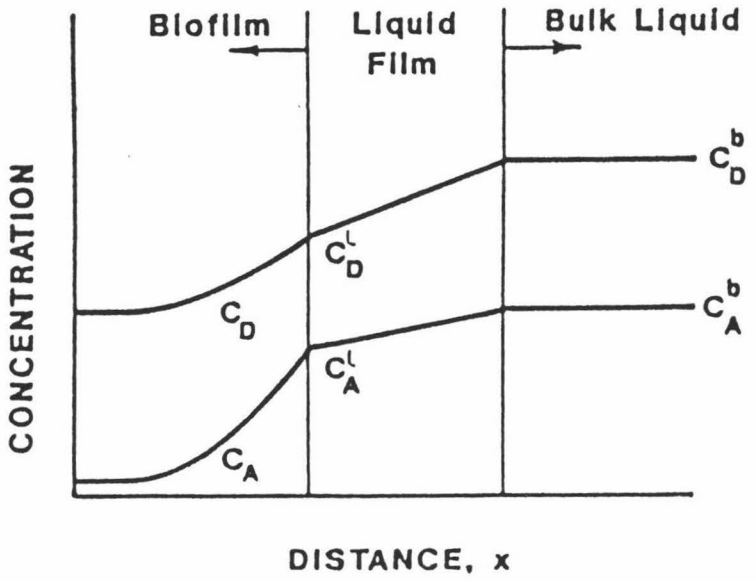

Figure 2.4 Idealized biofilm and stagnant liquid layer illustrating concentration profile of the organic substrate as electron donor (D) and oxygen as electron acceptor (A)

both the bulk substrate concentration and the maximum achievable reaction rate in the biofilm. Therefore, higher or lower values are possible.

2.2.2 Diffusion within the Biofilm

The diffusion of material in the biofilm follows Fick's Second Law (Rittman and McCarty, 1980; Chang and Rittman, 1987). The diffusivity of the biofilm may vary depending on the predominant organisms in the biofilm (Matson and Characklis, 1976). At the film-liquid interface and inwards to the film, diffusion of the substrate and oxygen and the reaction rate take place simultaneously. The concentration profiles in the biofilm will thus be the net result of reaction and diffusion, decreasing with depth. This can be observed in Figures 2.3 and 2.4. The effect of liquid velocity over the biofilm mentioned earlier in section 2.2.1 is extended to the diffusion within the biofilm by way of lowering the concentration at the film-liquid interface.

2.3 BIOFILM CHARACTERISTICS

Substrate removal or utilization rate of biofilm process determines the performance of the system. Such is the result of interaction between the rate of transport

(diffusion rate) and the intrinsic rate of reaction which in turn depends on the biofilm characteristics.

2.3.1 Thickness

When considering biofilm thickness, it is important that a distinction be made between the total film thickness and the active film thickness. Experimental results from a number of workers have shown that substrate removal by a biofilm increases linearly with increasing film thickness up to a maximum level (0.070mm - 0.100mm) at which it remains constant with further increase in film thickness (Tomlinson and Snaddon, 1966; Kornegay and Andrews, 1968; LaMotta, 1976(b)). This limiting value was the thickness of the aerobic portion of the film known as 'active layer'. Trulear and Characklis (1982) observed a similar phenomenon although they also found that the active depth increased as the substrate concentration in the liquid phase increased. The results of Bungay *et al* (1969) also indicated that the active thickness depends on substrate concentration in the bulk medium.

However, Sanders (1966) on the other hand, found that substrate removal rates dropped at thickness greater than the active layer depth. He attributed this to the diffusion of both fermentation products and the contents

of lysed cells back to the active layer which could reduce the concentration gradient of substrate between the liquid and the biofilm, and thus lower the removal rate.

These diverging views were reconciled by Hoehn and Ray (1973) who showed that substrate removal rates reached a peak value, and then decreased as the film grew thicker as shown in Figure 2.5. The removal rates increased again to the former levels or better as the film grew still further such that a quasi-steady state was attained. One explanation to this phenomenon is that the removal rate is reduced due to metabolization of the fermentation products diffusing to the active layer instead of substrate in the bulk liquid. Another explanation is the inhabitance of microbial activity in the active layer by some of the anaerobic fermentation products. The recovery to the previous rate could then occur when the microoganisms in the active layer become adjusted to the effects of the anaerobic zone.

It is generally accepted that the active thickness is a result of transport limitation within the biofilm. Only when the film is very thin and when the substrate and oxygen concentrations are very high; or when the rates of transport are large in relation to the reaction rates will the active film thickness approach the total film

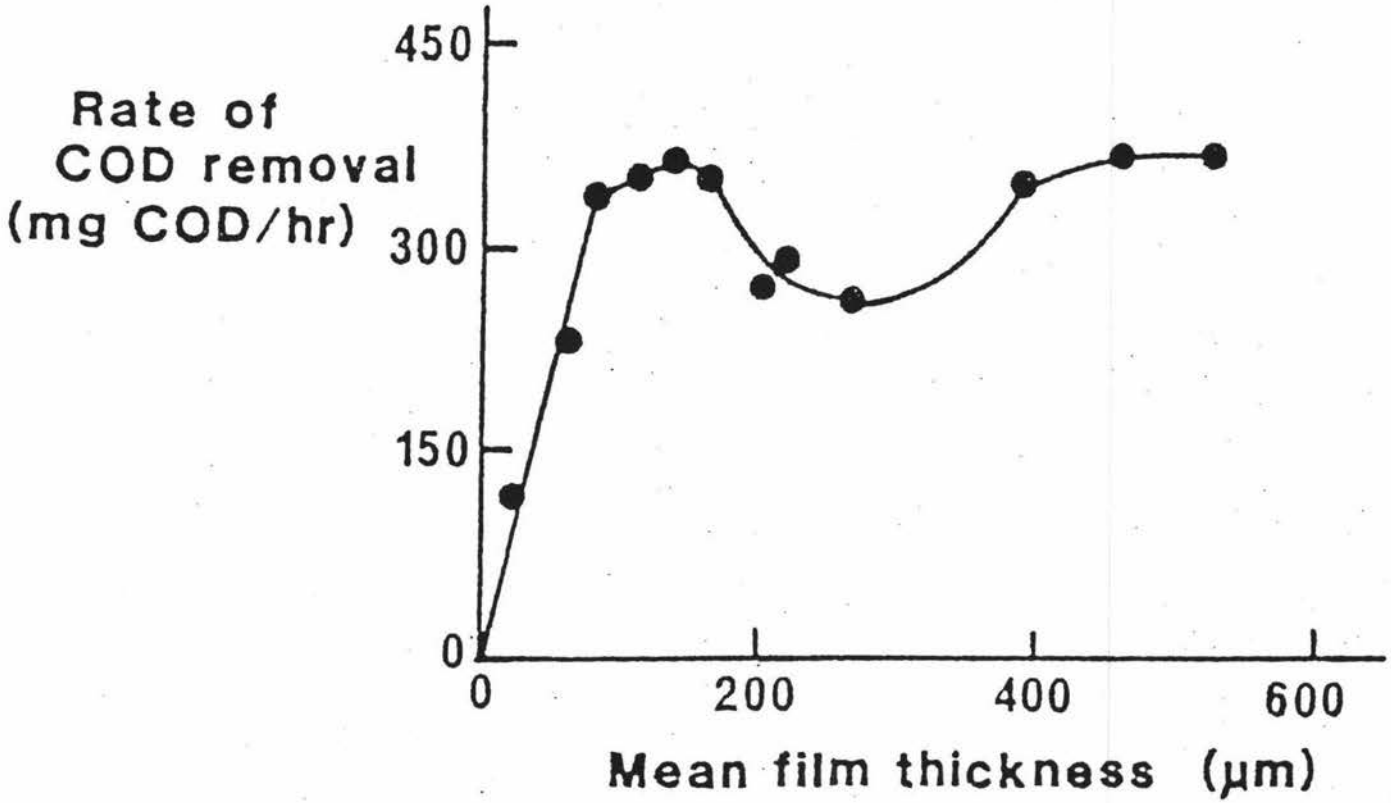

Figure 2.5 Rate of COD (representing substrates) removal as a function of film thickness (Hoehn and Ray, 1973)

thickness. However, because of the unsteady-state process, these conditions if exist will not be maintained unless film thickness is controlled by some means.

The work of Whalen *et al* (1969) showed that oxygen was present in excess throughout the biofilm fed with low substrate concentration and was limiting at greater depths (>0.100mm) with high substrate concentration. This suggests that oxygen becomes a limiting factor of active layer thickness at high feed substrate concentration, and at low feed concentration a completely active thin film can exist.

In a review of various papers by Atkinson and Fowler (1974) it was found that the total film thickness was between 0.07 and 4.0mm. The thickness was generally less than 0.2 mm for those subjected to mechanical or hydrodynamic control, while those under uncontrolled conditions, were as thick as 4.0 mm although it has been observed that under turbulent condition the thickness seldom exceed 1.0 mm (Characklis, 1981). The film thickness giving maximum effiency in wastewater treatment system has been quoted as 0.25 mm (Jenkin, 1963). The results of Tomlinson and Snaddon (1966); Kornegay and Andrews (1968) indicate critical depths between 0.07 and 0.15 mm, and those of LaMotta (1976(b)) between 0.012

and 0.065 mm depending on the substrate concentration in the bulk liquid. However, in contrast, Huang et al (1985) observed that the active film thickness in their experiment could reach 1.5 mm. They suggested that this was attributed to the much higher substrate and dissolved oxygen concentrations they used, or probably due to higher degradable substrate.

The ideal case for maximizing productivity in an aerobic system is to operate under maximum active film thickness attainable at that feed substrate concentration since this will provide maximum active biomass in the system to maintain maximum substrate utilization/removal rate. Unfortunately, the effective control of the biofilm thickness within a fixed-film reactor is currently the least developed area primarily because little fundamental study has been devoted to the factors governing biofilm development.

2.3.2 Density

The biofilm density is usually expressed as the dry cell mass per wet biofilm volume (dry density) rather than wet density (wet cell mass per wet biofilm volume) because of the difficulties in evaluating wet density. As the system performance (in terms of substrate removal efficiency) is

reflected by the reactor biomass concentration, density has an indirect effect since it determines the mass of the microorganisms present for a given film thickness in a particular reactor configuration.

Although it has been generally assumed that the density is constant and independent of film thickness, there is evidence that this is not the case. The results of Hoehn and Ray (1973) in Figure 2.6 show the density of a biofilm depends on its thickness. The density increases to a maximum value at a thickness consistent with the active film thickness. It was thought that changes in density were due to variations in the microbial populations within the biofilm. Maximum density was thought to be caused by tight packing of the aerobic layer, whereas the lower densities were due to lysis of cells in the anaerobic region. Shieh *et al* (1981) have observed similar reductions in density with increasing thickness but observed no region of increasing density. Trulear and Characklis (1982) also observed changes in biofilm density and suggested that this was attributed to changes in biofilm morphology which was also being observed during thickness measurement. They observed that the density in their film approached a maximum value as the substrate (glucose) loading rate was increased at a constant shear stress. However, evidence from the work of

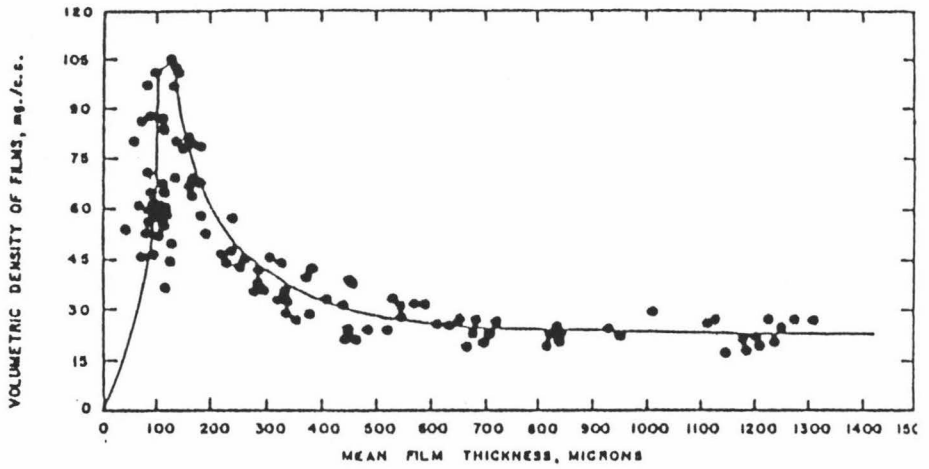

Figure 2.6 Effect of biofilm thickness on the density of the biofilm growing on a rotating drum (Hoehn and Ray, 1973)

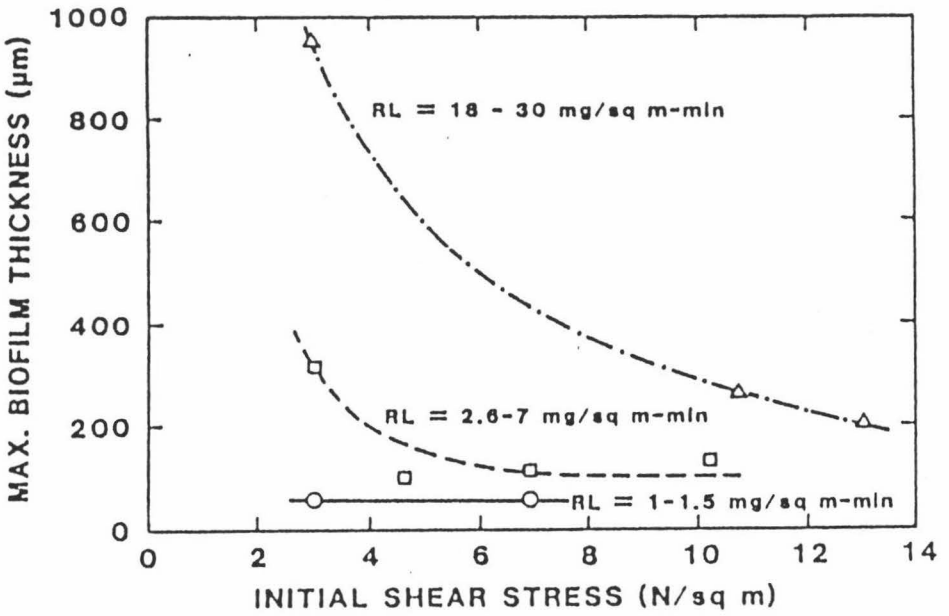

Figure 2.7 Effect of fluid shear stress and organic loading (R_L) on the maximum biofilm thickness attained in an annular reactor (Data from Zelver, 1979 as presented by Characklis, 1981)

Zelver (1979) presented by Characklis (1981) showing that biofilm thickness associated with a given shear stress as shown in Figure 2.7 was also a function of substrate loading raises questions as to whether thickness or loading influences the density. Further, it was shown that density is also influenced by fluid shear stress as shown in Figure 2.8 presented by Characklis *et al* (1982).

Study by Huang *et al* (1985) with sucrose as substrate showed that density is also influenced by dissolved oxygen in the bulk liquid. They observed that density decreases with increased dissolved oxygen (Figure 2.9). They attributed this to changes of microbial species which affect the structural matrix of the biofilm when they observed that at high dissolved oxygen the film appeared to be dense whilst at low dissolved oxygen the texture was loose and porous.

As there are many factors being proposed which could be responsible for changes in film density, more fundamental research will be required to delineate the mechanism and the significance of each individual factor.

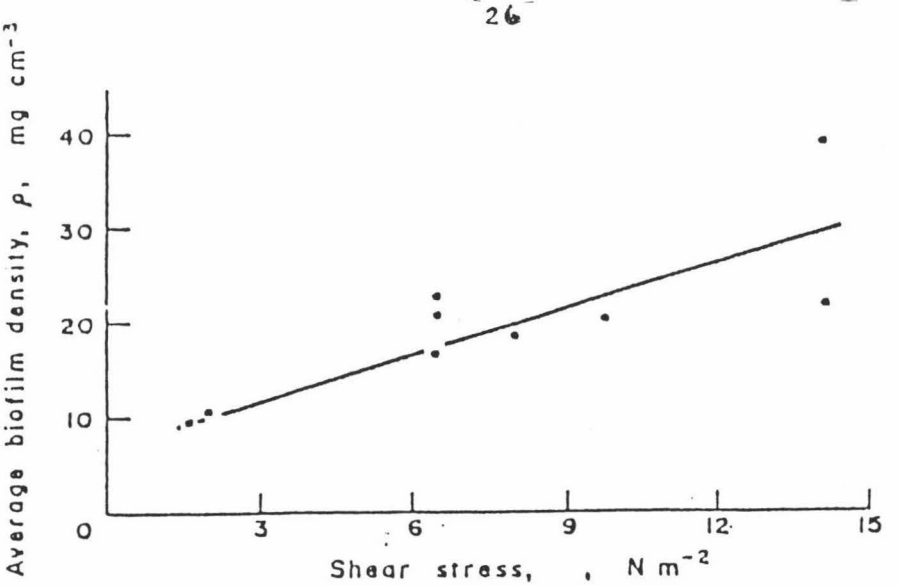

Figure 2.8 Influence of fluid shear stress on biofilm density (Data from Zelver, 1979 as presented by Characklis *et al*, 1982)

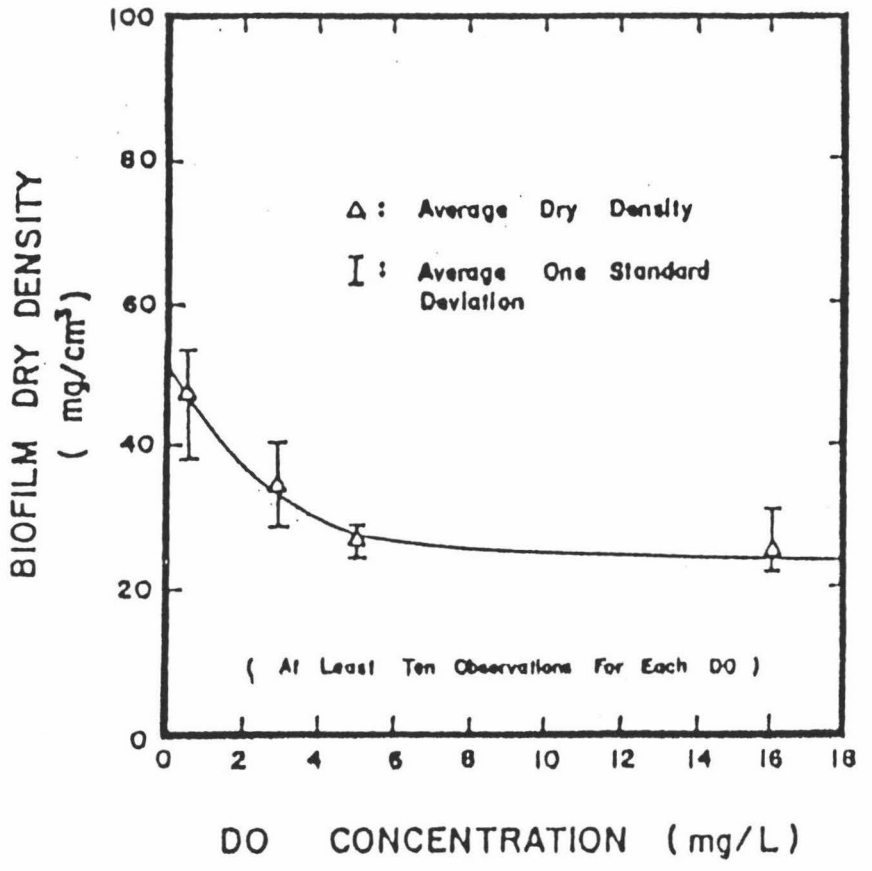

Figure 2.9 Effect of dissolved oxygen (D.O.) on dry density of biofilm (Huang *et al*, 1985)

2.4 BIOFILM DETACHMENT

Biofilm loss is resulted from decay and hydrodynamic shear stress caused by liquid flowing over the biofilm. Among these factors, hydrodynamic shear can vary depending on the hydraulic conditions around the biofilm. Until recently, little was known regarding loss due to hydrodynamic shear. Trulear and Characklis (1982) in their experiment showed that film detachment is highly dependent on hydrodynamic conditions, and observed a film thickness reaching a plateau phase where no further accumulation was seen. They explained this to be the result of shearing equilizing production rate. They also reported that detachment rate increased with liquid velocity as shown in Figure 2.10. This suggests that the rate of biofilm detachment increases as the shear stress at the interface increases. Further, the detachment rate also increases as the biofilm mass increases as shown in Figure 2.11 (Trulear and Characklis, 1982). This suggests the presence of a mechanism whereby films of different thickness can be attained in a reactor with a fixed shear stress as substrate is applied at various rates. At higher substrate application rates, however, the biofilm would be growing faster and thus a greater mass (and so is thickness for a given density) would develop before the detachment rate balanced the production rate. This can be

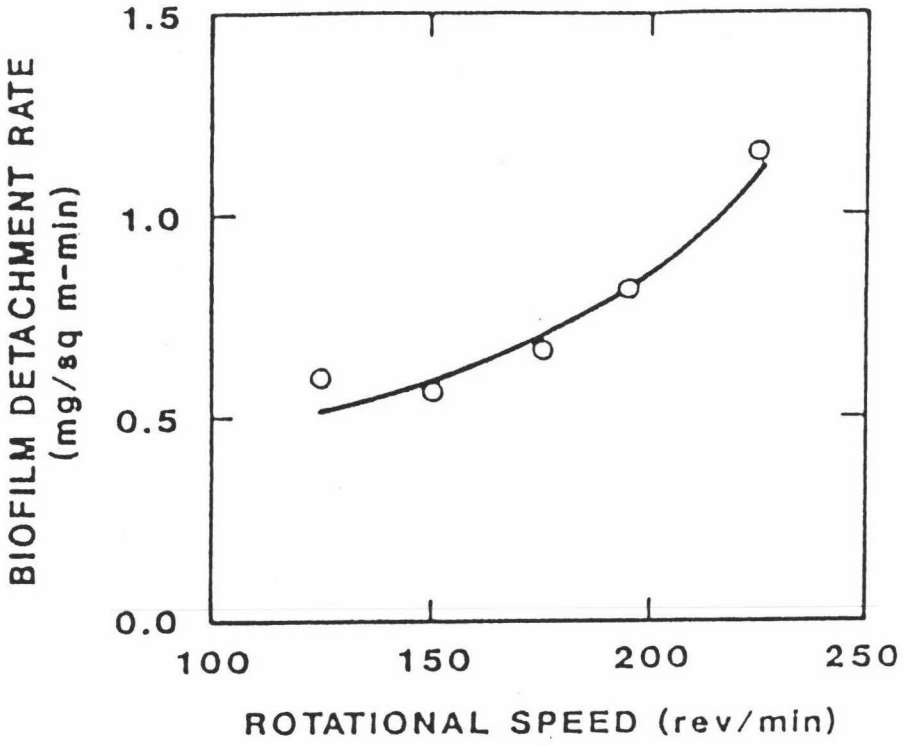

Figure 2.10 Effect of rotational speed in an annular reactor on the detachment rate of a biofilm with a mass of 150-160 mg (Trulear and Characklis, 1982)

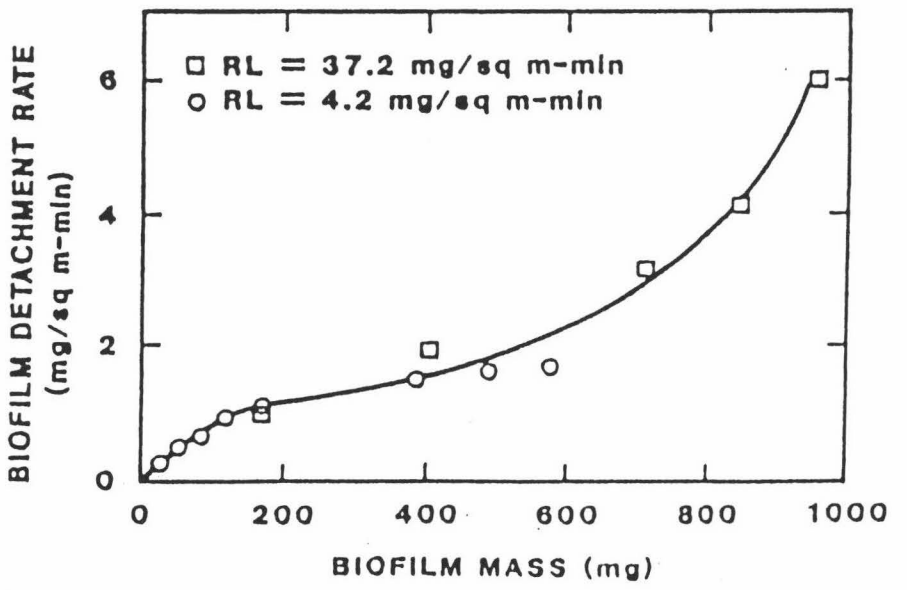

Figure 2.11 Effect of biofilm mass (proportional to thickness) in an annular reactor rotating at constant speed on the detachment rate of biofilm. R_L refers to the organic loading rate. (Trulear and Characklis, 1982)

seen in Figure 2.7 as presented by Characklis, 1981 (from the work of Zelver, 1979).

The results of Trulear and Characklis (1982) in Figure 2.11 suggest that detachment rate associated with a given shear stress will increase as thickness increases since biofilm mass is a function of thickness. Their results which further showed that density is a function of the applied substrate loading rate means that the thickness of a given mass will be greater at lower loading rate, thus suggesting that detachment rate is a function of both thickness and density.

Detachment may not depend on severing the film-surface adhesive bond, but may result from rupture of the layer of cells adjacent to the surface in a multilayer film. In such cases, a sheet of biofilm may detach leaving the inner layer or cell debris on the surface and so the result will depend on the mechanical strength of the cells and not the cell or film-surface adhesive bond (Fowler, 1986). This will occur only when the film-surface adhesion is stronger than the inter-layer film adhesion.

2.5 CONCLUDING REMARKS

The review covers the various processes involved in surface attachment, growth and loss of biofilms, and identifies the areas which are least understood so that more studies can be directed towards those areas. A review of various studies gave evidence that a number of events occur within the biofilms during growth. Among the many interfering factors, shear loss is the least understood.

The ultimate objective in the practical sense is to achieve maximum system productivity and efficiency, which appears to be very much dependent of the maximum active film thickness attainable under a set of operating conditions and the ability to maintain that condition under steady-state in the system.

The complete biofilm behaviour can be quantified only if a theory for a broad range of processes can be developed which may involve a complex mechanistic model or semi-empirical correlation. To this end, there is more knowledge yet to be gained. However, with the renewed interest in biofilm processes, more studies can be set to fill the remaining gaps in knowledge so that more effective biofilm utilization can be achieved in the future.

CHAPTER 3

MATERIALS AND METHODS

3.1 MICROBIAL CULTURE AND LIQUID MEDIUM

A commercial culture, 'Phenobac' was used to develop the biofilm which degrades phenol in solution. Single substrate, phenol, in aqueous solution with distilled water was used as a medium for growth composing of other trace elements (organic salts) as nutrients. The composition of the aqueous phenol solution is shown in Table 3.1. The microbial culture was grown in shake flasks maintained at 30 ^{o}C on a shaker for 24 hours.

Table 3.1 Composition of aqueous phenol solution

Potassium Phosphate Monobasic, $KH_2 PO_4$	0.420 g
Potassium Phosphate Dibasic, $K_2H PO_4$	0.375 g
Ammonium Sulphate, $(NH_4)_2 SO_4$	0.244 g
Sodium Chloride, Na Cl	0.030 g
Magnesium Sulphate 7-hydrate, $Mg SO_4 7H_2O$	0.030 g
Calcium Chloride dihydrate, $Ca Cl_2 2H_2O$	0.030 g
Ferrous Chloride, $Fe Cl_2$	0.003 g
Phenol, $C_6 H_5 OH$	0.150 g
Distilled Water, $H_2 O$	1.000 litre
pH 6.7	

Source: Rao, 1985.

3.2 MEASUREMENT OF CELL CONCENTRATION

Cell concentration in the liquid medium was determined via a pre-established relationship between absorbance reading and dry cell mass concentration. This relationship was determined by measuring the absorbance of various samples of different cell concentration using a spectrophotometer set at a wavelength of 620 nm (visible range). The established relationship is shown in Figure 3.1 which can be expressed as $Y_{av} = 0.001727\ X_c$. The samples were put under vibration as shown in Figure 3.2 to obtain a homogeneous suspension of samples for all tests, otherwise various particle size from different samples will have different settleability which will affect the results. Such problem was encountered during the initial trial.

The cell concentration in terms of dry cell mass per unit volume of liquid medium was determined by measuring the dry cell mass of the residue (dried at 105 ^{o}C for 24 hours to 72 hours until constant weight was achieved) after the same samples were filtered through 0.45 µm micropore membranes. The filters were predried at 60 ^{o}C for about 24 hours before used.

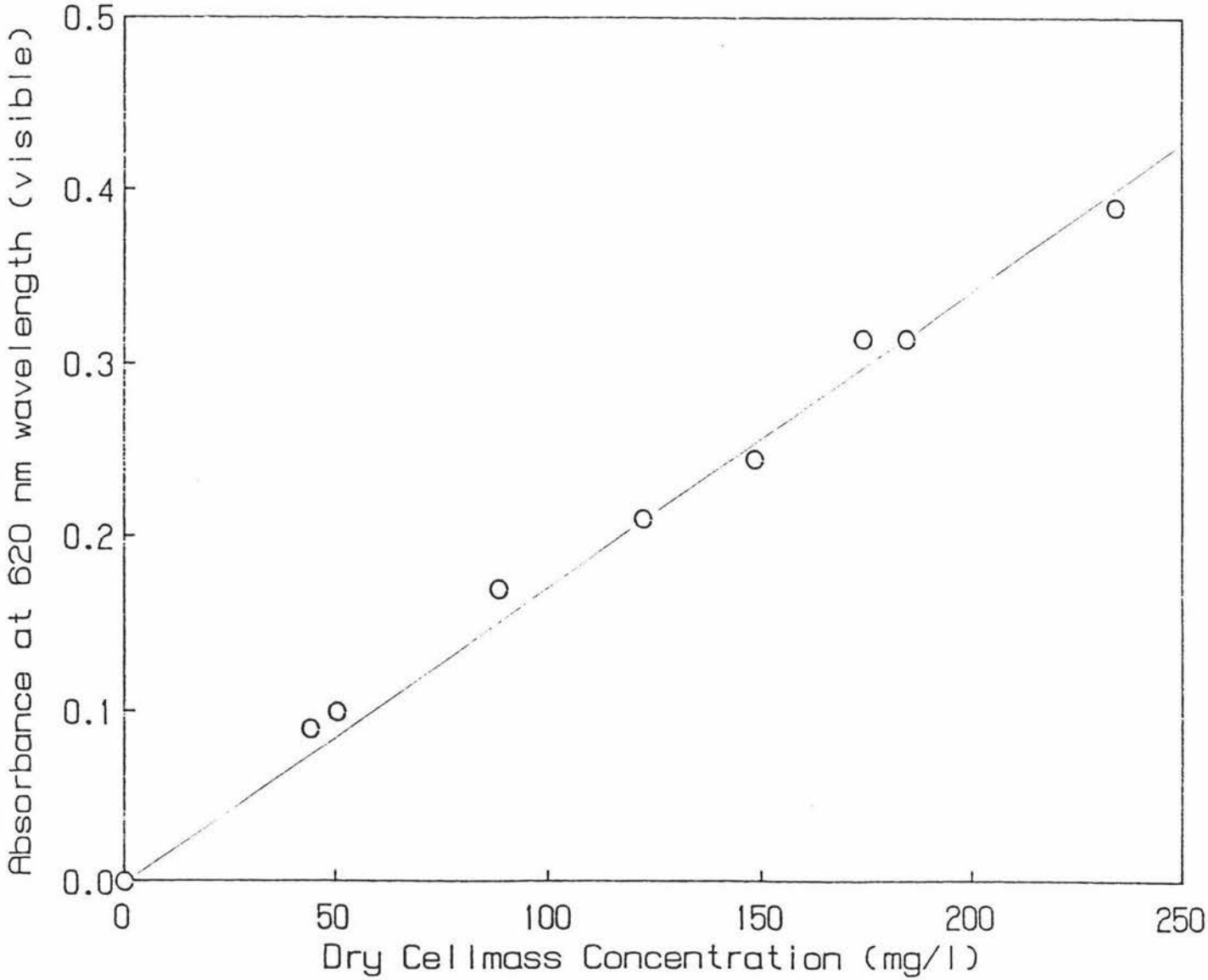

Figure 3.1 Relation between dry cell mass concentration and absorbance

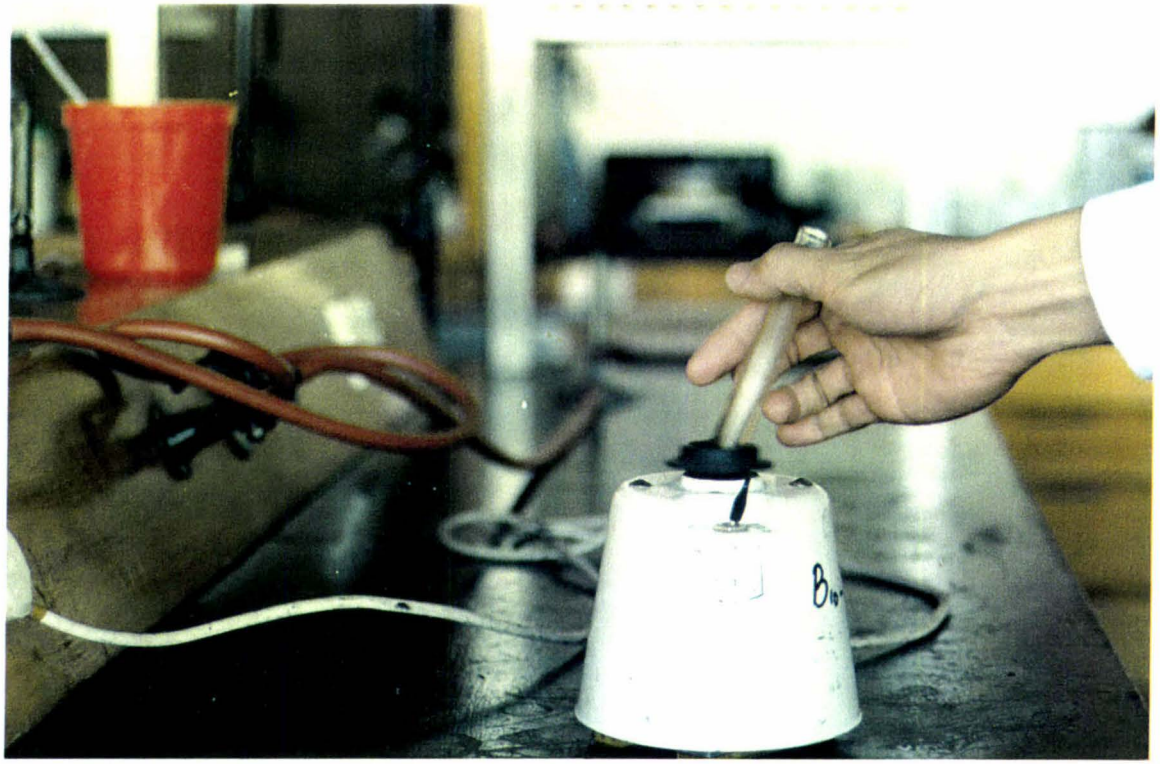

Figure 3.2 Photograph of vibrating equipment

3.3 MEASUREMENT OF PHENOL CONCENTRATION

The unique property of phenol that absorbs UV light permits direct measurement of the UV absorbance of the phenol solution via a UV spectrophotometer set at a wavelength of 279 nm. A standard relationship between the UV absorbance and phenol concentration was established after measuring the absorbance of samples with different known phenol concentration. The relationship is shown in Figure 3.3 which can be expressed as $Y_{au} = 7.9967\ X_p$ for $0 <= X_p <= 150$.

3.4 THE BIOREACTOR

The reactor used in the study consisted of two concentric cylinders made of acrylic plastic, a stationary outer cylinder and a rotating inner cylinder. Details of the reactor are illustrated in Figures 3.4. The average dimensions of the reactor are presented in Table 3.2. The inner cylinder can be attached to a variable speed stirrer motor.

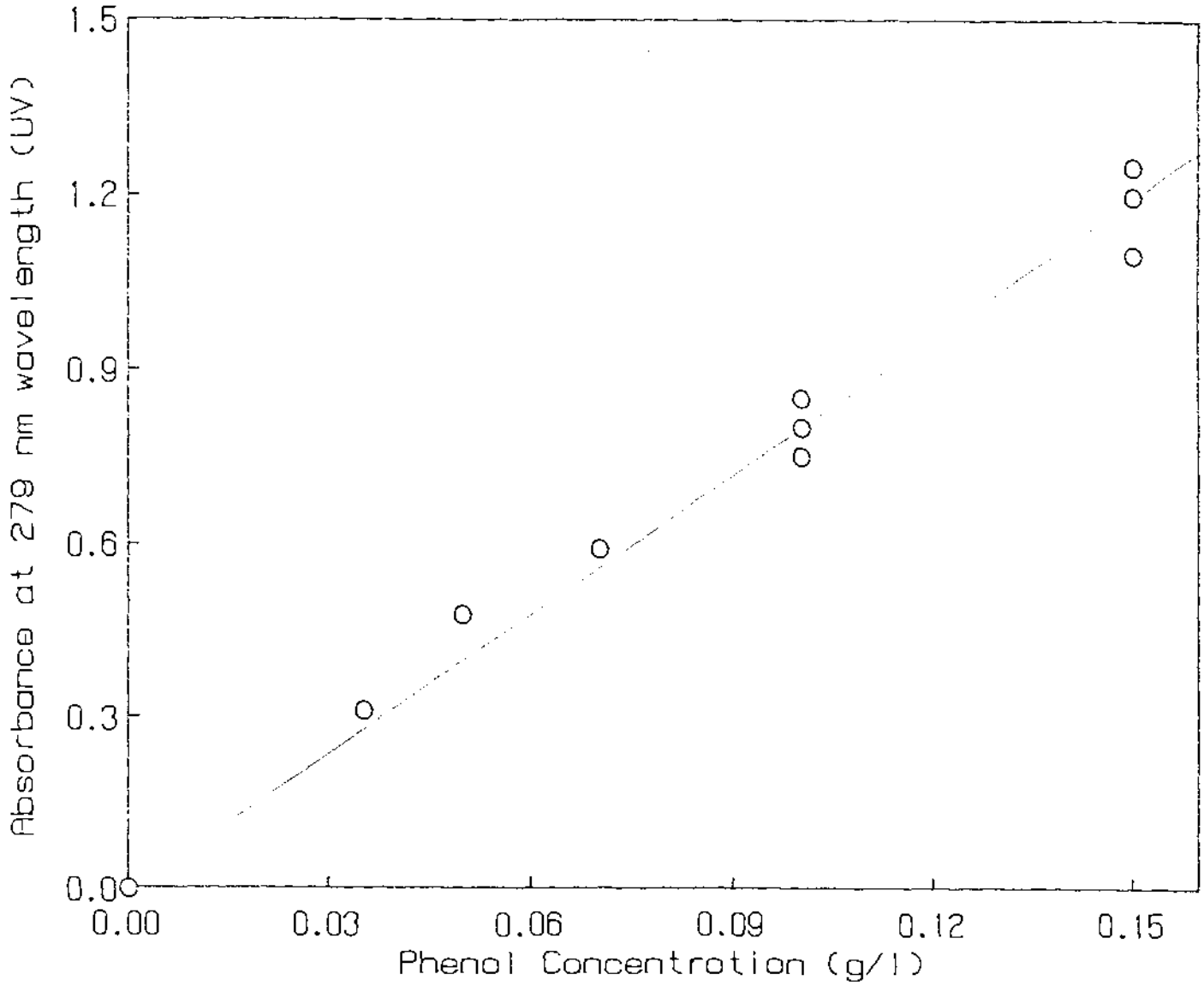

Figure 3.3 Relation between phenol concentration and absorbance

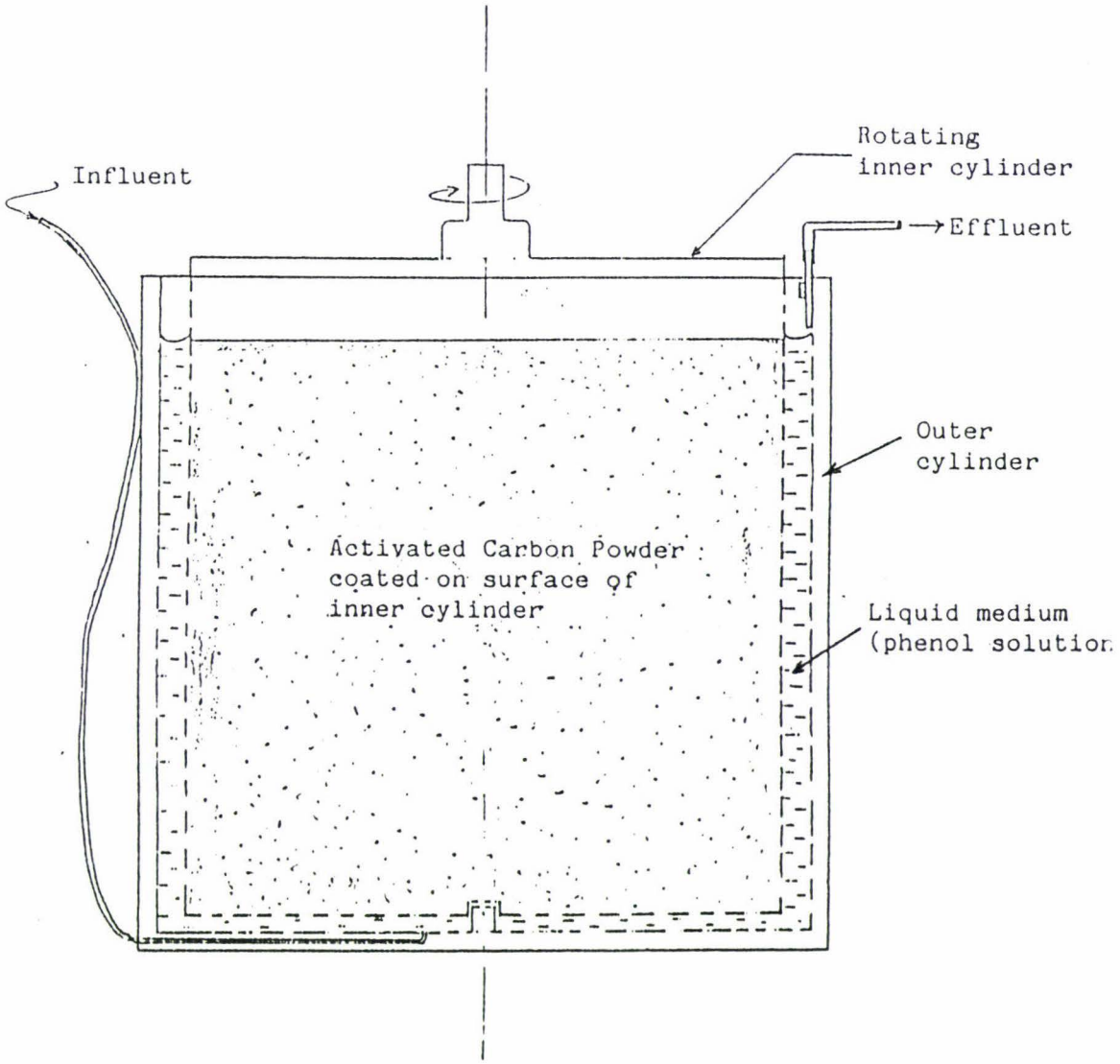

Figure 3.4 Diagram of a concentric cylindrical bioreactor

Table 3.2 Dimensions of reactor

Total height of reactor (inner and outer)	~ 12 cm
Inner cylinder wetted surface area corresponding to area coated with A.C. powder (excluding bottom end area)	314.348 cm^2
Wetted height of inner cylinder corresponding to height coated with A.C. powder	10 cm
Outer Diameter of inner cylinder	10.006 cm
Internal Diameter of outer cylinder	11.068 cm
Width (gap) between inner and outer cylinder	0.531 cm

NB: A.C. refers to Activated Carbon.

The reactor configuration has the following advantages:

i) shear stress on the surface can be varied independently of liquid residence time.

ii) with a small gap between the two concentric cylinders, it has relatively high surface area to reactor volume ratio so that a small hydraulic retention time, which is necessary to prevent suspended growth, can be achieved at a reasonably low flowrate.

The surface of the inner cylinder is coated with a layer of activated carbon powder for better biofilm-surface adhesion, especially for initial attachment (Chang and

Rittman, 1988). The coating of the activated carbon particles to the inner cylinder surface was done using a solution of acrylic plastic in chloroform. Chloroform evaporates readily on exposure to atmosphere, and the acrylic plastic which is a similar material as the reactor is harmless to the microbial film.

3.5 EXPERIMENTAL SYSTEM AND PROCEDURES

The system was operated in a continuous-flow well-mixed mode without recycle. The experimental set-up is shown in Figures 3.5 and 3.6. The reactor is set in a water bath maintaining the reactor contents temperature at 30 ^{o}C. Prior to the commencement, the reactor was filled with similar phenol solution for at least one hour to allow surface conditioning. The experiment was then initiated by filling the reactor with fresh medium innoculated with phenobac culture at about the same initial cell concentration for all sets of experiment. This eliminates the possibilities of the effect of initial attachment due to differential initial cell concentration in the bulk liquid (Duddridge *et al*, 1982). The reactor was operated in a batch mode for 8 hours to 10 hours during this initial stage to allow some surface colonization with the inner cylinder rotating continuously to provide a well mixed condition, before continous

1 - Oxygen gas supply
2 - Feed reservoir with oxygenated sterilized phenol solution
3 - Magnetic stirrer
4 - Sparger
5 - Masterflex tubing pump with variable speed drive
    (a) feed pump
    (b) effluent pump
6 - Variable speed stirrer, Heidalph No. 50115 Type RZR50
7 - Thermometer
8 - Water bath (set at 30 °C)
9 - Bioreactor
10 - Effluent

→ Direction of flow

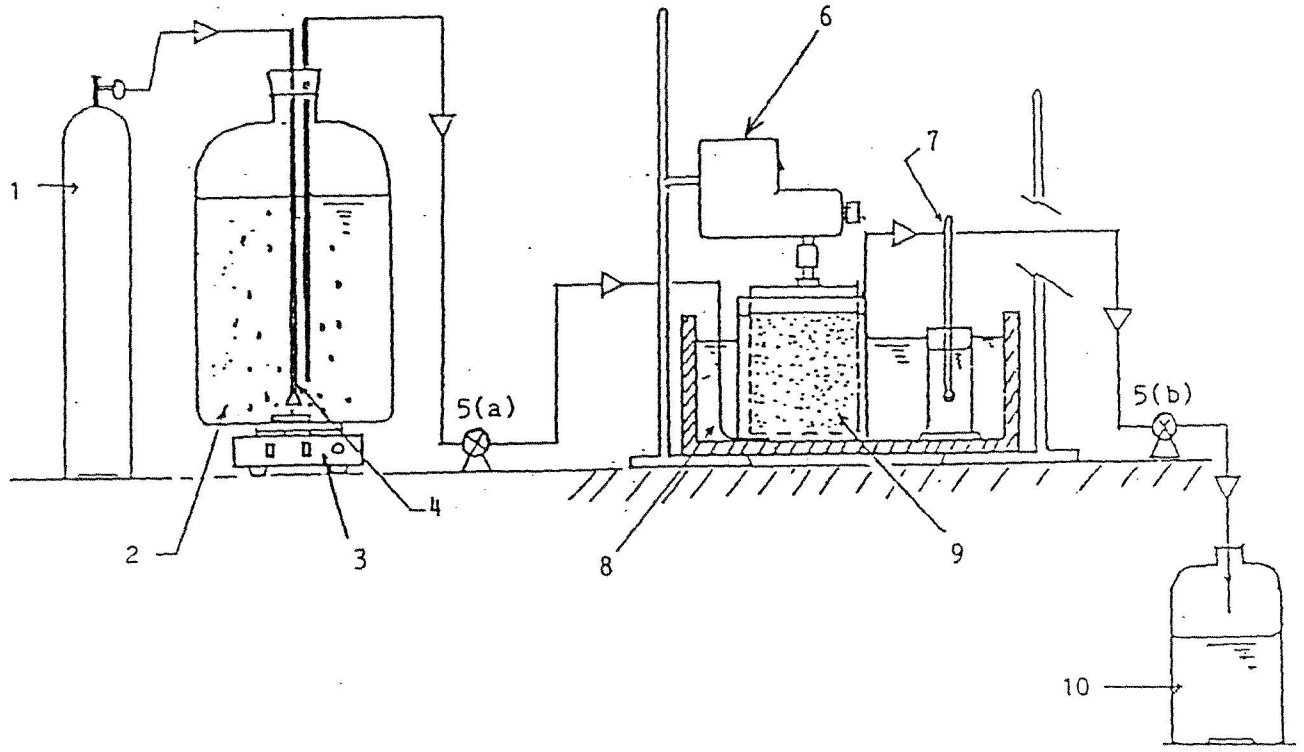

Figure 3.5 Schematic diagram of the experimental set-up

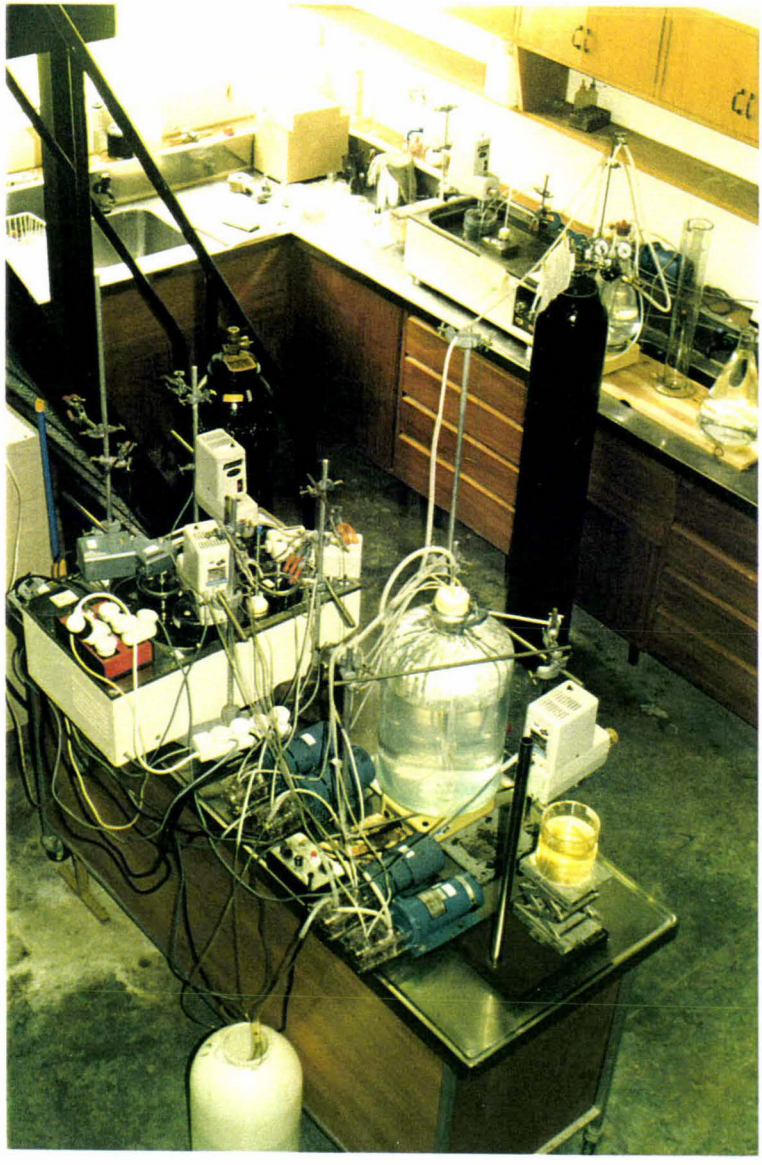

Figure 3.6 Photograph of the overall arrangement of the experimental equipment

feeding of fresh medium commenced. The phenol and cell concentrations in the reactor were measured periodically, and the flowrate checked occasionally.

The system was maintained under aerobic condition by a continous supply of oxygen gas to the sterilized fresh medium in the feed reservoir via a sparger. A magnetic stirrer was installed to disperse the gas bubbles and to maintain a uniform oxygen and substrate concentration.

The liquid volume in the reactor was maintained constant via an outlet (effluent) pump operating at a much higher rate than the inlet pump to prevent the possibility of reactor overflowing due to blockage in the outlet tubing as the cells accummulate on it. Maximum liquid level in the reactor can be adjusted by lowering or raising the suction end of the outlet tubing. The operating parameters for the experiment are listed in Table 3.3.

Table 3.3 Operating parameters

Reactor liquid volume	200 cm^3
Hydraulic Residence Time	1.48 hr.
Flowrate	135 ml/hr.
Initital reactor phenol concentration	~150 mg/l
Inffluent phenol concentration	150 mg/l

As the study only requires biofilm growth on the inner cylinder surface, the surface of the outer cylinder was cleaned every alternate day to eliminate the effect of cell attachment and growth on this surface.

The study was divided into two parts:

1) Biofilm growth study ,and
2) Shear loss study which involved growing of the biofilm to some thickness at low operating speed before subjecting to shear tests at much higher operating speeds.

The operating speeds are shown in Table 3.4. After each shear test, the reactor (now with a thinner biofilm on it) is reset for further growth so that subsequent shear test can be performed again.

Table 3.4 Operating speeds of inner cylinder of reactor

		R.P.M
1)	Biofilm growth study	30, 80, 125, 150, 175, 200 250, 300, 350, 400, 500, 550
2)	Shear loss study	
	- Biofilm growth phase	~ 35
	- Shear tests	100, 125, 150, 175, 200

3.5.1 Measurement of Biofilm Growth

The quantity of biofilm accumulated on a surface may be determined by applying the principles of displacement. The initial quantity (volume) of water required to fill the clean reactor up to the height of the carbon coated surface was measured. The reactor must be dry and there should be no air pockets within the liquid, especially at the bottom end between the inner and outer cylinders, otherwise the accuracy of the measurement will be affected. For the study of growth rate (net attachment) the measurements were made about once every two days during the growth period using the same quantity of liquid. The cummulative volume of biomass attached to the surface on each measurement is represented by the volume displaced. The mass can be computed from the average dry density measured for the range of film thickness tested. The surface of the outer cylinder as well as the bottom end surface of the inner cylinder in contact with the liquid medium were cleaned, and extra growth on the area beyond the coated surface of the inner cylinder removed before the measurement. The method of film thickness measurement adopted by Trulear and Characklis (1982) involving a stage micrometer of a microscope was tried but proved to be time consuming and impractical for this work due to the large number of measurements required.

3.5.2 Shear Test

The shear test consists of two parts, viz. measuring the applied shear stress, and measuring biofilm loss due to shear.

3.5.2.1 Measurement of Torque and Determination of Shear Stress

A torque measuring device was designed and constructed for this experiment to determine the torque on the outer cylinder when the inner cylinder was set to rotate at a constant speed. Details of the torque measuring device are illustrated in Figure 3.7 to 3.9 which consists of a turn-table made up of two acrylic plastic discs connected to one another via a central shaft. One end of the shaft is fixed to the centre of the disc at the top while the other end is attached to the centre of the bottom disc via a free-rotating, frictionless bearing. The bottom disc is attached to a Lab Jack while the disc at the top is free to rotate together with the shaft. The theory of torque and shear stress determination for the system with smooth surface is discussed in Appendix 1.

During shear test and torque measurements, the reactor is mounted on the turn-table (top disc). As the inner cylinder is made to rotate by the stirrer motor, a torque

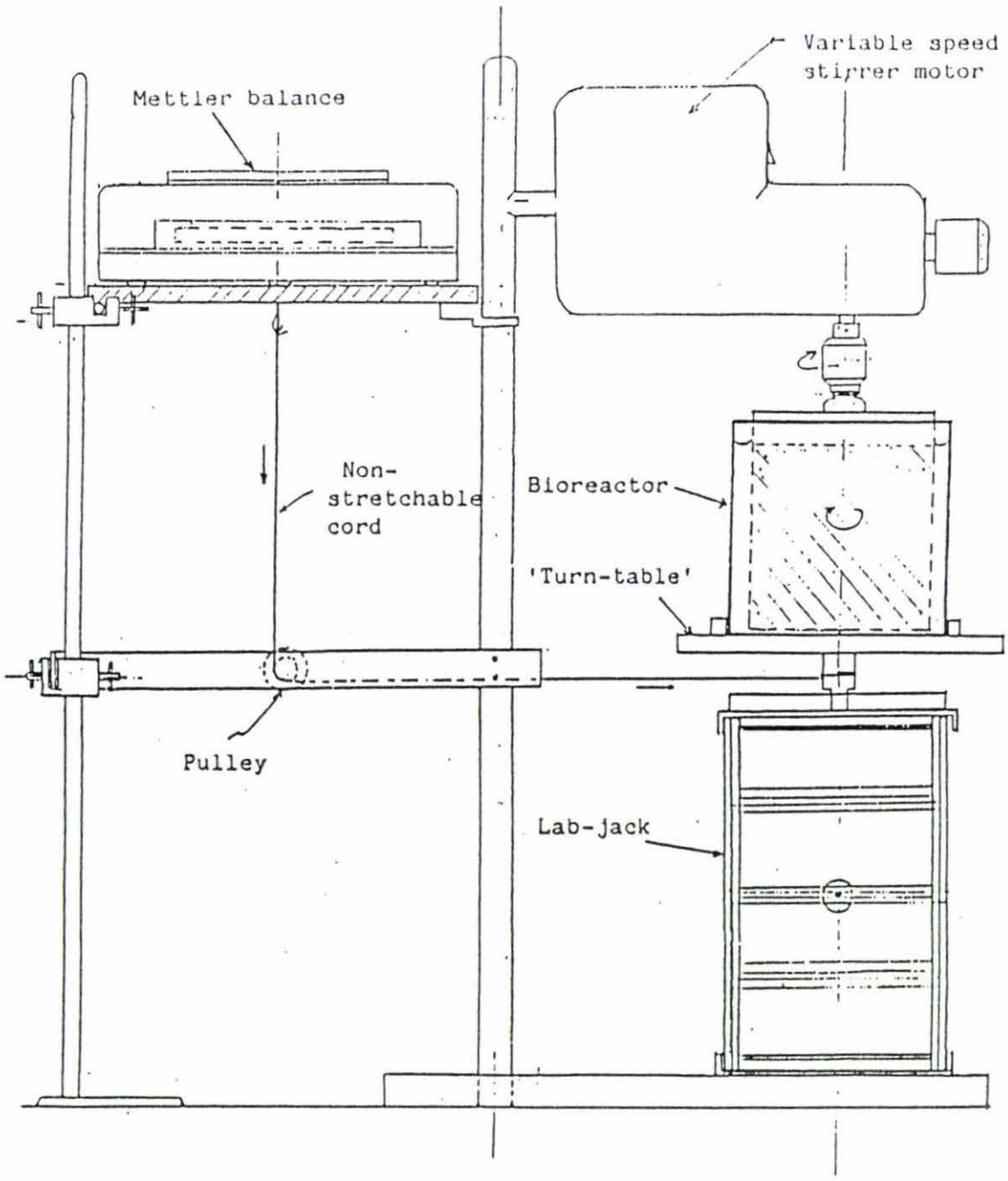

Figure 3.7 Schematic diagram of the torque measuring device

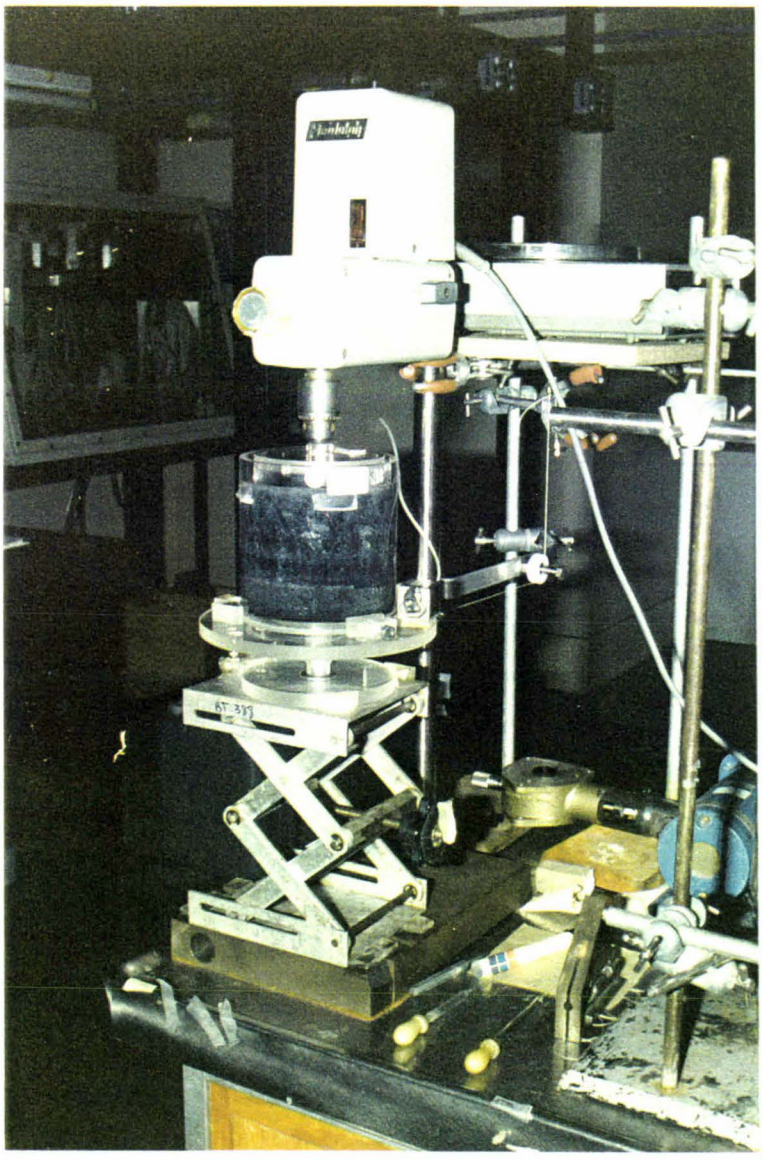

Figure 3.8 Photograph of the torque measuring device for shear test

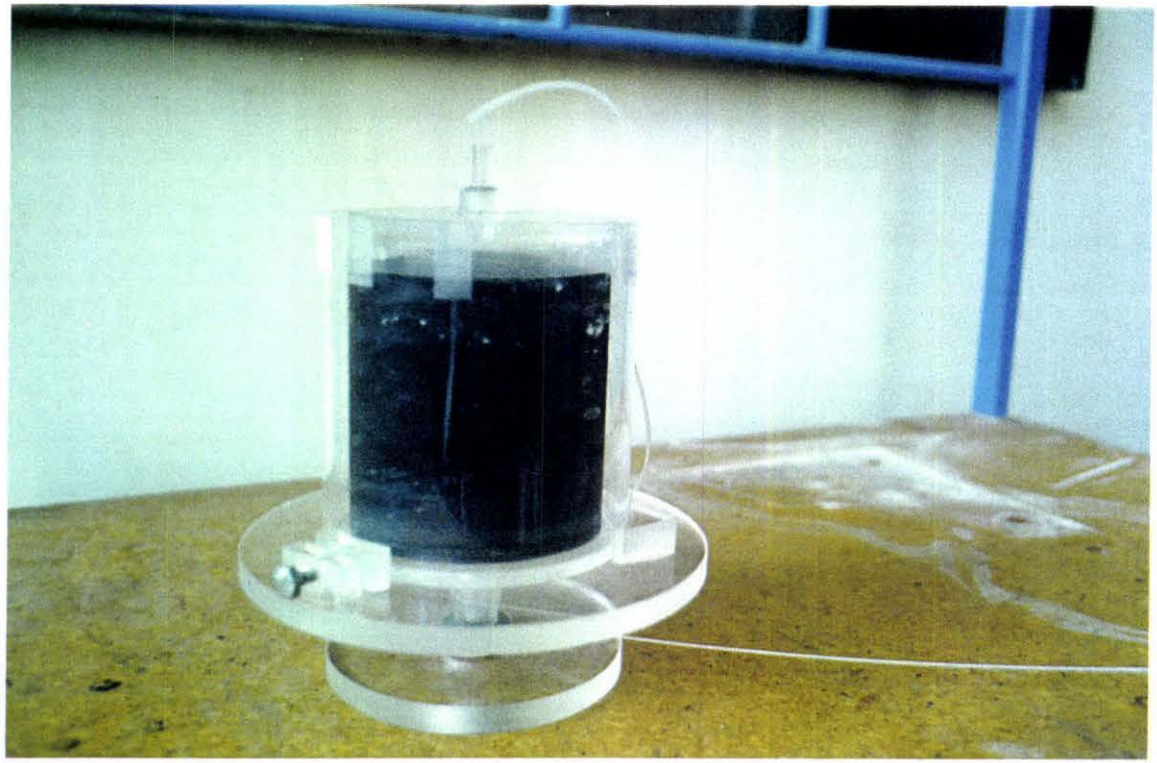

Figure 3.9 Photograph of 'Turn-Table' of the torque measuring device with bioreactor mounted

applied to the outer cylinder via the liquid medium in the reactor is displayed as unit of force, i.e. measuring the tension in the non-stretchable cord connected from the shaft to the digital display balance. The device has to be zeroed initially with the cord held in a tort condition.

The sizing of the shaft diameter will affect the reading or the amount of tension in the cord for an applied torque. A suitable diameter was chosen to give a reasonably large reading for the range of torque expected in the experiment. Calculations to determine the appropriate shaft size are presented in Appendix 2. The torque produced by the inner cylinder rotation and the shear stress exerted at the liquid-solid surface interface can be computed from these basic data using equation (i) in Appendix 2 and equation (4) in Appendix 1, respectively.

3.5.2.2 Measurement of Biofilm Loss due to Shear

Biofilm loss due to shear was determined by measuring the cell mass loss from the attached surface when the surface is subjected to shear stress. During shear test, samples from the reactor were taken at various time intervals to determine the cell mass concentration. The method is

explained in section 3.2. However, after each measurement the sample has to be put back into the reactor again so that there will be no volume change which can affect the concentration of the subsequent test.

3.5.3 Biofilm Dry Density Measurement

The measurement of biofilm density involved first measuring the quantity (wet volume) of the attached biofilm. The method is similar to that in section 3.5.1. Once the quantity has been determined, the biofilm is removed from the solid surface by jets of distilled water followed by filtration using grade GF/A (standard laboratory glass fibre paper) and a series of micropore membrane of pore size ranging from 8 μm to 0.45 μm. The drying procedure is similar to the one discussed in section 3.2. Direct scraping of the biofilm from the reactor surface is avoided to prevent the activated carbon coating from being removed in the process.

CHAPTER 4

RESULTS AND DISCUSSIONS

4.1 TORQUE ON SUPPORT SURFACE WITH AND WITHOUT BIOFILM

Torque on three (3) types of surface have been examined and compared. Surface with activated carbon coating (rough) with and without biofilm growth were measured experimentally, while a theoretical relationship was derived for a smooth surface. The torque on reactor surface (rough) fits a quadratic function (Figure 4.1). For surface coated with activated carbon without biofilm growth (clean surface), the following function was found to be applicable:

$$\text{Torque, } T = (3.23\times10^{-3}N + 0.42\times10^{-4}N^2) \pm 0.28 \text{ Nmm}$$

at 95% confidence level,

where N is the rotational speed in rpm.

This differs significantly from the theoretical torque for smooth surface which follows linear relationship with the angular velocity as derived in Appendix 1, where

$$T = 4\pi h\mu\omega R^2 \frac{k^2}{1 - k^2}$$

Surface coating giving a rougher texture results in higher resistance to liquid flow over it, and consequently,

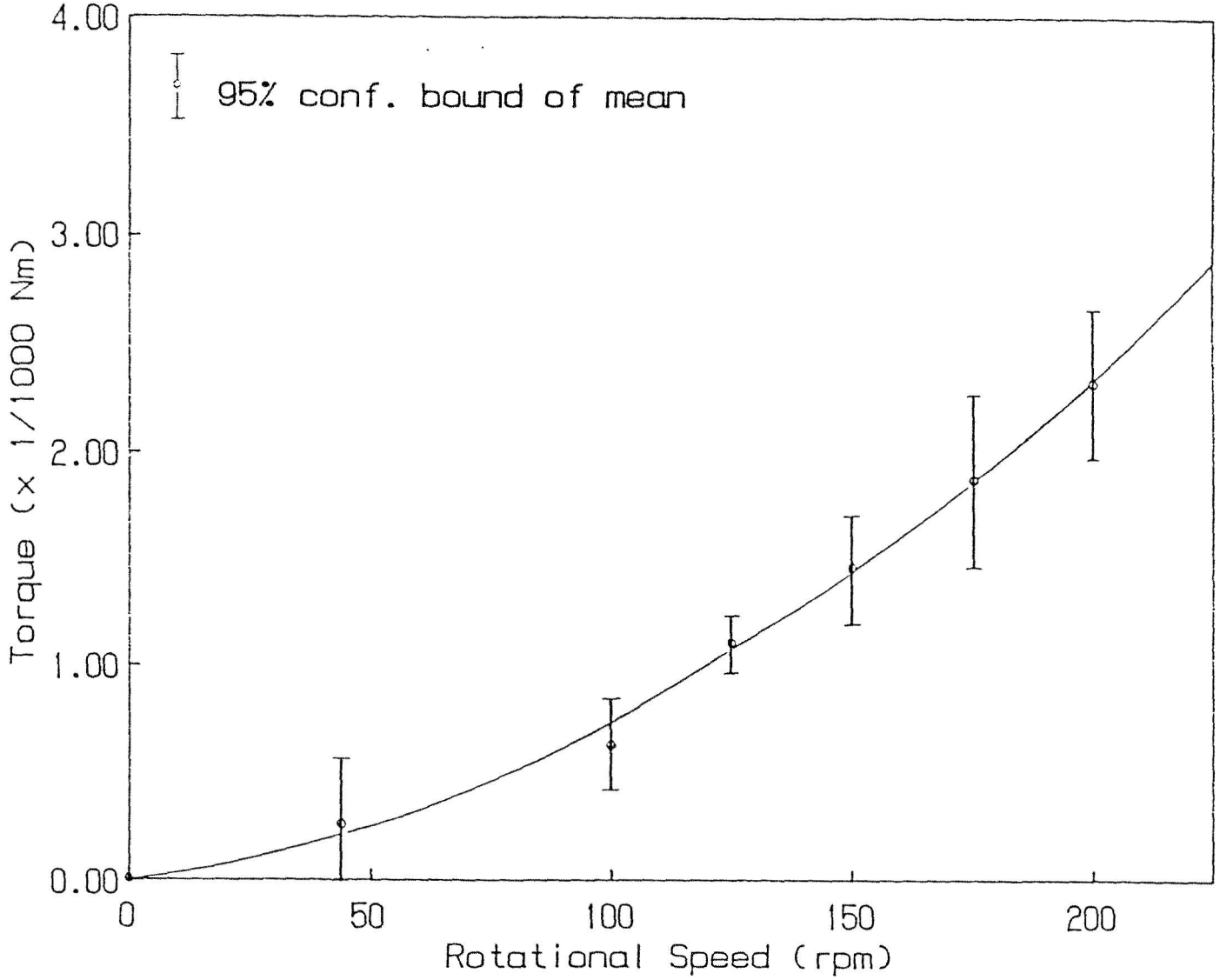

Figure 4.1 Variation in torque with rotational speed without biofilm

produces a higher torque than smooth surface.

The torque due to biofilm attachment and growth on the rotating bioreactor surface as shown in Figure 4.2 also fits a quadratic function as follows:

$$T = 2.51\times10^{-3}N + 0.77\times10^{-4}N^2) \pm 0.67 \text{ Nmm}$$

at 95% confidence level.

The effect of film thickness was insignificant. No consistent variation in torque at constant rotational speed for different film thicknesses was observed. The regression lines in Figure 4.3 indicating slopes of near zero (giving almost constant torque at each constant rotational speed) for the range of film thickness further justifies the insignificance of the effect of film thickness on torque for the system studied.

The thickness of the biofilm on the surface may vary, giving rise to irregularities on the film surface in contact with the liquid. The method of thickness determination adopted which employs the principles of volume displacement only enables computation of average thickness. Variations in surface irregularities could have attributed to the inconsistent variation of torque with film thickness. However, analysis of the experimental results by statistical method indicates

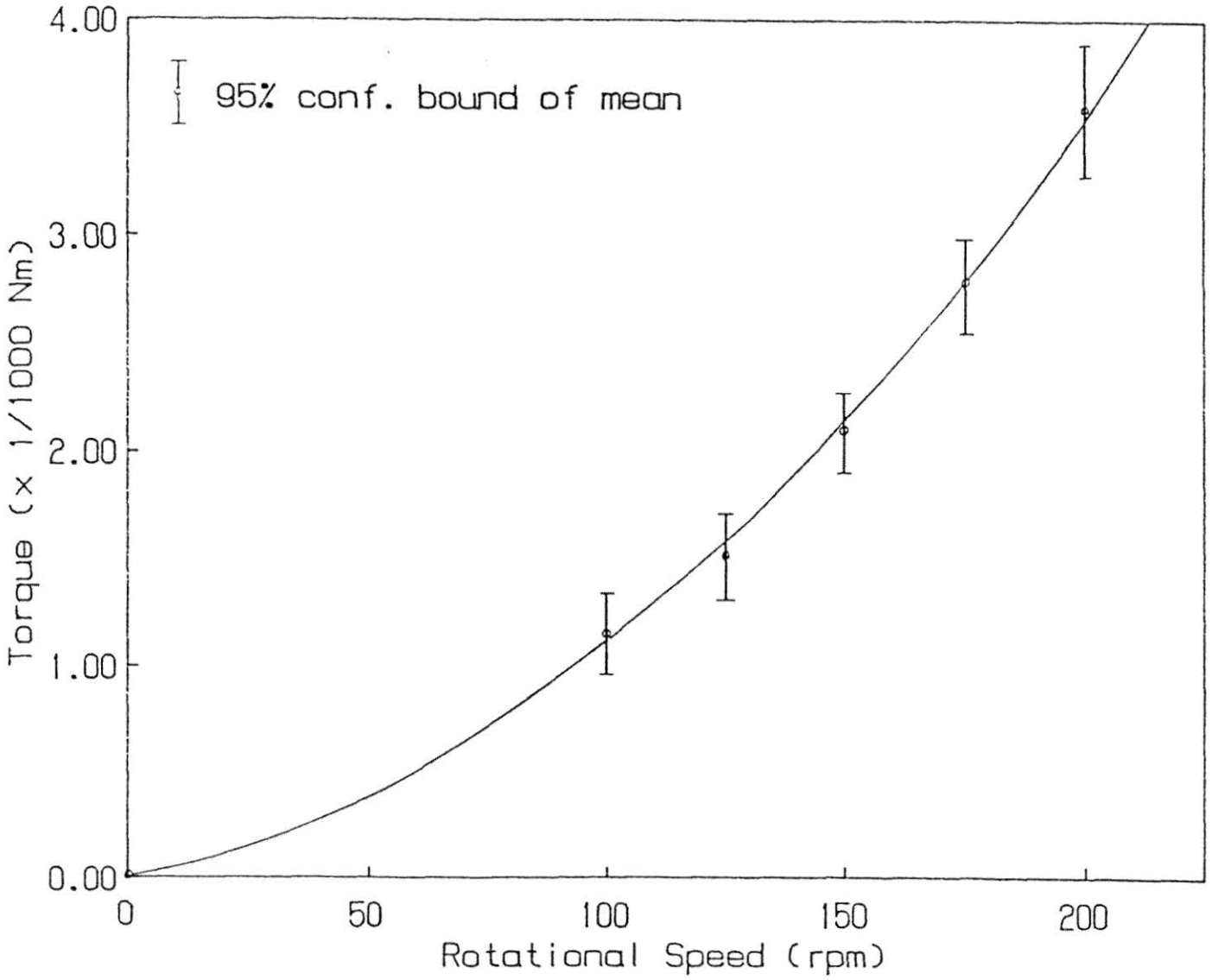

Figure 4.2 Variation in torque with rotational speed with biofilm

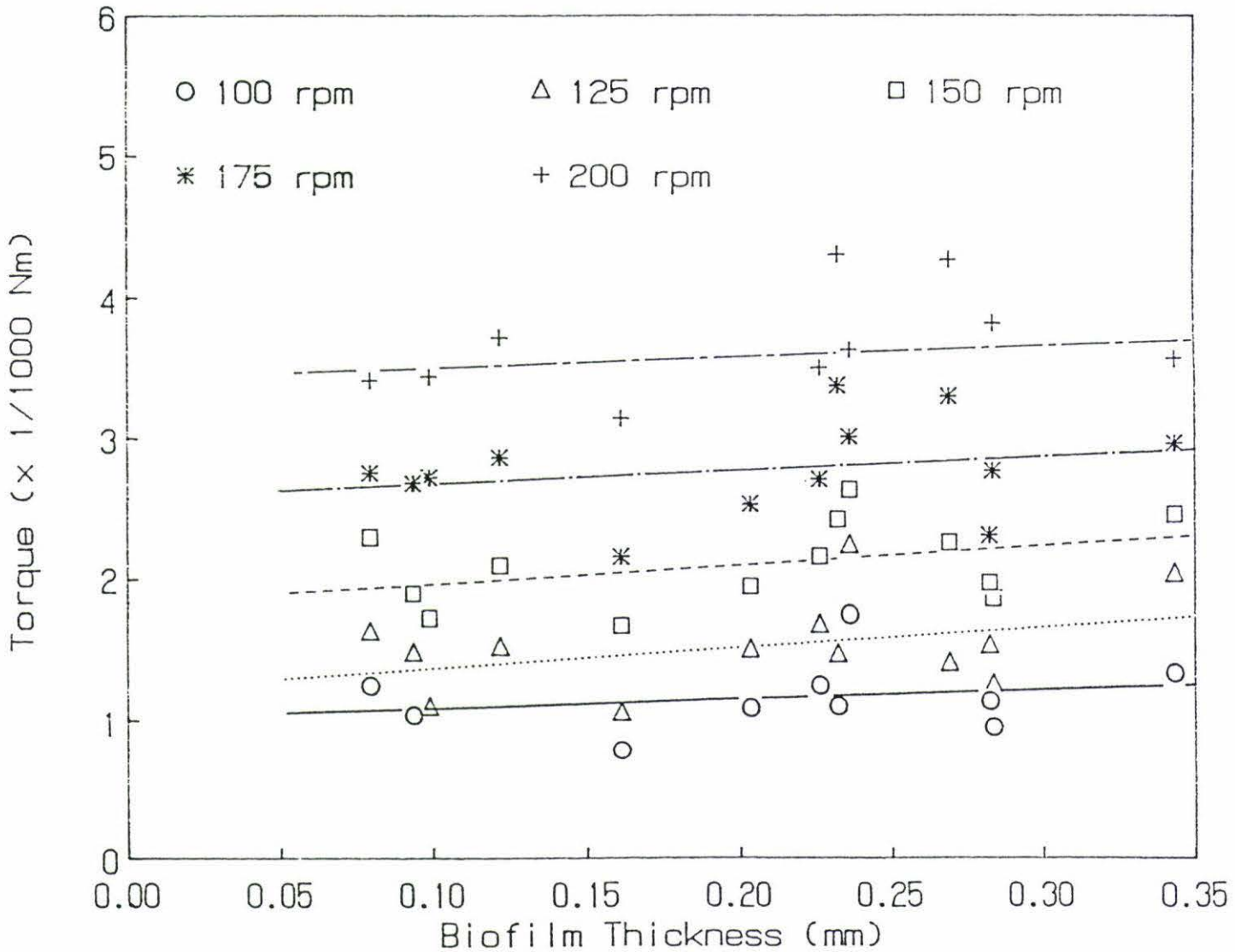

Figure 4.3 Effect of biofilm thickness on torque

reasonably small variations within the confidence limit chosen, and therefore justifies the use of a single quadratic function of torque for all film thicknesses eventhough theoretically, thicker film should cause a higher torque (and hence higher shear stress) for a constant rotational speed (disregarding the surface irregularities).

Comparisons of the torque due to different surface types can be seen in Figure 4.4.

4.2 BIOFILM GROWTH AND ACCUMULATION

Biofilm accumulation is the net result of biomass attachment, continous production or growth and detachment (loss) by shearing and decay. The net biofilm accumulation on the bioreactor surface and the substrate (phenol) concentration in the bulk liquid of the reactor were examined simultaneously during the biofilm growth. The activated carbon coated surface with and without biofilm are illustrated in figures 4. 5 and 4.6, respectively.

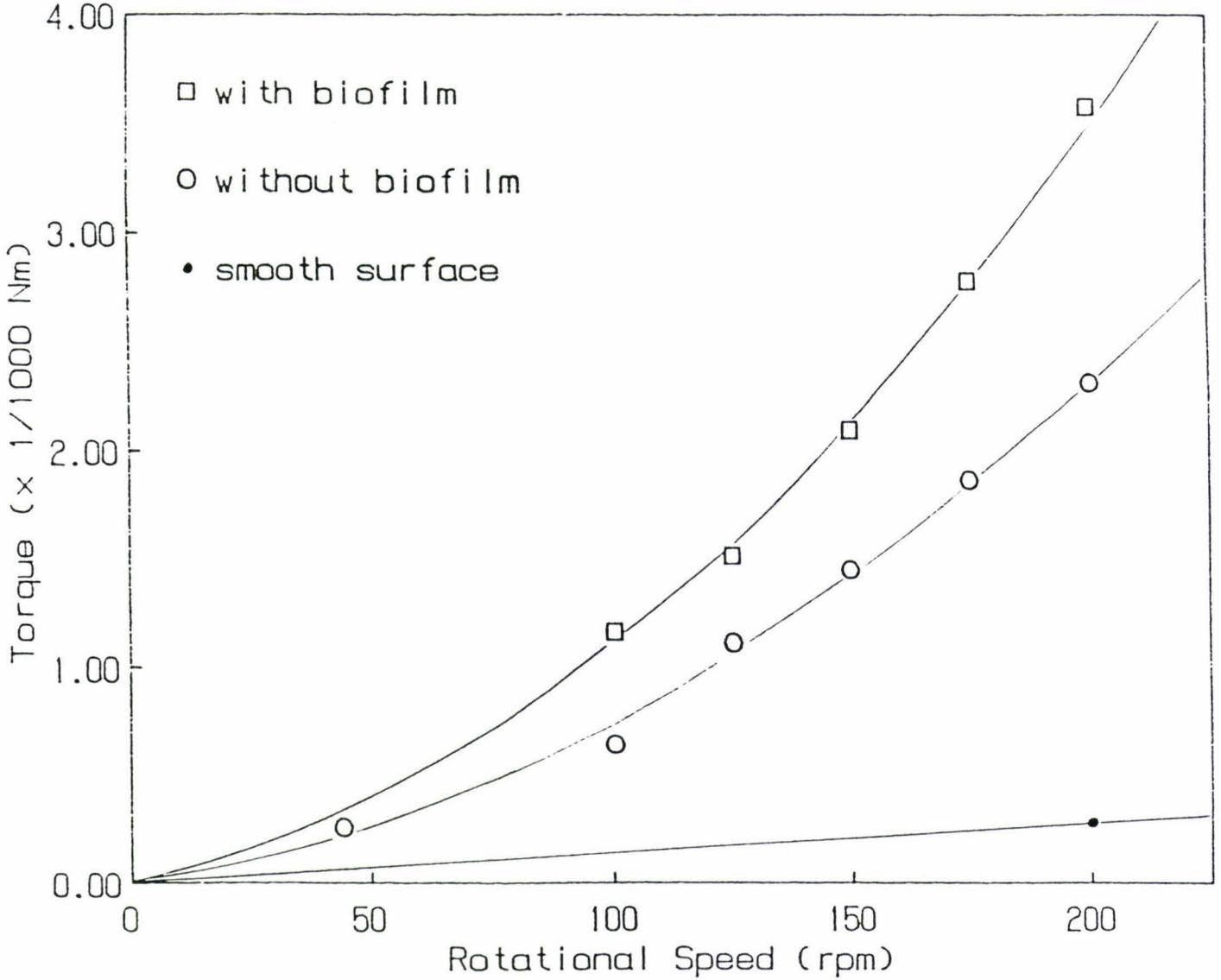

Figure 4.4 Torque variation with rotational speed for different surface types

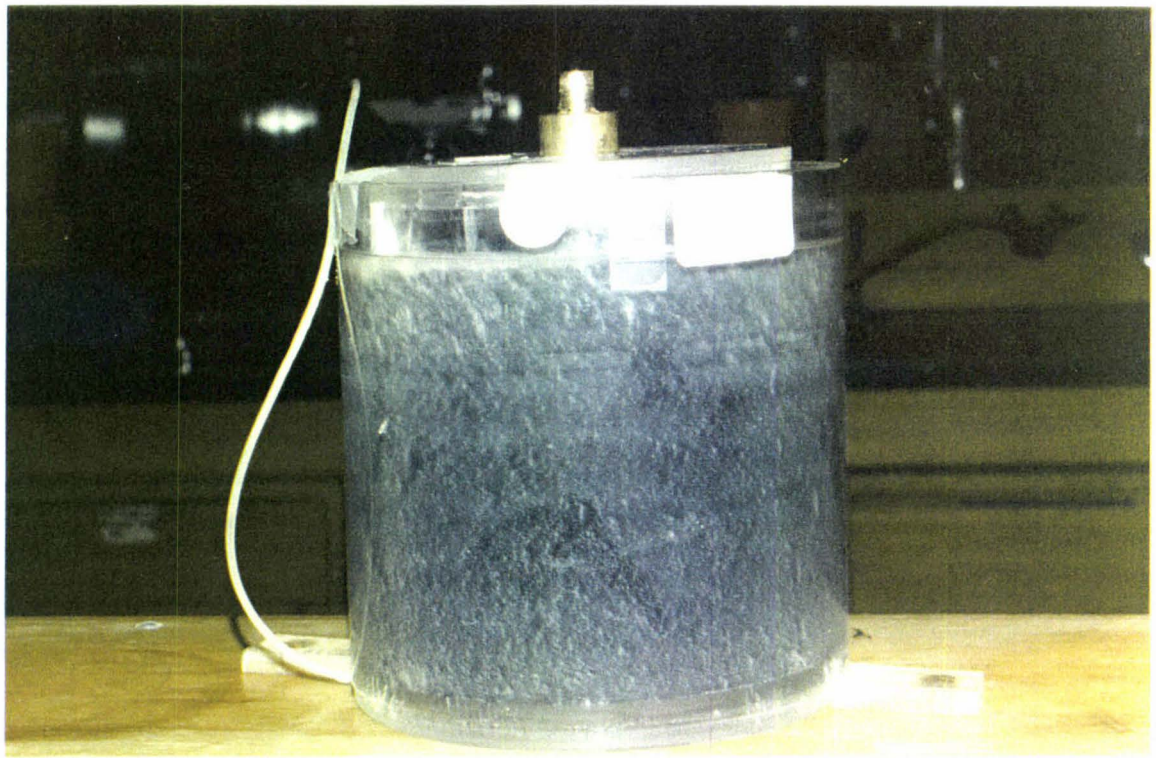

Figure 4.5 Photograph of activated carbon coated surface reactor with biofilm

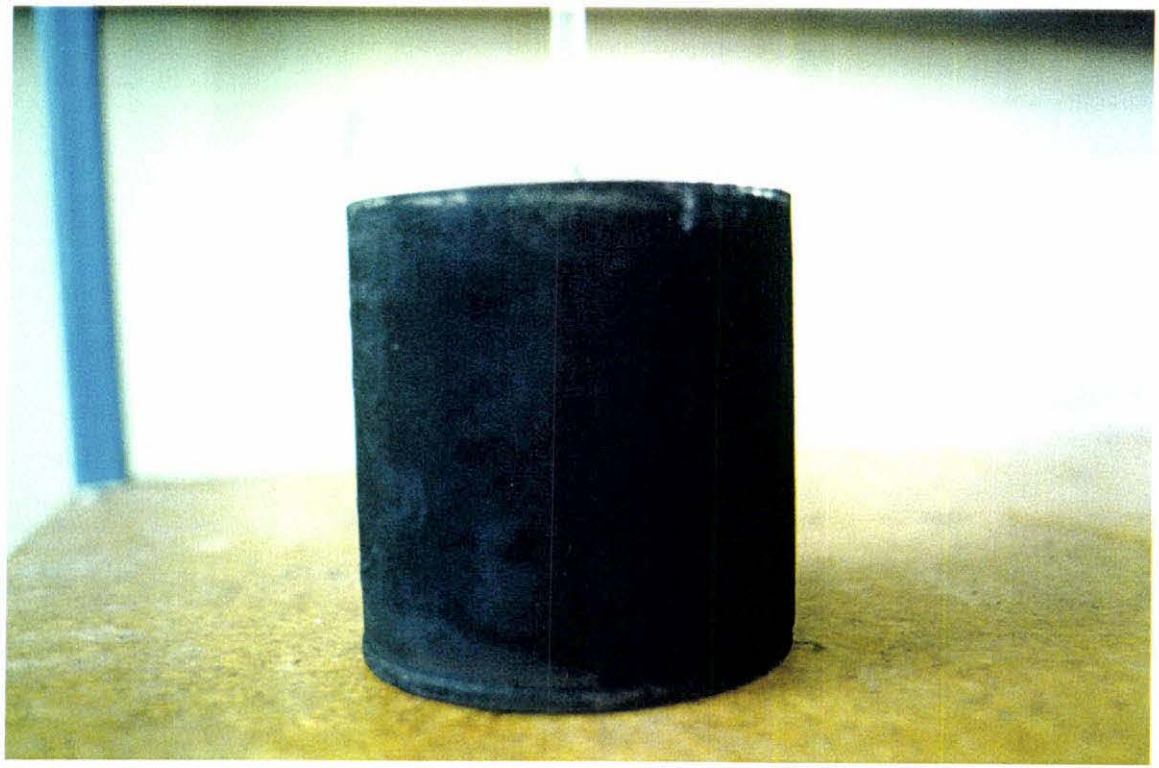

Figure 4.6 Photograph of actived carbon coated surface reactor without biofilm

4.2.1 Substrate Removal or Consumption

The substrate removal rate was observed to increase with film thickness to a steady-state similar to that found by Tomlinson and Snaddon (1966); Kornegay and Andrews (1968); Hoehn and Ray (1973); and LaMotta (1976(b)). The steady-state rate is reached at film thickness of between 0.050mm and 0.100 mm approximately, for rotational speed of 30 rpm to 550 rpm as can be seen in Figure 4.7. This agrees with that observed by Tomlinson and Snaddon (1966); and Kornegay and Andrews (1968). However, steady-state values vary in increasing order exponentially with increasing applied shear stress (or rotational speed) as demonstrated in Figure 4.8 which reached a maximum constant value at and beyond a critical shear stress of about 3.44 N/m^2 (~ 250 rpm). Incidentally, this is also the maximum substrate removal efficiency for the system. Similar phenomenon was also observed by LaMotta (1973(a)); Trulear and Characklis (1982), although the critical speed or shear stress they obtained was lower than that observed in this study. This can be attributed to the decreased in diffussion resistance of the 'stagnant liquid film' to a minimum as the 'moving liquid' velocity over the biofilm was increased by the action of reactor rotational speed.

The substrate (phenol) mass balance across the bioreactor

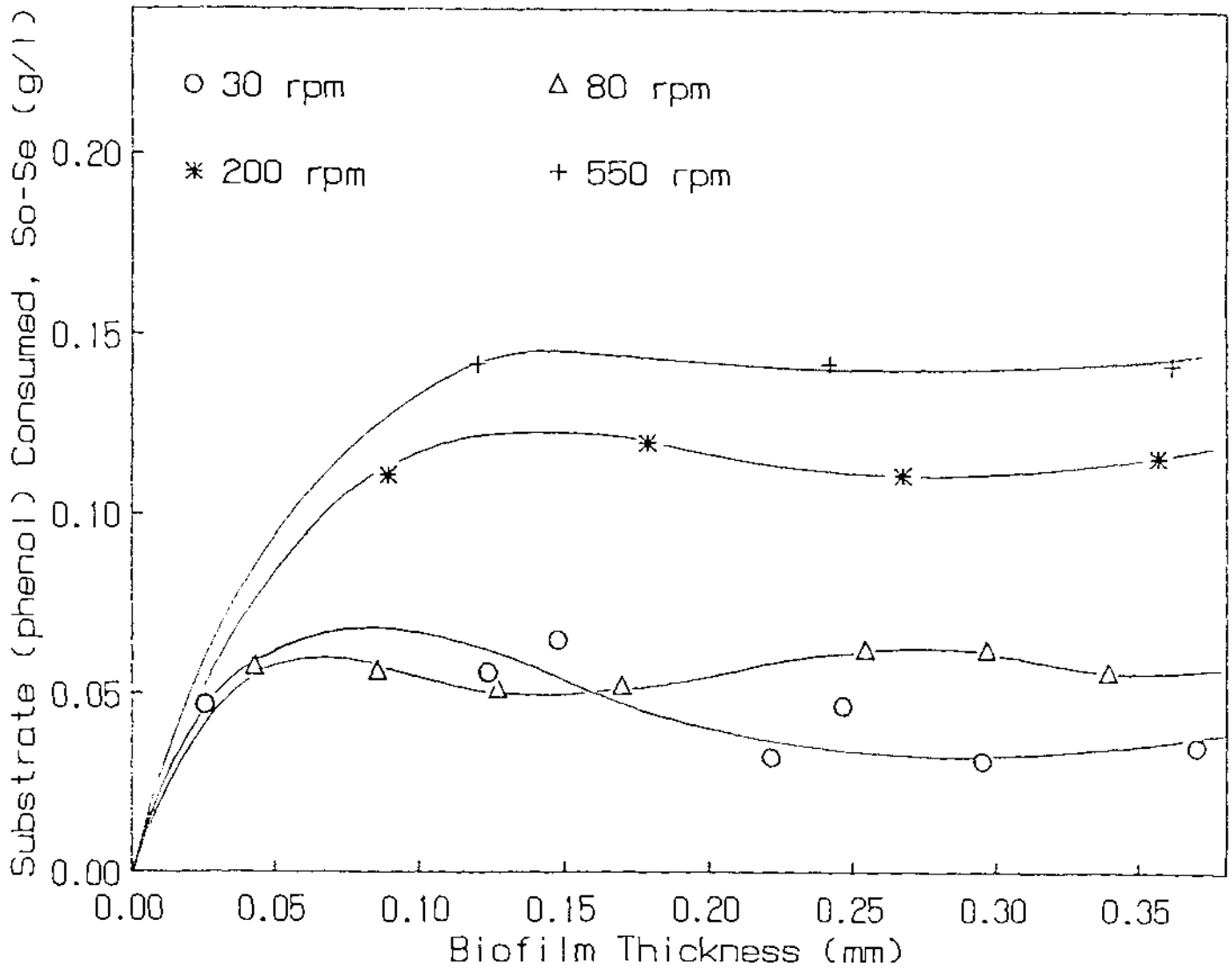

Figure 4.7 Variation in substrate removal with film thickness for various rotational speeds

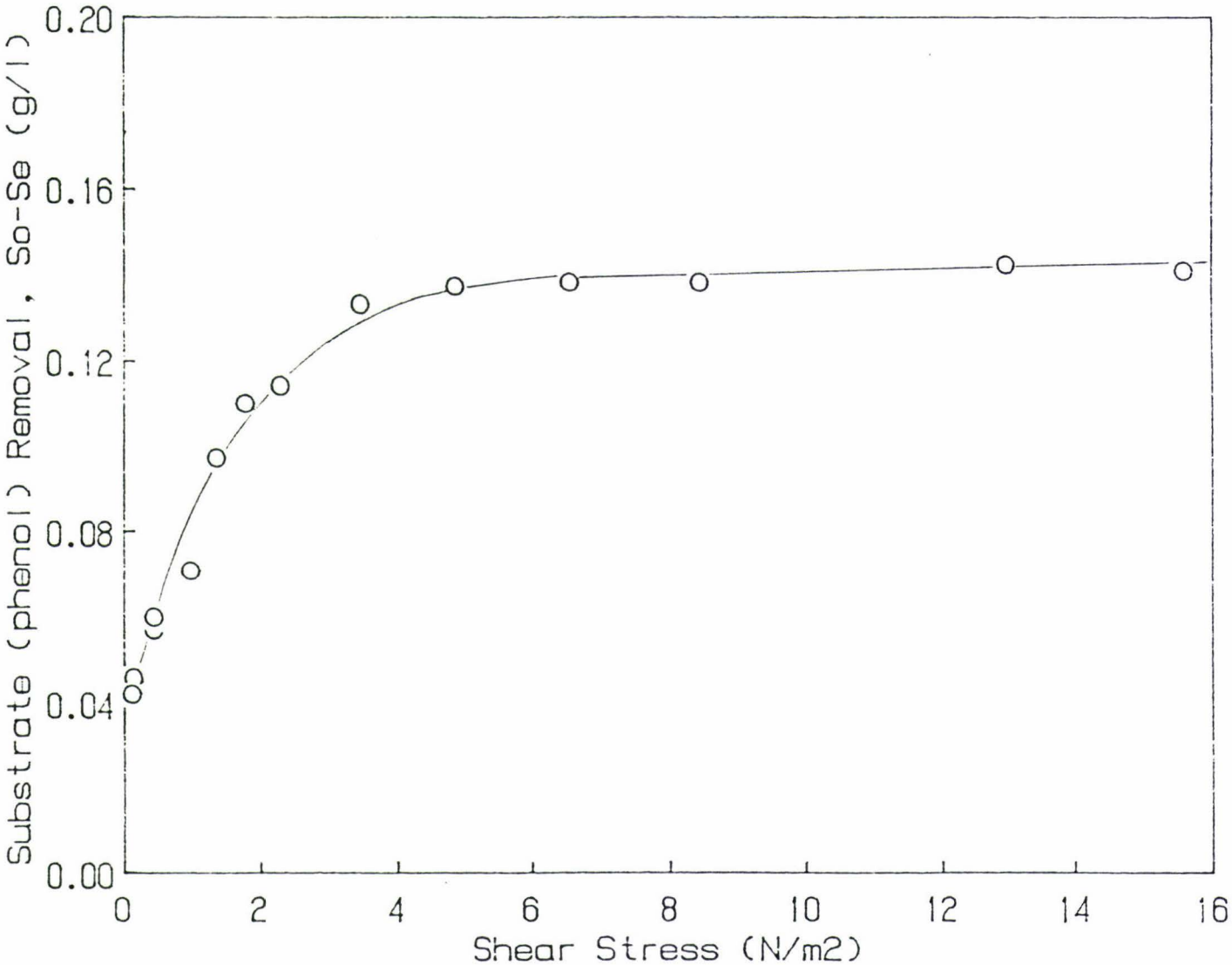

Figure 4.8 Effect of shear stress on steady-state substrate removal

can be expressed as follows:

Substrate net accumulation = inflow - outflow - consumed by attached biofilm - consumed by suspended biomass

$$V\left.\frac{dS}{dt}\right|_{\substack{\text{net}\\ \text{accum.}}} = QS_o - QS_e - A.z.R_c - V\left.\frac{dS}{dt}\right|_{\substack{\text{cons.}\\ \text{by s.}\\ \text{biomass}}}$$

where A is the surface area of reactor with biofilm (m^2), z, the biofilm thickness (m) and R_c, the rate of substrate consumption per unit volume of biofilm ($g/m^3.hr$).

As the suspended growth can be neglected due to low HRT, giving the mean cell residence time much less than the minimum mean cell residence time (i.e. $\theta_c \ll \theta_c^M$), the last term can be omitted.

At steady-state of substrate consumption, $R_c = \frac{Q(S_o-S_e)}{A.z}$

so that for any constant shear stress, R_c the steady-state consumption rate is inversely proportional to z where z > minimum thickness, z_a (the active thickness according to Kornegay and Andrews (1968), and Hoehn and Ray (1973)). At $\sigma > 3.44$ N/m^2 (~250 rpm), S_o-S_e (constant) reaches maximum so that maximum R_c also decreases linearly with film thickness greater than the active thickness. Beyond the active thickness the inner region becomes starved of substrate resulting in lower overall reaction rate ,and so

maintaining thickness greater than this will not give any higher removal efficiency.

4.2.2 Net Biofilm Accumulation

The cummulative biofilm mass accumulation measured at different time can be approximated to a linear relationship representing constant growth rate for each reactor operating speed as presented in Figures 4.9 and 4.10. The net growth rate increases with increasing operating speed to a maximum beyond which the rate begins to fall, for a constant feed substrate concentration (Figure 4.11). Similarly, a parabolic relationship with shear stress is found as follows:

$$\text{Net Growth Rate, } G_n = (14.28 + 27.53\sigma - 1.51\sigma^2) \times 10^{-3} \text{ g/d} \quad \ldots (1)$$

where σ is the shear stress in N/m^2.

Studies on the effect of shear stress on net biofilm growth reveal that a shear stress of 19 N/m^2 is required to achieve zero net growth rate, which is the stress at which total biofilm loss rate equals total growth rate.

The film thickness was observed to have little effect on the shear stress at the biofilm surface for a constant speed of rotation in contrast to the results of Trulear

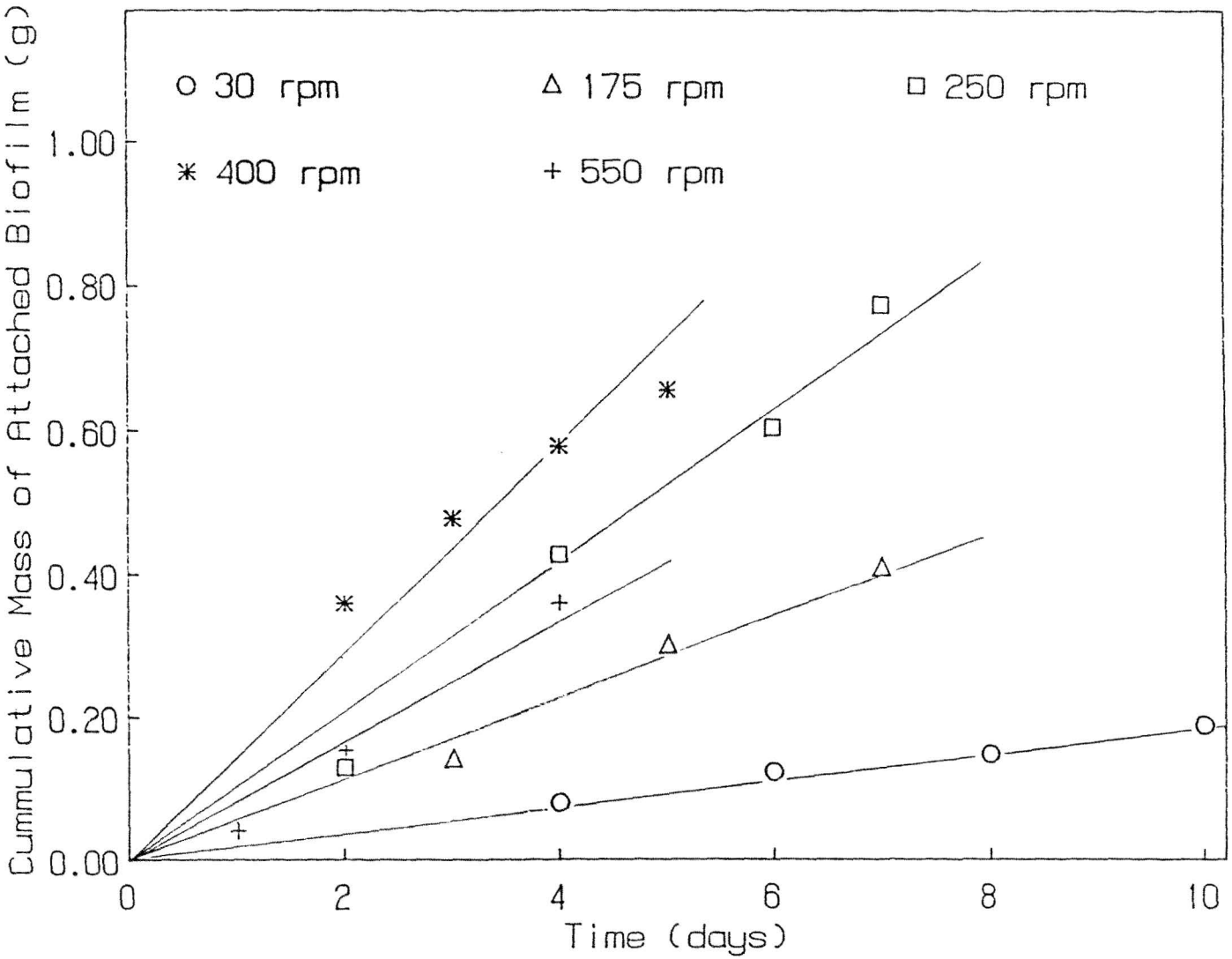

Figure 4.9 Variation in net biofilm accumulation with time

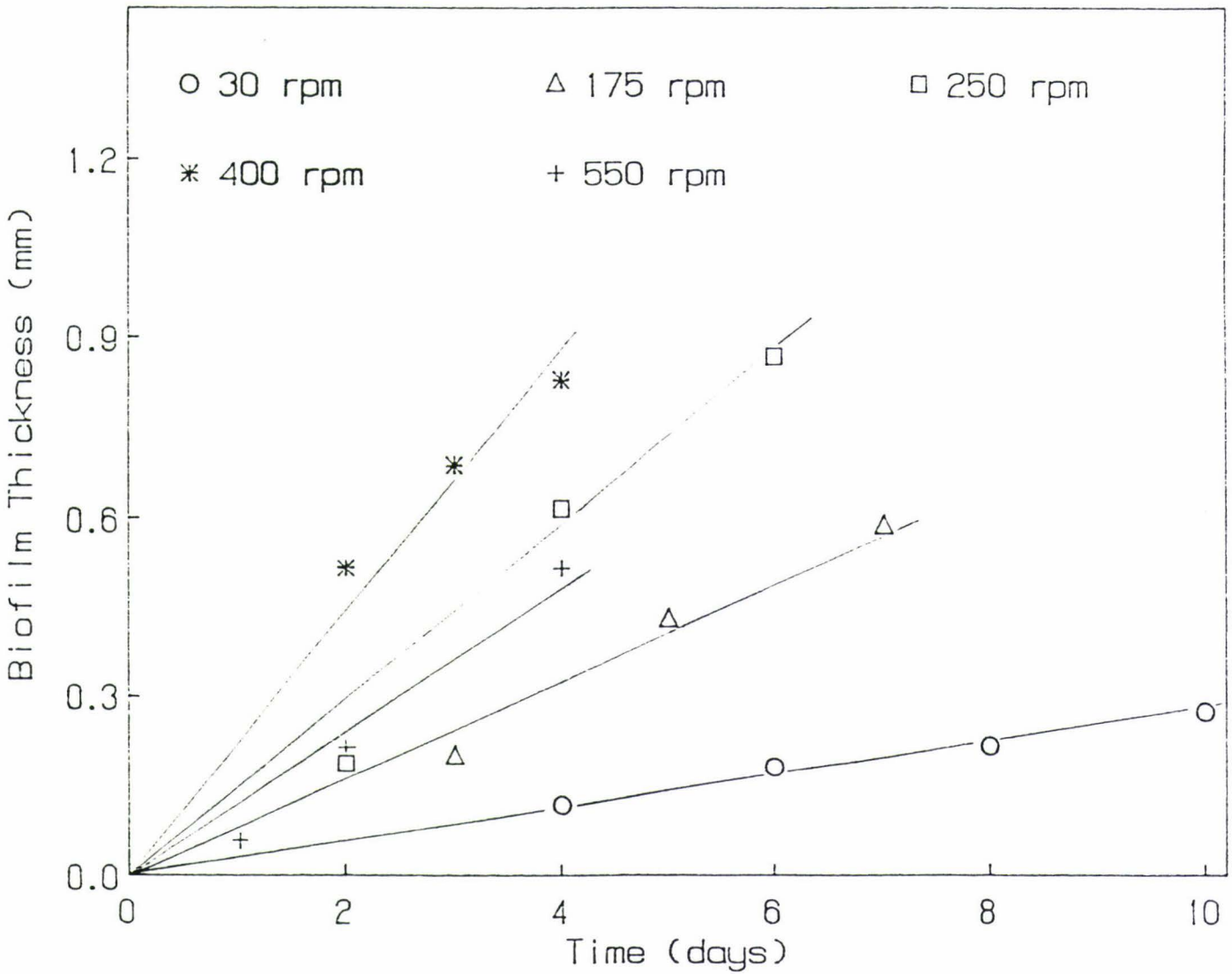

Figure 4.10 Variation in biofilm thickness with time

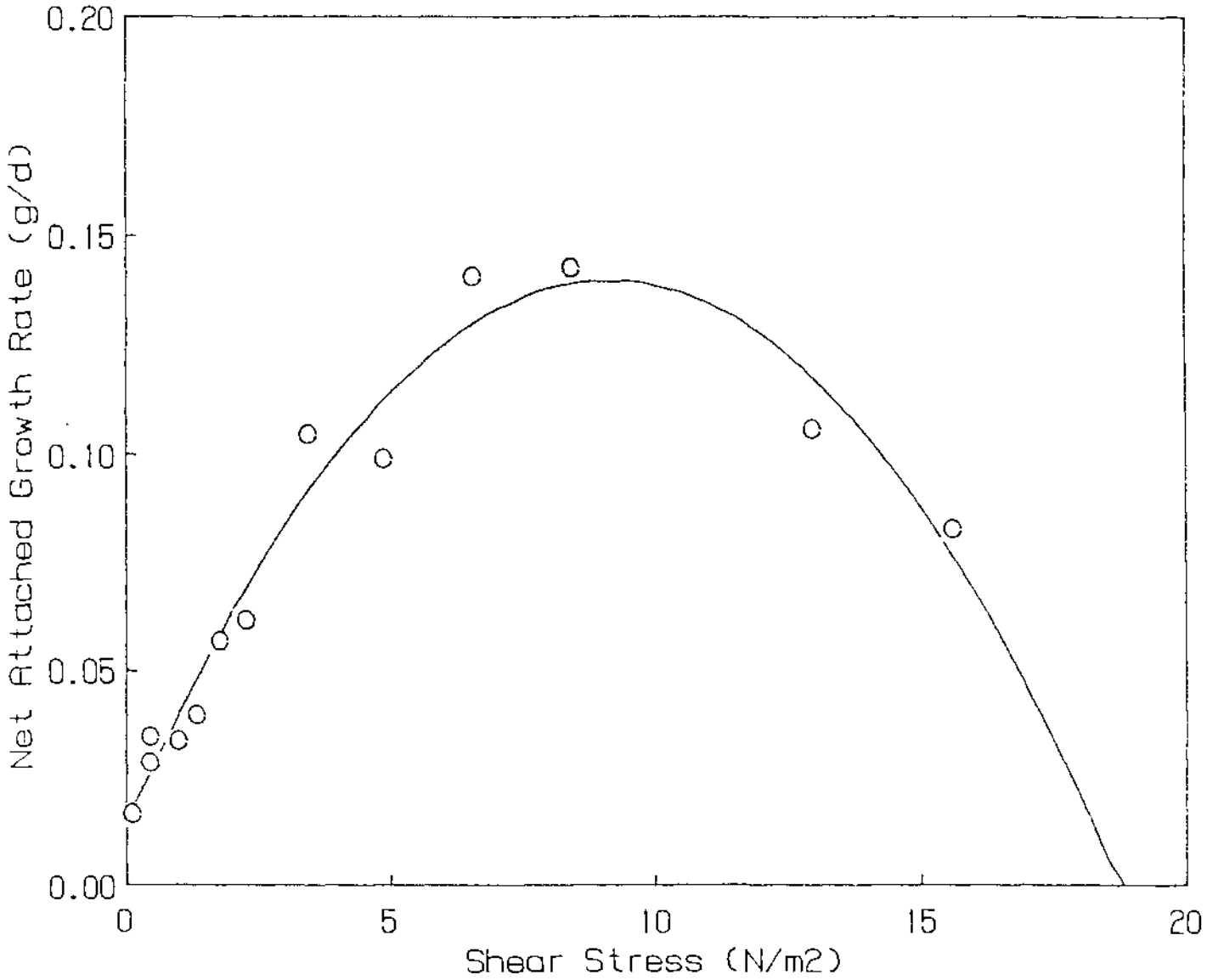

Figure 4.11 Effect of shear stress on net biofilm growth rate

and Characklis (1982) who observed that thickness increased to a point where it remained constant when production balanced shear loss due to increasing shear stress with film thickness, although their substrate concentration was much lower. Within the range of film thickness studied, the net biofilm accumulation appears to continue to increase even up to a thickness of about 1.0 mm, as demonstrated in Figure 4.10. This confirms the validity of adopting a single relationship between torque and rotational speed for all film thicknesses as discussed in section 4.1 by neglecting the effect of film thickness.

4.3 BIOFILM LOSS DURING GROWTH

The total substrate (phenol) consumed as discussed in section 4.2.1 whether at increasing or constant rate will be utilized for cell synthesis and maintenance. Although no data on shear loss during growth are available, it can be calculated from total growth rate and the observed net growth rate. The total growth rate was estimated by adopting a yield of 0.92 g/g found by Rao (1985) for the same culture and substrate, together with the substrate removal rate at steady-state. Dispersed growth can be neglected at low HRT as explained in section 4.2.1. The estimated total growth curve as a function of shear stress is shown in Figure 4.12 comprising of both decay

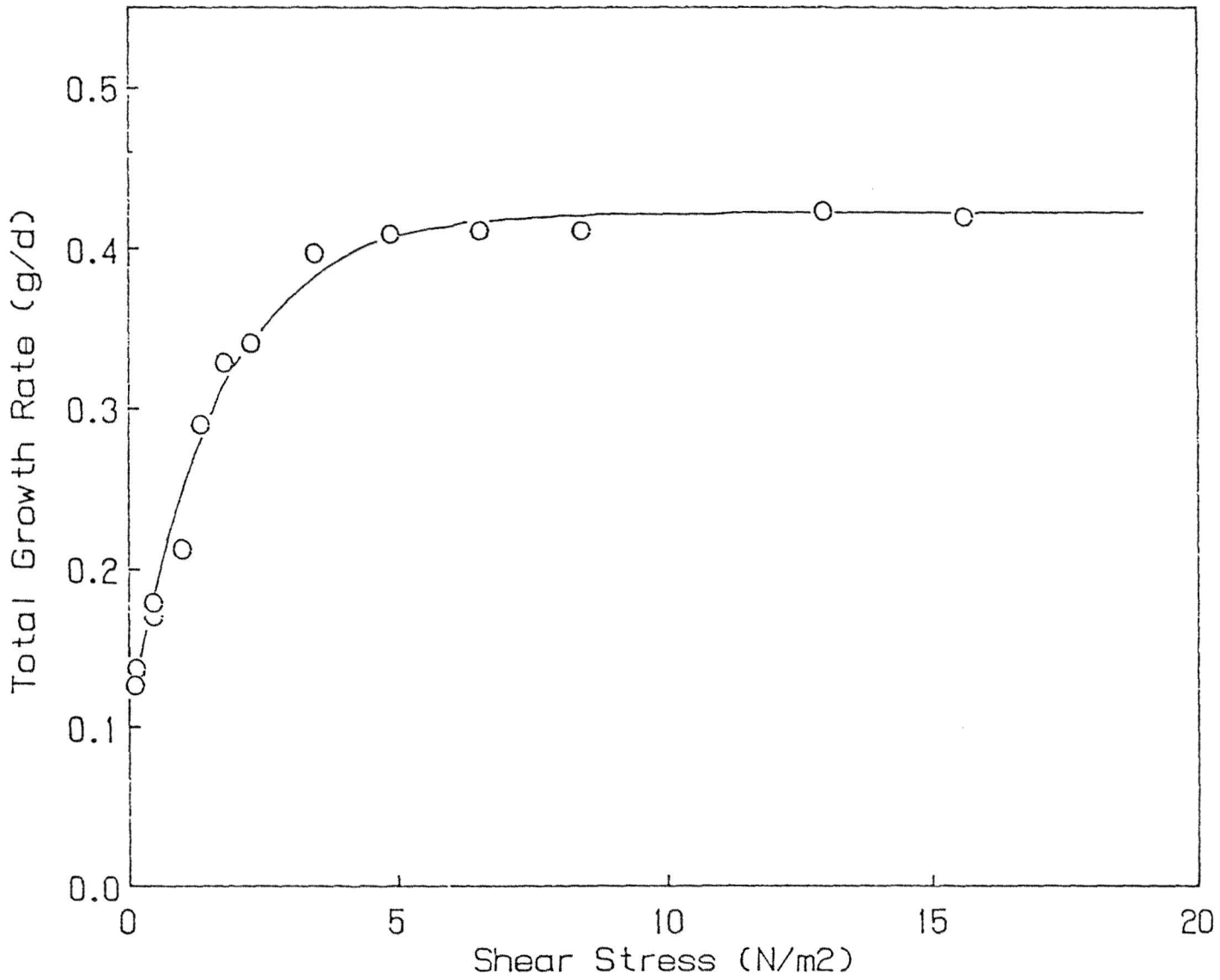

Figure 4.12 Variation in biofilm total growth rate with shear stress

loss and shear loss components. This follows the function,

$$\text{Total Growth Rate, } G_t = 0.42 - 0.32e^{-0.61\sigma} \text{ g/d} \quad \ldots (2)$$

The loss due to cell decay will be negligible compared to shear loss and will be even more so at higher shear stress so that shear loss rate can be reasonably approximated to the total loss rate, neglecting the decay loss. The relationship of shear loss rate with shear stress in Figure 4.13 therefore can be obtained by combining equations (1) and (2) as follows:

$$\text{Shear Loss Rate, } R_s = (40.82 - 2.75\sigma + 0.15\sigma^2 - 31.83e^{-0.61\sigma}) \times 10^{-2} \text{ g/d} \quad \ldots (3)$$

The effect of shear stress on both the growth and loss rates is presented in Figure 4.14. The initial increasing loss rate which tends to reduce after shear stress of about 1.77 N/m^2 (~175 rpm) to more or less constant until shear stress of about 9 N/m^2 indicates an increase in shear resistance. What causes the increase in shear resistance? From the results of Trulear and Characklis (1982) who found that biofilm density increases with increasing substrate loading rate, it follows that as reactor substrate concentration increases, density also increases, and hence its resistance to shear loss since higher density film will be more compact. However, in

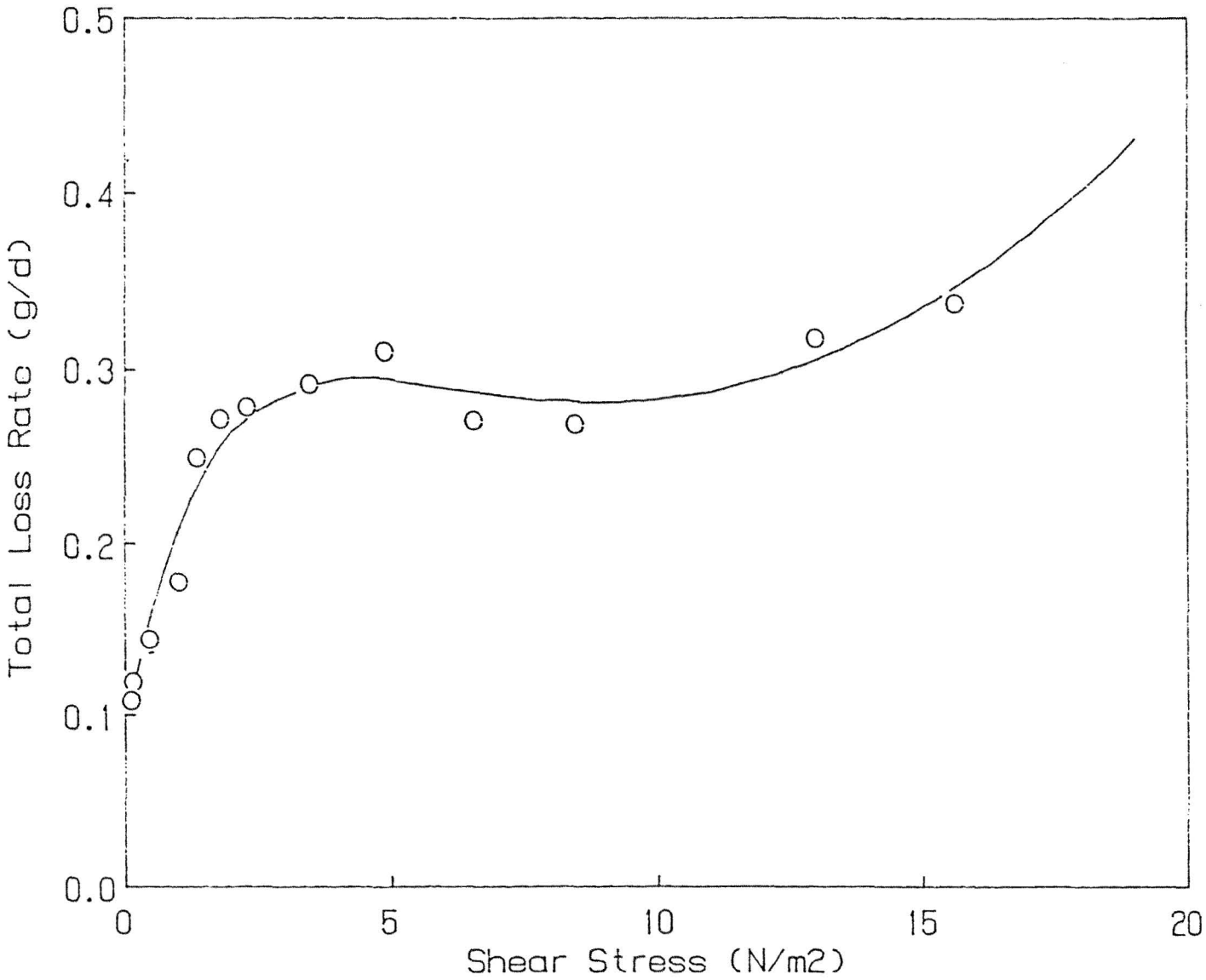

Figure 4.13 Variation in biofilm total loss rate with shear stress

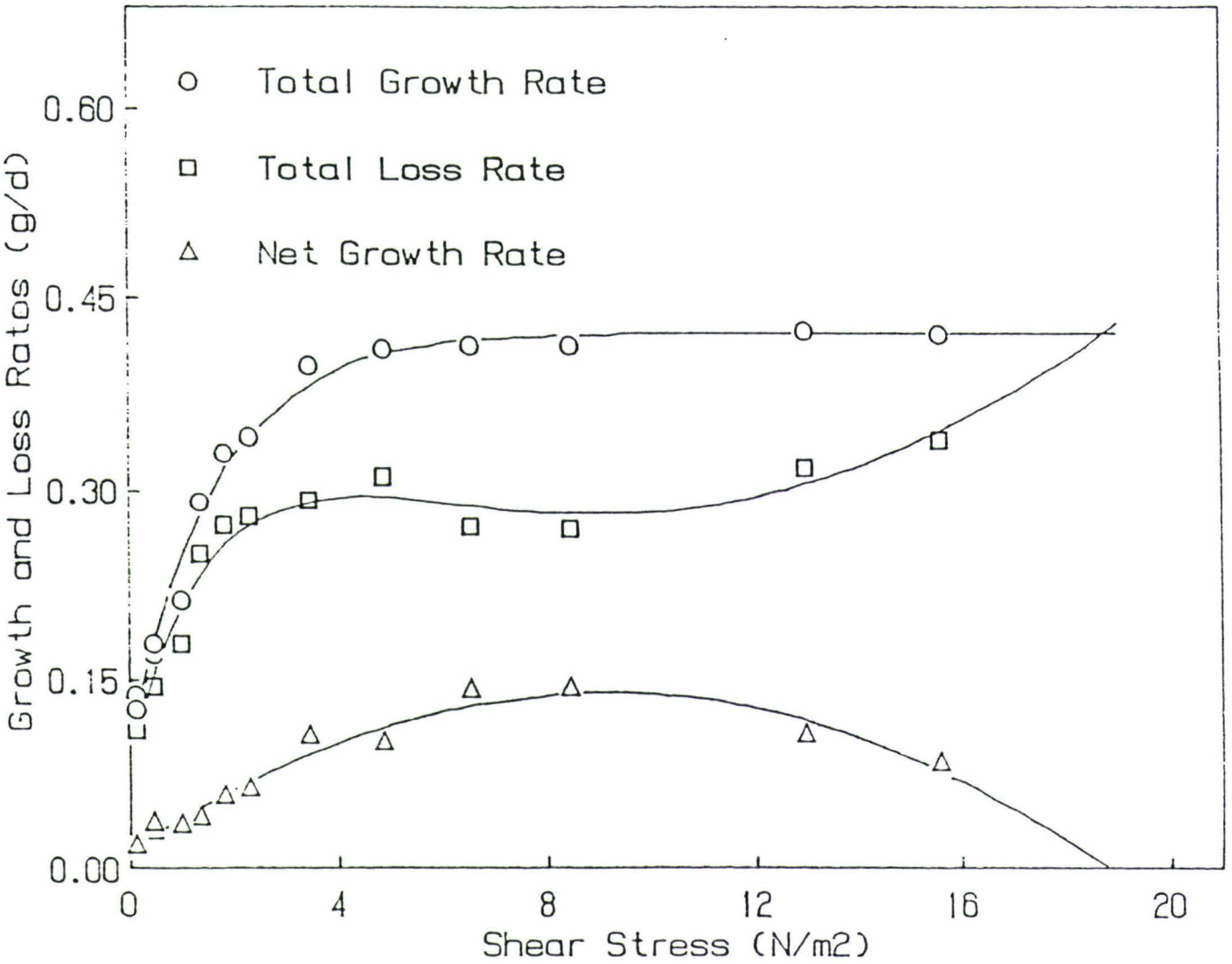

Figure 4.14 Effect of shear stress on biofilm growth and loss rates

contrast, reactor substrate concentration was decreasing at increasing shear stress in this study, suggesting that reactor concentration may not be the factor affecting the shear resistance. Thus, it can be deduced that increasing shear stress is the main cause of increasing the shear resistance. This agrees with Zelver (1979) who also found density, which reflects its strength, increases linearly with increasing shear stress.

The sensitivity of reactor substrate concentration effect on film density was only significant at low concentration levels as observed from the results of Trulear and Characklis (1982). At high substrate concentration levels the density remains approximately constant. Therefore, it may well be the fact that the reactor substrate (phenol) concentration in this study was within this high range such that there is insignificant effect on shear strength. Equally possible is a dual effect, one due to reactor substrate concentration decreasing tending to cause decreasing shear strength while the other due to increasing applied shear stress tending to cause increasing shear resistance; both occurring simultaneously giving rise to either increase or decrease in shear strength depending on the magnitude of each influencing factor.

Beyond a shear stress of 9 N/m^2, the effect of reactor substrate concentration could be neglected since this remains constant after this point for an inlet concentration of 150 mg/l. However, the loss rate begins to increase again. The possible reasons for this are:

1. shear resistance remains constant or decreases after this point, and/or
2. shear stress exceeding the bonding strength (adhesion) between biofilm and reactor surface before loss by detachment at inter-film layer equalizes total growth.

The latter was evident in Figure 4.15 where there are obvious patches of uneven surface detachment resulting in large film thickness variations over the surface. When this occurs, control of biofilm for maintaining a constant film thickness by applying shear stress hydrodynamically becomes impossible which is highly probable for high reactor substrate concentration. Under such condition, zero net growth will only represent constant biomass quantity, and not constant thickness. Only under a condition whereby film to surface adhesion remains greater than the average film to film adhesion until steady-state is reached, will it be possible to truly achieve a constant film thickness, more or less uniform over the surface. Further investigations on a similar system under different conditions by varying the

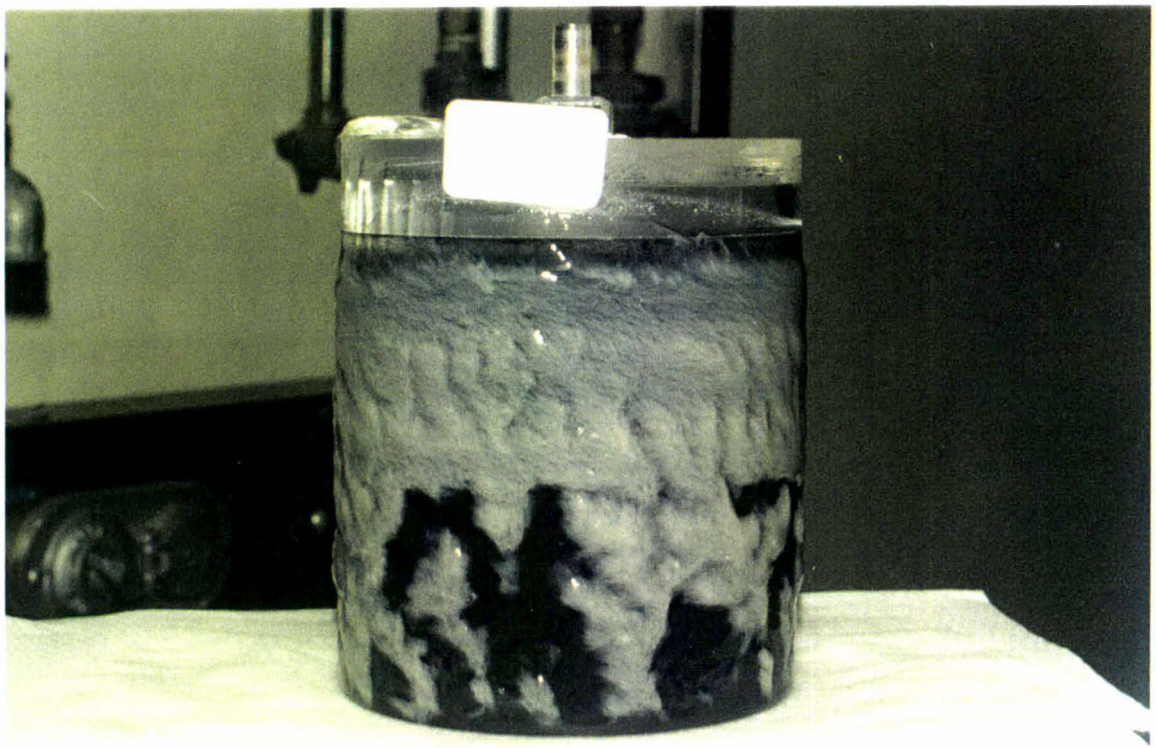

Figure 4.15 Photograph of net biofilm accumulation for 'thick' film (after 4 days of growth, at 350 rpm)

parameters such as feed substrate concentration, HRT or reactor temperature, and a study on the film to surface adhesion providing additional information will be necessary to supplement the present study.

4.4 EFFECT OF SHEAR CONDITIONS DURING GROWTH

The cummulative mass of biofilm loss with time at different rotational speeds is shown in Figure 4.16 which increases to a constant when detachment ceased. The detachment ceased at shorter shearing time for higher rotational speed irrespective of film thickness, viz. 10 to 15 minutes for 100 rpm; 5 to 10 minutes for 125 rpm, 150 rpm and 175 rpm; less than 5 minutes for 200 rpm. This suggested that the loosely packed outer layers of the film with lower resistance to shear loss were quickly removed. At higher speeds (> 175 rpm) larger quantity of mass was observed to have been removed from thick films than the thinner ones. Fragments of biofilm were found particularly at the speed of 200 rpm indicating that detachment has occurred at the support surface to biofilm interface because the inner most region of the thicker films may be starved of substrate, and therefore, have weak adhesion.

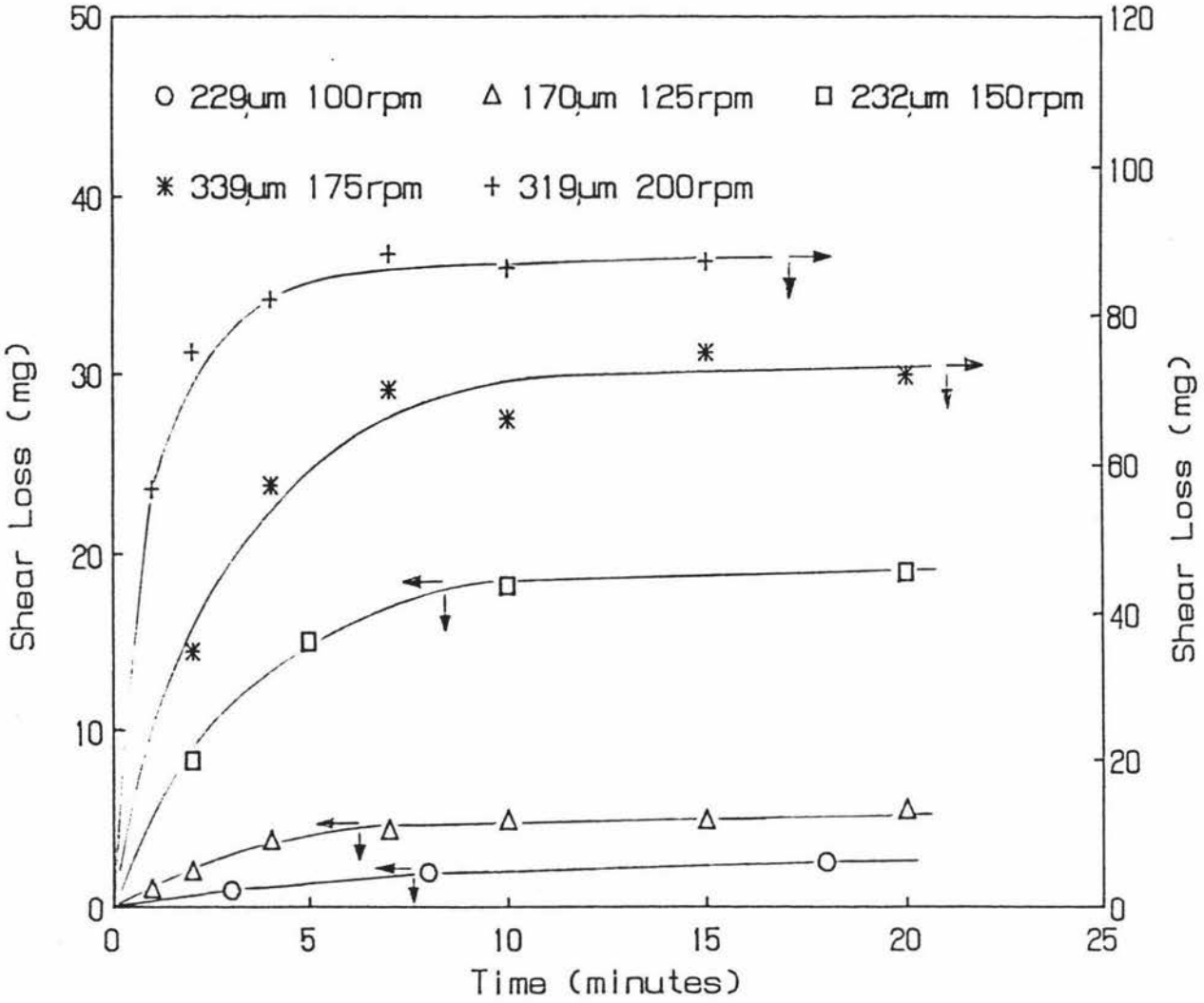

Figure 4.16 Variation in biofilm loss with shearing time for different rotational speeds

The initial loss rate at different rotational speeds varies approximately linearly with biofilm thickness as shown in Figure 4.17. A significant effect of film thickness on initial shear loss rate was observed. Higher loss rate is associated with thicker film for a given constant shear stress. As shear stress variation with changing film thickness at a constant speed is insignificant based on the validity of the single relationship between torque and rotational speed as discussed in section 4.1, it is likely that increasing loss rate with increasing film thickness is not due to shear stress but possibly caused by changes in biofilm structure, particularly at the support-biofilm interface, where lysis of microorganisms due to nutrient or oxygen starvation would occur.

At low shear stress, less than about 2 N/m^2, the initial loss rate per unit thickness follows a linear relationship with shear stress (Figure 4.18). Higher shear stress, above 2 N/m^2 (~ 200 rpm), results in massive biofilm loss for reasons explained earlier especially for film thicker than 0.150 mm which do not warrant further consideration.

Comparison with the loss rate in section 4.3 shows that shear loss rate due to applied shear stress greater than that adapted during biofilm growth are unreasonably high,

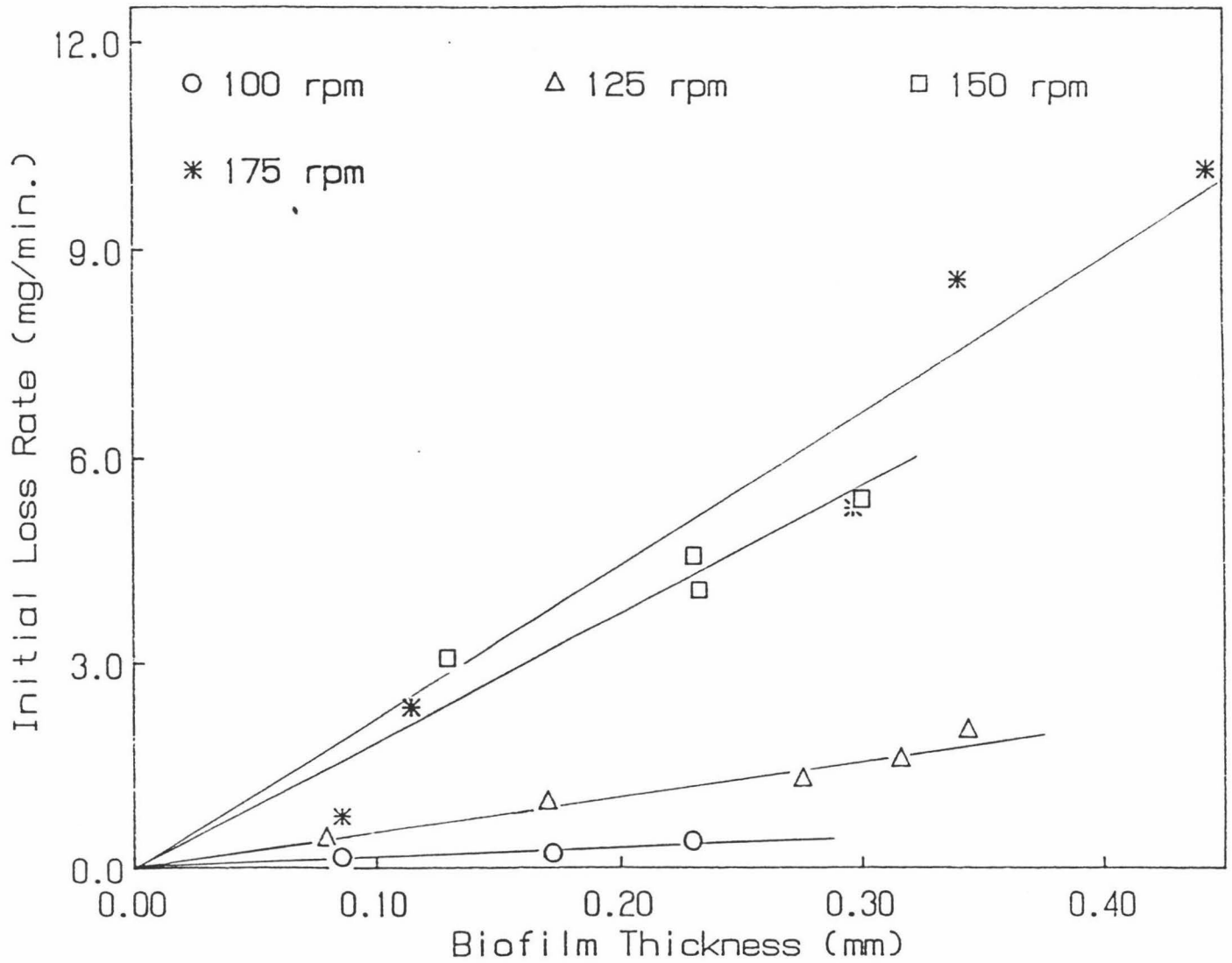

Figure 4.17 Variation in initial loss rate of biofilm with film thickness for different rotational speeds

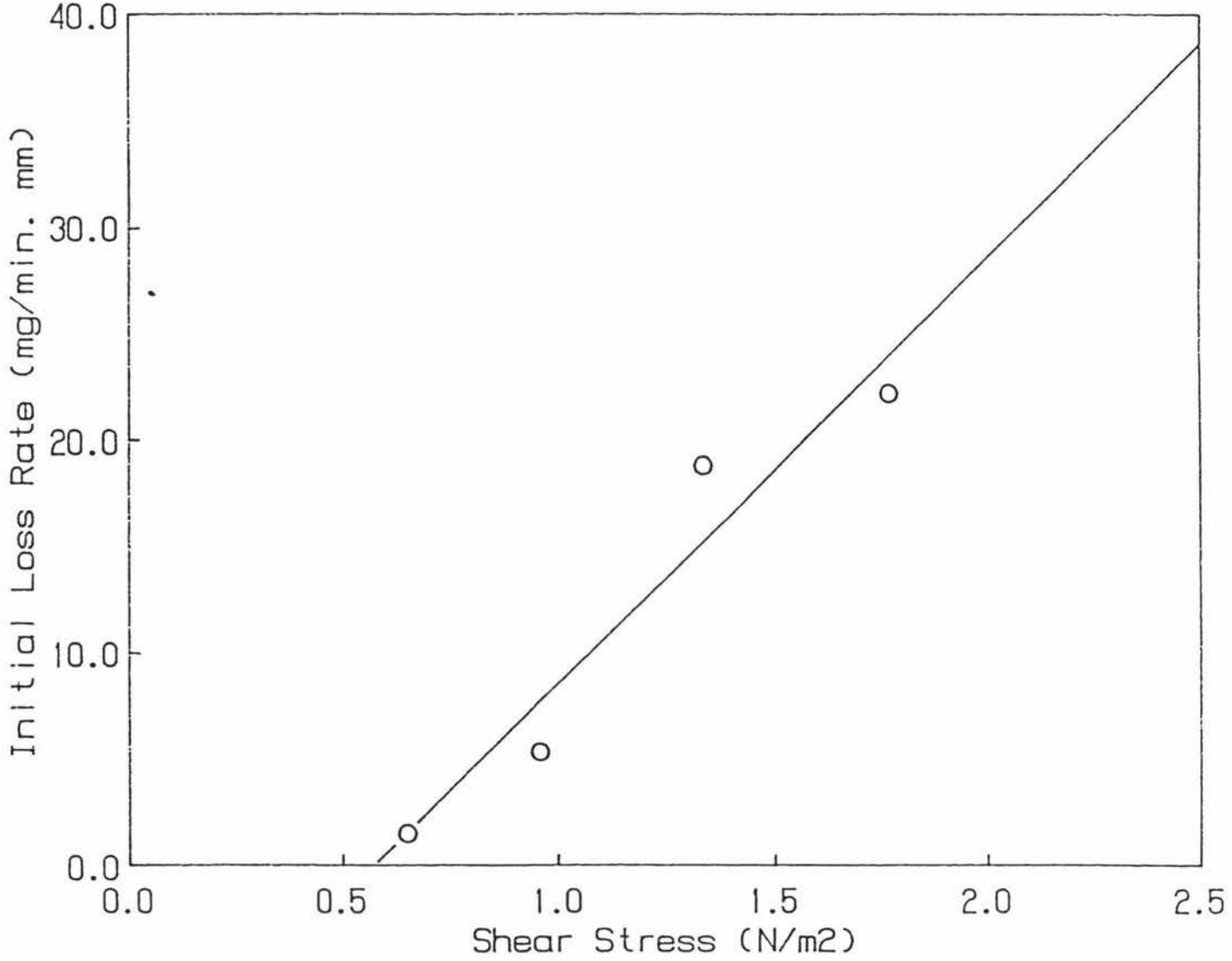

Figure 4.18 Variation in initial loss rate per unit film thickness with shear stress

i.e. higher than the possible total growth rate, suggesting that biofilm shear loss resistance increases with increasing shear stress adapted during growth phase.

CHAPTER 5

CONCLUSIONS

The present work on the aerobic biofilm growth and loss characteristics were studied under a limited operating condition. Further study under a wider range of condition will be necessary for more complete understanding of its processes and behaviour. However, for the system studied the following conclusions are arrived at:

1. There is no significant change in torque with increasing film thickness so that a general quadratic relationship of torque and rotational speed is adopted for all film thicknesses for determining shear stress at the film-liquid interface in the reactor. Consequently, shear stress can be assumed to remain constant for all film thicknesses at a given rotational speed.

2. The substrate consumption or removal is directly proportional to film thickness up to a critical thickness of about 0.050 mm to 0.100 mm only. Beyond this critical thickness, removal becomes independent of film thickness.

3. The steady-state substrate consumption rate increases with increasing shear stress during growth according to an exponential function,

$$S_o - S_e = 0.14 - 0.11e^{-0.61\sigma} \quad g/l$$

so that the maximum substrate removal efficiency is achieved after shear stress of about 3.4 N/m^2.

4. The cummulative attachment of biofilm at a constant rotational speed follows linear relationship with time so that a constant net growth rate can be assumed. The net growth rate varies with shear stress according to a quadratic function as follows:

$$G_n = (14.28 + 27.53\sigma - 1.51\sigma^2) \times 10^{-3} \quad g/d$$

which predicts a zero net growth at shear stress of about 19 N/m^2.

5. The shear loss rate increases with increase in shear stress, but at the same time shear loss resistance of the biofilm also increases with increasing applied shear stress during growth.

6. The liquid phase diffusion resistance appears to reach a minimum at shear stress greater than 3.4 N/m^2 (~250 rpm).

7. Besides shear loss at the exterior layers of the biofilm, shearing may occur at the interface of support surface and biofilm if adhesion at the support surface is weakened due to cell lysis, and under such circumstances, maintenance of constant film thickness by applying shear stress will not be possible.

CHAPTER 6

RECOMMENDATIONS FOR FURTHER STUDY

The results of current research study, because of various constraints, are valid within limited conditions only. More extensive studies of the similar system performed under a wider range of different conditions such as loading rate, HRT and temperature are required to enable the establishment of general relationships between each significant influencing parameter. In addition, the following areas are emphasized:

a) the factors affecting the dry density of biofilm and their significance need to be identified.

b) the strength of adhesion of biofilm on various surface types need to be further studied and comparisons made with the inter-film layer adhesion.

c) a more refined experimental device need to be developed so that the torque and all other parameters can be measured and monitored simultaneously without time lapse to eliminate any possible experimental discrepancies. This includes measurement of biomass concentration of the effluent during the growth phase to enable direct determination of the total biofilm loss rate.

Finally, a general mechanistic model must be developed to explain the experimental observations, which will be useful for predicting the performance of the biofilm system under various operating conditions.

NOMENCLATURE

A	Wetted surface area of inner cylinder, excluding bottom end surface, m^2
G_n	Biofilm Net Growth Rate, g/d
G_t	Biofilm total Growth Rate, g/d
HRT	Hydraulic Retention Time, hr
h	Wetted surface height of inner cylinder, m
Δh	Height of liquid displaced by attached biofilm in the reactor, mm
k	Dimensionless ratio of outer radius of inner cylinder to inner radius of outer cylinder
N	Bioreactor rotational speed, rpm
Q	Volumetric flowrate, in and out of the bioreactor, l/hr
R	Inner radius of the outer cylinder, m
R_c	Steady-state substrate consumption rate, $g/m^3.hr$
R_s	Biofilm shear loss rate, g/d
S	Bioreactor bulk liquid substrate concentration, g/l
S_e	Effluent substrate concentration, g/l
S_o	Feed (or inffluent) substrate concentration, g/l
T	Torque on wetted vertical surface of inner cylinder, (with or without biofilm), Nm (unless otherwise defined)
V	Bioreactor liquid volume, litres (l)
X_c	Cell concentration (dry mass), mg/l
X_p	Phenol concentration, mg/l
Y_{au}	Absorbance reading at 279 nm UV wavelength
Y_{av}	Absorbance reading at 620 nm Visible wavelength

z	Total biofilm thickness, m (unless otherwise defined)
z_a	Active biofilm thickness, m
μ	Bioreactor liquid viscosity, $N.s/m^2$
ω	Angular velocity of inner cylinder, rad/s
σ	Shear stress at wetted vertical surface of inner cylinder (with or without biofilm), N/m^2
θ_c	Mean cell residence time, hr
θ_c^M	Minimum mean cell residence time, hr

REFERENCES

Atkinson, B. and Fowler, H. W. (1974) 'The Significance of Microbial Film in Fermenters' Advances in Biochemical Engineering (Ghose, T.K., Fiechter, A. and Blakebrough, N., eds.), Springer Verlag, Berlin 3., 221-277.

Bajpai, A. C.; Mustoe, L. R. and Walker, D. (1974) 'Engineering Mathematics' John Wiley and Sons, Chichester, 704-715.

Bungay, H. R.; Whalen, W. J. and Sanders, W. M. (1969) 'Microprobe Techniques for Determining Diffusivities and Respiration Rates in Microbial Slime Systems' Biotechnology and Bioengineering, Vol. 11, 765-772.

Castaldi, F. J. and Malina, J. F., Jr. (1982) 'Velocity-dependent Reaction Rates in a Slime Reactor' Journal of Water Pollution Control Federation, Vol. 54, 261-269.

Chang, H. T. and Rittman, B. E. (1987) 'Mathematical Modelling of Biofilm on Activated Carbon' Environmental Science and Technology, Vol. 21, No. 3, 273-279.

Chang, H. T. and Rittman, B. E. (1988) 'Comparative study of Biofilm Shear Loss on Different Adsorptive Media' Journal of Water Pollution Control Federation, Vol. 60, No. 3, 362-368.

Characklis, W. G. (1981) 'Fouling Biofilm Development: A Process Analysis' Biotechnology and Bioengineering, Vol. 23, 1923-1960.

Characklis, W. G.; Trulear, M. G.; Bryers, J. D. and Zelver, N. (1982) 'Dynamics of Biofilm Processes: Methods' Water Research, Vol. 16, 1207-1216.

Chen, Y. S. and Bungay, H. R. (1981) 'Microelectrode Studies of Oxygen Transfer in Trickling Filter Slimes' Biotechnology and Bioengineering, Vol. 23, 781-792.

Cleland, A. C.; Cleland, D. J.; Hearn, C. R.; Mawson, A. J. and Rao, B.S.M. (1989) 'Process Engineering Principles - Laboratory Work' Massey University, Department of Biotechnology, Palmerston North, New Zealand., 3-10.

Cooper, J. R. and Le Fevre, E. J. (1969) 'Thermophysical Properties of Water Substance' Edward Arnold (Pub.) Ltd., London.

Duddridge, J. E.; Kent, C. A. and Law, J. F. (1982) 'Effect of Surface Shear Stress on the Attachment of Pseudomonas Fluorescens to Stainless Steel under Defined Flow Conditions' Biotechnology and Bioengineering, Vol. 24, 153-164.

Eckenfelder, W. W. Jr. (1980) 'Principles of Water Quality Management' CBI Publishing Co., Inc., Massachusetts, Chap. 9.

Fletcher, M. and Floodgate, G. D. (1973) 'An Electron Microscopic Demonstration of an Acidic Polysaccharide involved in the Adhesion of a Marine Bacterium to Solid Surfaces' Journal of General Microbiology, Vol. 74, 325-334.

Fowler, H. W. (1986) 'The Evaluation of the Forces involved in Cell/Surface Attachment' in Process Engineering Aspects of Immobilized Cell Systems (Webb, C.; Black, G.M. and Atkinson, B., eds.), The Institution of Chemical Engineers, Rugby, England, 253-263.

Greenfield, P. F. (1987) 'Fundamentals of Biological Wastewater Treatment' in Wastewater Treatment Principles and Practices (Rao, B.S.M., eds.), Vol. 2, Department of Biotechnology, Massey University, Palmerston North, New Zealand, Chap. 3.

Hoehn, R. C. and Ray, A. D. (1973) 'Effect of Thickness on Bacterial Film' Journal of Water Pollution Control Federation, Vol. 45, 2302-2320.

Holman, J. P. (1978) 'Experimental Methods for Engineers' 3rd Edn., McGraw-Hill, New York.

Huang, J. C.; Chang, S. Y.; Liu, Y. C. and Jiang, Z. (1985) 'Biofilm Growths with Sucrose as Substrate' Journal of Environmental Engineering, Vol. 111, No. 3, 353-363.

Huskins, D. J. (1982) 'Quality Measuring Instruments in On-Line Process Analysis' Ellis Horwood Ltd., Chichester, England, 138-139.

Jenkins, D. (1963) 'Sewage treatment' Biochemistry of Industrial Micro-organisms (Rainbow, C. and Rose, A.H., eds.), Academic Press, Chap. 15, 508-536.

Kornegay, B. H. and Andrews, J. F. (1968) 'Kinetics of Fixed-Film Biological Reactors' Journal of Water Pollution Control Federation, Vol. 40, 460-468.

LaMotta, E. J. (1976 (a)) 'External Mass Transfer in a Biological Film Reactor' Biotechnology and Bioengineering, Vol. 18, 1359-1370.

LaMotta, E. J. (1976 (b)) 'Internal Diffusion and Reaction in Biological Films' Environmental Science and Technology, Vol. 10, No. 8, 765-769.

Marshall, K. C. (1976) 'Interfaces in Microbial Ecology' Harvard University Press, Cambridge, Massachusetts.

Marshall, K. C. (1980) 'Bacterial Adhesion in Natural Environments' in Microbial Adhesion to Surfaces (Berkeley, R.C.W.; Lunch, J.M.; Melling, J.; Rutter, P.R. and Vincent, B., eds.), Ellis Horwood Ltd., Chichester, England, Chap. 9, 187-196.

Matson, J. V. and Characklis, W. G. (1976) 'Diffusion into Microbial Aggregates' Water Research, Vol. 10, 877-885.

McCormack, P. D. and Crane, L. (1973) 'Physical Fluid Dynamics' Academic Press, London, 164-167.

Merrington, A. C. (1949) 'Viscometry' Edward Arnold and Co., London, Chap. 3.

Metcalf and Eddy, Inc. (1979) 'Wastewater Engineering: Treatment/Disposal/Reuse' 2nd Edn., McGraw-Hill Book Co. New York.

Rao, B. S. M. (1985) 'Biofilm Characteristics and Their Role in a Fluidized-Bed Bioreactor' Ph.D. Thesis, University of Queensland, Australia.

Rao, B. S. M. (1987) 'Principles of Attached Growth Wastewater Treatment Processes' in Wastewater Treatment Principles and Practice (Rao, B.S.M., ed.), Department of Biotechnology, Massey University, Palmerston North, New Zealand.

Rittman, B. E. and McCarty, P. L. (1980) 'Model of steady - State-Biofilm Kinetics' Biotechnology and Bioengineering, Vol. 22, 2343-2357.

Round, G. F. and Garg, V. K. (1986) 'Application of Fluid Dynamics' Edward Arnold, London, 133-134.

Sanders, W. M. (1966) 'Oxygen Utilization by Slime Organisms in Continuous Culture' International Journal of Air and Water Pollution, Vol. 10, 253-276.

Shieh, W. K.; Sutton, P. M. and Kos, P. (1981) 'Predicting Reactor Biomass Concentration in a Fluidized Bed System' Journal of water Pollution Control Federation, Vol. 53, 1574-1584.

Tadros, T. F. (1980) 'Particle-Surface Adhesion' in Microbial Adhesion to Surfaces (Berkeley, R.C.W.; Lunch, J.M.; Melling, J.; Rutter, P.R. and Vincent, B., eds.), Ellis Horwood Ltd., Chichester, England, Chap. 5, 93-116.

Tomlinson, T. G. and Snaddon, D. H. M. (1966) 'Biological Oxidation of Sewage by Films of Micro-organisms' International Journal of Air and Water Pollution, Vol. 10, 865-881.

Trulear, M. G. and Characklis, W. G. (1982) 'Dynamics of Biofilm Processes' Journal of Water Pollution Control Federation, Vol. 54, No. 9, 1288-1301.

Walshaw, A. C. and Jobson, D. A. (1972) 'Mechanics of Fluids' 2nd Edn., Longman Group Ltd., London, 172-173.

Whalen, W. J.; Bungay, H. R. and Sanders, W. M. (1969) 'Microelectrode Determination of Oxygen Profiles in Microbial Slime systems' Environmental Science and Technology, Vol. 3, 1297-1298.

Zelver, N. (1979) 'Biofilm Development and Associated Energy Losses in Water Conduits' M.S. Thesis, Rice University, Houston, Texas.

APPENDIX 1

THEORY OF TORQUE AND SHEAR STRESS IN A CONCENTRIC CYLINDRICAL REACTOR SYSTEM

1. Shear Stress Distribution in the Liquid Layer Between the Vertical Surfaces of the Concentric Cylinders with Inner Cylinder Rotating only.

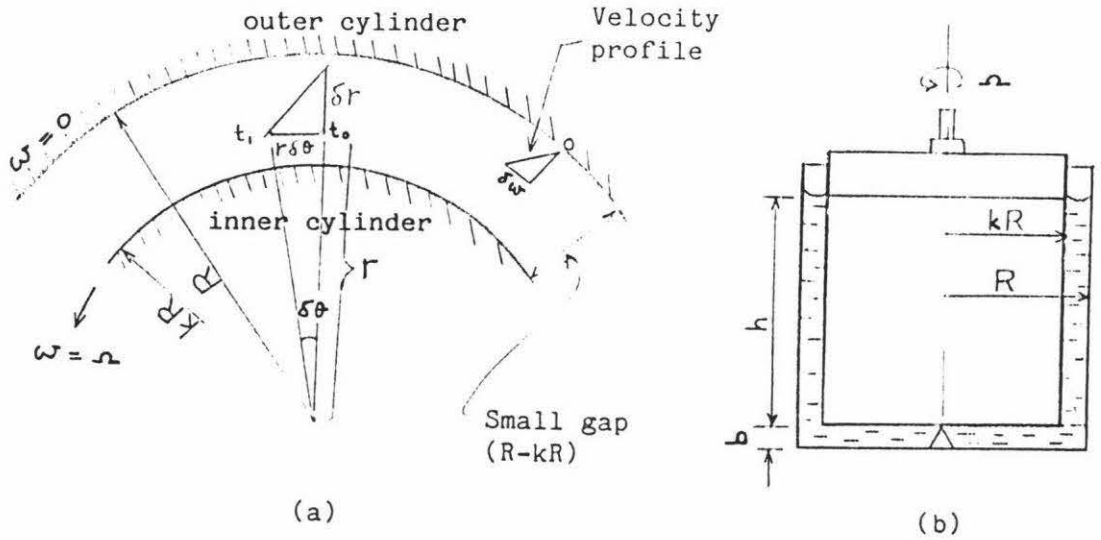

Figure A1.1 Diagram of concentric cylindrical reactor with inner cylinder rotating.

The following assumptions are made in deriving the shear stress distribution in the annular gap in the radial direction:

i. the boundary surface is smooth.

ii. the gap between the two concentric cylinders is small compared to the radius kR, where k<1.

iii. the flow is laminar and entirely tangential (i.e. no

axial and radial flows) and the liquid rotates in layers concentric with the cylinders.

iv. no slip at the boundaries so that the liquid in contact with the rotating cylinder has the same velocity as the periphery of the cylinder, and the liquid in contact with the stationary cylinder is at rest.

v. liquid is incompressible and of constant viscosity.

Consider Figure A1.1,

The inner cylinder rotates at a constant angular velocity, Ω radian/sec. The liquid immediately at the surface of the inner cylinder will also be rotating at Ω rad./s., whilst the surface of the outer cylinder will be 0.0 rad./s. At radius r, the distance travelled from time, t to t will be ~ $r\,\delta\Theta$. If the liquid layer travels at dw rad./s., then

$$r\,\delta\Theta = r\,\delta w\,dt$$

Now, shear strain, $\delta\gamma = r\,\delta\Theta / \delta r$

$$= r\,\delta w\,\delta t / \delta r$$

Therefore, $\delta\gamma/\delta t = r\,\delta w / \delta r$ = rate of shearing

As $\delta r \to 0$, $d\gamma/dt = r\,dw/dr$

But Shear Stress, $\sigma_{r\theta}$ = μ x rate of shearing (Walshaw and Jobson, 1972)

$$= \mu\,d\gamma / dt$$

$$= \mu\,r\,dw / dr \qquad .. \quad .. \quad (1)$$

where μ is the dynamic viscosity.

Now, the viscous force exerted on the liquid at radius, r will be

$$\sigma_{r\theta} \times \text{area}$$

$$= \mu\, r \frac{dw}{dr} 2\pi r h$$

$$= 2\pi r^2 \mu h \frac{dw}{dr}$$

This force will result in a couple or torque tending to retard the motion. The resisting torque will be

$$- 2\pi r^2 \mu \frac{dw}{dr} r$$

$$= - 2\pi r^3 \mu \frac{dw}{dr}$$

At constant speed, acceleration = 0

Therefore, the externally applied torque, T to maintain rotation must equal that due to viscous resistance.

Therefore, $$T = - 2\pi r^3 \mu h \frac{dw}{dr}$$

$$T \frac{dr}{r^3} = - 2\pi \mu h\, dw \qquad \ldots\ldots (2)$$

Integrating equation (2), for limits, r = kR to R
and w = Ω to 0,

gives $$\left[\frac{-T}{2r^2}\right]_{kR}^{R} = - 2\pi \mu h \left[w\right]_{\Omega}^{0}$$

$$T = 4\pi h \mu \Omega R^2 [k^2/(1 - k^2)] \qquad .. \quad (3)$$

(Round and Garg, 1986).

Shear Stress Distribution, $\sigma_{r\theta}$

$$\sigma_{r\theta} = \frac{\text{Torque, } T}{2\pi h r^2} \qquad .. \quad .. \quad (4)$$

Substituting for Torque,

$$\sigma_{r\theta} = \frac{4\pi h \mu \Omega R^2 k^2}{2\pi h r^2 (1 - k^2)}$$

$$= \frac{2 \mu \Omega R^2 k^2}{r^2 (1 - k^2)} \quad .. \quad .. \quad (5)$$

The point of interest in the study is the shear stress at the interface of inner cylinder surface and the liquid, $r = kR$.

Therefore at $r = kR$,

$$\sigma_{r\theta} = \frac{2 \mu \Omega}{(1 - k^2)} \quad .. \quad .. \quad (6)$$

If the apparatus is constructed with sufficient accuracy, the critical speed, below which the linear relationship between torque and angular velocity in equation (3) can be maintained, is expressed as follows:

$$\frac{\Omega_c^2 (kR)^2 d^3}{0.5 (kR + R) \nu} = \frac{\pi^4 f}{0.0571 f^2 + 0.00056} \quad .. \quad .. \quad (7)$$

(Merrington, 1949)

where $d = (R - kR)$ cm.

$f = 1 - 0.652\ d / (kR)$

ν = kinematic viscosity (centistokes, cs)

and $d/(kR)$ is assumed to be small

2. Torque on Bottom of Inner Cylinder

If gap 'b' is much smaller than the radius, kR and there is no radial and axial flow so that v_r and v_z equal zero,

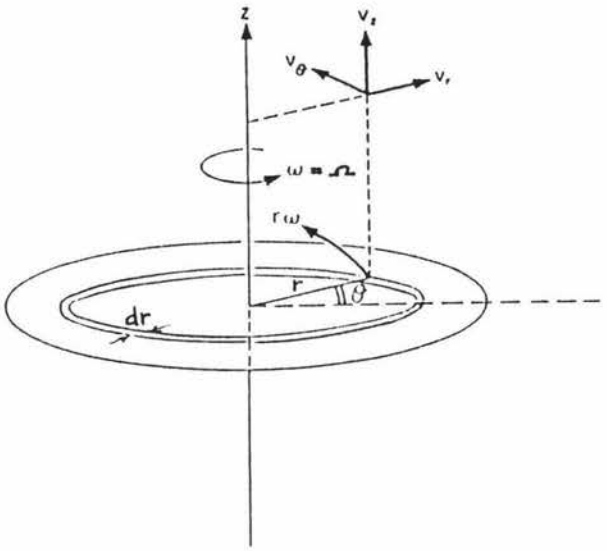

Figure A1.2 Coordinate system for bottom surface of inner cylinder of a bioreactor in rotation.

the torque on the bottom of the inner cylinder can be derived as follows:

The incremental turning moment or Torque of the bottom end element of width, dr, at radius, r is

$$dM = (2\pi r\, dr)\tau_{z\theta}|_{z=0} . r ,$$

[McCormack and Crane, 1973]

Integrating gives,

$$\text{Total Moment or Torque, } M = 2\pi \int_0^{kR} r^2 \tau_{z\theta}|_{z=0} . dr$$

Now,

The circumferential component of shear stress, $\tau_{z\theta}|_{z=0} = \frac{\mu \Omega r}{b}$, at $z = 0$

$$\therefore \quad M = 2\pi \int_0^{kR} r^2 \frac{\mu \Omega r}{b}\, dr$$

or $$\text{Torque, } T = \frac{\pi \mu \Omega R^4 k^4}{2b} \quad .. \quad .. \quad (8)$$

[Huskins, 1982; Round and Garg, 1986]

3. To Determine the Critical speed,

$kR = 5.003$ cm; $d = 0.531$ cm; $R = 5.534$ cm

$\therefore$ $f = 0.9308$

$\nu = 0.8042$ cs. for water at $30^{o}C$ (Merrington, 1949)

Substituting in equation (7),

gives $\Omega_c = 45.25$ rad/s

$= 432$ rpm

Therefore, theoretically, turbulence sets in when the speed exceeds 432 rpm for smooth surface reactor.

4. To Determine the Significance of Torque on the Bottom of Inner Cylinder.

For gap 'b' ~ 5 mm.

Using equation (8),

at $\Omega = 100$ rpm, Torque = 0.000016 Nm

at $\Omega = 500$ rpm, Torque = 0.000082 Nm

Therefore within the operating range, Torque is less than 0.0001 Nm. Thus, the Torque due to the bottom end of the inner cylinder is insignificant and can be neglected.

APPENDIX 2

SIZING OF SHAFT DIAMETER FOR TORQUE MEASURING DEVICE

From equation (3) in Appendix 1,

$$T = 4\pi h \mu \Omega R^2 \frac{k^2}{(1-k2)}$$

at 30 ^{o}C, $\mu = 797 \times 10^{-6}$ Ns/m^2 (Cooper & Le Fevre, 1969)

Minimum operating speed for shear test = 100 rpm

$\therefore$ $\Omega = 10.47$ rad/s

For clean surface, k = 0.904

Therefore Torque, T = 0.0001436 Nm (or 14.64 g.mm)

also Torque = F x r .. .. .. (i)

where F is the tension in the cord around the shaft of radius, r.

Now, tension in the cord is displayed in unit, g. So, to give a reasonably large reading, say > 1 g., the radius, r should be < 14.64 mm.

Therefore, choosing radius of 10 mm will theoretically give a reading of 1.46 g on smooth surface reactor; and for surface coated with activated carbon powder (rough) the reading may be much higher.

APPENDIX 3

BIOREACTOR DIMENSIONS

Table A3 Details of bioreactor dimensions

Bioreactor Nos.	Internal Diameter of Outer Cylinder D (mm)	Outer Diameter of Inner Cylinder (mm)	
		w.o. coating d_i	w. coating d_o
R1	110.73	99.78	100.099
R2	110.63	99.86	100.178
R3	110.69	99.81	99.937
R4	110.67	99.79	100.108
R5	110.59	99.69	99.945
R6	110.79	99.77	100.089
Average	110.68	99.78	100.059

N.B.: h for height of activated carbon coated surface (site for biofilm attachment and growth), 100 mm.

H, overall height of outer cylinder, ~ 120 mm.

a, the gap between the vertical sides of inner and outer cylinders, 5.31 mm.

b, the gap between the lower ends of inner and outer cylinders, ~ 5 mm.

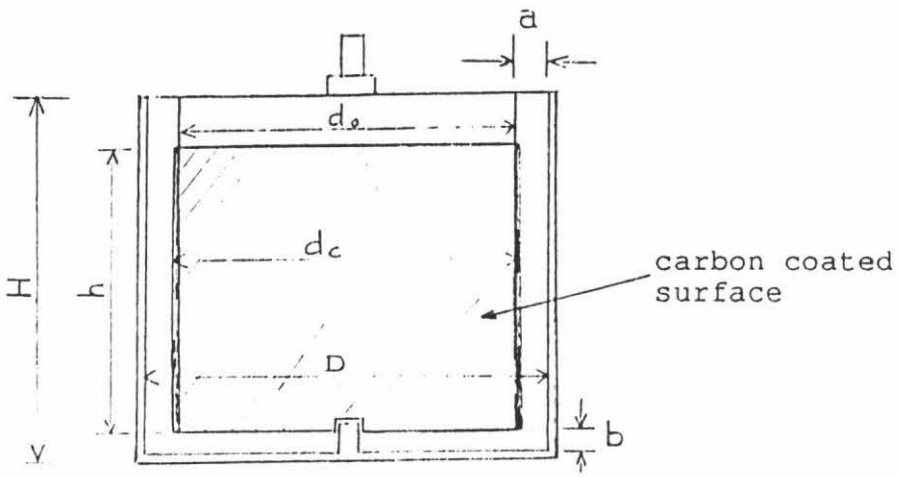

Fig.A3 Diagram of bioreactor dimensions without biofilm.

APPENDIX 4

DERIVATION OF FUNCTIONS FOR COMPUTATION OF VOLUME AND THICKNESS OF BIOFILM

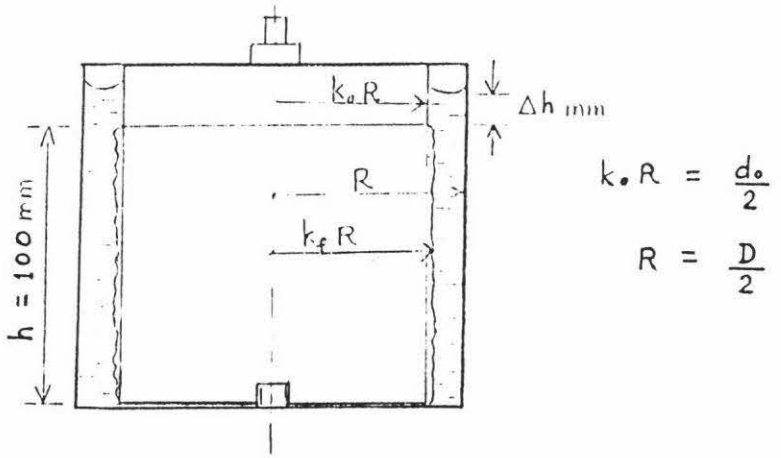

Fig. A4 Diagram of bioreactor dimensions with biofilm.

A4.1 VOLUME OF ATTACHED BIOFILM

The volume of liquid displaced, V_{df} = Volume of biofilm attached

$$= \pi(R^2 - k_o^2 R^2)\,\Delta h$$

Substituting appropriate values for R and $k_o R$ based on the dimensions in Appendix 3, the following relationships between volume, V_{df}, of biofilm growth and rise in liquid height, Δh (mm), are obtained for the respective reactors:

R1	$V_{df} = 1810.409\,\Delta h$ mm3
R2	$V_{df} = 1780.480\,\Delta h$ mm3
R3	$V_{df} = 1798.750\,\Delta h$ mm3
R4	$V_{df} = 1798.408\,\Delta h$ mm3
R5	$V_{df} = 1800.173\,\Delta h$ mm3
R6	$V_{df} = 1822.415\,\Delta h$ mm3

A4.2 THICKNESS OF ATTACHED BIOFILM

Equating the above volume (as function of Δh) to $\pi(k_f^2R^2 - (d_c/2)^2)100$ for the respective reactors, and substituting k_fR with $(z + d_c/2)$, the following relationships between film thickness, z (mm) and rise in liquid height, Δh (mm) are obtained:

R1 $\quad z(z + 100.099) = 5.763\,\Delta h$

R2 $\quad z(z + 100.178) = 5.667\,\Delta h$

R3 $\quad z(z + 99.937) = 5.726\,\Delta h$

R4 $\quad z(z + 100.108) = 5.725\,\Delta h$

R5 $\quad z(z + 99.945) = 5.730\,\Delta h$

R6 $\quad z(z + 100.089) = 5.801\,\Delta h$

when z is small, i.e. $z < 1$ mm, say,

R1 $\quad z \sim 0.0575\,\Delta h$

R2 $\quad z \sim 0.0565\,\Delta h$

R3 $\quad z \sim 0.0573\,\Delta h$

R4 $\quad z \sim 0.0572\,\Delta h$

R5 $\quad z \sim 0.0573\,\Delta h$

R6 $\quad z \sim 0.0580\,\Delta h$

Substituting for Δh (from section A4.1, Δh can be expressed as function of volume, V_{df}) in the above equations,

gives R1 $\quad z \sim (0.0575/1810.409)V_{df}$

R2 $\quad z \sim (0.0565/1780.480)V_{df}$

R3 $\quad z \sim (0.0573/1798.750)V_{df}$

R4 $\quad z \sim (0.0572/1798.408)V_{df}$

R5 $\quad z \sim (0.0573/1800.173)V_{df}$

R6 $\quad z \sim (0.0580/1822.415)V_{df}$

APPENDIX 5

DATA FOR ESTABLISHING STANDARD CURVES TO DETERMINE THE BIOREACTOR CELL MASS AND PHENOL CONCENTRATIONS

A5.1 CELL MASS CONCENTRATION AND ABSORBANCE RELATIONSHIP

Table A5.1.1 RAW DATA: Absorbance at 620 nm wavelength for various dry cell mass concentrations

Sample Dilution	Absorbance @ 620 nm	Dry filter mass, g	Dry cell & filter, g	Net cell mass, g
Data Set No. 1				
25% c.s. 75% d.w.	0.100	0.0855	1) 0.0880 2) 0.0880	0.0025
50% c.s. 50% d.w.	0.210	0.0852	1) 0.0914 2) 0.0913	0.0061
75% c.s. 25% d.w.	0.315	0.0858	1) 0.0946 2) 0.0945	0.0087
100% c.s.	0.390	0.0854	1) 0.0971 2) 0.0971	0.0117
Data Set No.2				
25% c.s 75% d.w.	0.090	0.0854	1) 0.0876	0.0022
50% c.s. 50% d.w.	0.170	0.0854	1) 0.0898	0.0044
75% c.s. 25% d.w.	0.245	0.0858	1) 0.0932 2) 0.0932	0.0074
100% c.s.	0.315	0.0853	1) 0.0949 2) 0.0945 3) 0.0942	0.0092

N.B.: Sample size, 50 ml per sample.
c.s. for liquid containing cells in suspension.
d.w. for distilled water only.
1), 2) and 3) for after 1, 2 and 3 day(s) resp'ly.

Table A5.1.2 Calculated dry cell mass for various absorbance at 620 nm wavelength (Visible)

Sample Dilution	Absorbance @ 620 nm	Dry Cellmass, mg/l
Data Set No. 1		
25% c.s. 75% d.w.	0.100	50
50% c.s 50% d.w.	0.210	122
75% c.s. 25% d.w.	0.315	174
100% c.s.	0.390	234
Data Set No. 2		
25% c.s. 75% d.w.	0.090	44
50% c.s. 50% d.w.	0.170	88
75% c.s. 25% d.w.	0.245	148
100% c.s.	0.315	184

Curve fit equation: $Y_{av} = 0.001727\ X_c \pm 0.0266$

at 95% confidence level.

Filename: see m*x

Curve fit for Absorbance Vs. cell mass

*** Stopping after 3 iterations

Coefficents after last iteration :

Chi Square	M
1.546935320E-04	0.001727
E format	1.72665856E-03

Std devs	0.0000303576
%	1.7582
Dependencies	0.0000

Correlation Coefficients
1.00000

Degrees of Freedom : 8
Finial Lamda : 0.00000100

Data and fitted values

i	x(i)	y(i)	Pred Y	Residual	Z Resid
1	0.00000000	0.00000000	0.00000000	0.00000000	0.00000
2	50.00000000	0.10000000	0.08633293	0.01366707	1.09885
3	44.00000000	0.09000000	0.07597298	0.01402702	1.12779
4	88.00000000	0.17000000	0.15194595	0.01805405	1.45157
5	122.00000000	0.21000000	0.21065234	-0.00065234	-0.05244
6	148.00000000	0.24500000	0.25554547	-0.01054547	-0.84787
7	174.00000000	0.31500000	0.30043859	0.01456141	1.17075
8	184.00000000	0.31500000	0.31770518	-0.00270518	-0.21750
9	234.00000000	0.39000000	0.40403810	-0.01403810	-1.12868

ANOVA

Source of variation	df.	SS	MS	F
Model	1	0.12630134	0.12630134	816.46167774
Residual	8	0.00123755	0.00015469	
Total	8	0.12753889		

R-sq. 99.03%
adjusted for df. 99.03%

A5.2 PHENOL CONCENTRATION AND ABSORBANCE RELATIONSHIP

Table A5.2 Absorbance at 279 nm wavelength (UV) for various phenol concentrations

Sample	Known Phenol Conc., g/l	Absorbance @ 279 nm
1	0.035	0.31
2	0.050	0.48
3	0.070	0.59
4	0.100	0.80
5	0.100	0.75
6	0.100	0.85
7	0.150	1.20
8	0.150	1.25
9	0.150	1.10

Curve fit equation: $Y_{au} = 7.9967\ X_p \pm 0.1134$

at 95% confidence level.

Curve fit for Absorbance Vs. phenol concentration

Filename: phenseer m*s

*** Stopping after 3 iterations

Coefficients after last iteration :

Chi Square	M
2.855427300E-03	7.99e702
E format	7.99670200E+00
std devs	0.164031291
%	2.051%
Dependencies	0.0000

Correlation Coefficients
1.00000

Degrees of Freedom : 9
Final Lamda : 0.000001000

Data and fitted values

i	x(i)	y(i)	Pred Y	Residual	Z Resi
1	0.000000000	0.000000000	0.000000000	0.000000000	0.0000
2	0.035000000	0.310000000	0.279988457	0.030011543	0.5635
3	0.050000000	0.480000000	0.399833510	0.080166490	1.5001
4	0.070000000	0.590000000	0.559776914	0.030223086	0.5657
5	0.100000000	0.800000000	0.799670200	0.000329800	0.0061
6	0.100000000	0.750000000	0.799670200	-0.049670200	-0.9295
7	0.100000000	0.850000000	0.799670200	0.050329800	0.9418
8	0.150000000	1.200000000	1.199505300	0.000494700	0.0092
9	0.150000000	1.250000000	1.199505300	0.050494700	0.9449
10	0.150000000	1.100000000	1.199505300	-0.099505300	-1.8621

ANOVA

Source of variation	df.	SS	MS	F
Model	0	1.413511115	1.413511115	495.026139960
Residual	9	0.025690885	0.002854543	
Total	9	1.439210000		

R-sq.	98.21%
adjusted for df.	98.21%

APPENDIX 6

TORQUE AND ROTATIONAL SPEED (RPM) RELATIONSHIP DATA

A6.1 CARBON COATED SURFACE BIOREACTOR WITH NO BIOFILM ATTACHMENT AND GROWTH

Table A6.1(a) Measured torque at various rotational speeds (rpm) with no biofilm on carbon coated surface bioreactor

Reactor	Torque in Nmm (or x 1/1000 Nm)					
	44rpm	100rpm	125rpm	150rpm	175rpm	200rpm
R1	0.515	0.760	1.177	1.521	1.962	2.453
R4	0.059	0.500	1.099	1.285	1.687	2.178
R5	0.233	0.749	1.171	1.386	1.962	2.330
R6	0.278	0.589	1.006	1.643	-	-

Curve fit equation: $T = (0.0032283N + 0.000042308N^2)$

$\pm$ 0.274 Nmm

at 95% confidence level

where N is the speed in rpm.

Table A6.1(b) Calculated 95% confidence interval of the mean of torque values in table A6.1(a)

Parameters	44rpm	100rpm	125rpm	150rpm	175rpm	200rpm
Mean $\bar{T}$	0.271	0.650	1.113	1.459	1.870	2.320
n	4	4	4	4	3	3
S_{n-1}	0.188	0.127	0.080	0.156	0.159	0.138
B	0.598	0.404	0.254	0.496	0.684	0.593
B_{mean}	0.299	0.202	0.127	0.248	0.395	0.343
$\bar{T} + B_{mean}$	0.570	0.852	1.240	1.707	2.265	2.663
$\bar{T} - B_{mean}$	-	0.448	0.986	1.211	1.475	1.977

N.B.: Mean Torque, $\bar{T}$ in Nmm (or x 1/1000 Nm)

A6.2 CARBON COATED SURFACE BIOREACTOR WITH BIOFILM ATTACHMENT AND GROWTH

Table A6.2(a) Measured Torque at various rotational speeds (rpm) with biofilm on carbon coated surface bioreactor

Reactor	Film Thn. (μm)		Torque in Nmm (or x 1/1000 Nm)				
	In.	Fin.	100rpm	125rpm	150rpm	175rpm	200rpm
R2	79	~79	1.251	1.619	2.291	2.757	3.409
R4	114	72	1.030	1.472	1.889	2.674	-
R5	126	72	-	1.079	1.717	2.710	3.434
R1	273	178	1.242	1.668	2.158	2.698	3.492
R1	129	115	-	1.511	2.086	2.868	3.712
R4	292	172	1.095	1.455	2.420	3.368	4.298
R5	172	149	0.769	1.046	1.668	2.149	3.139
R5	226	180	1.079	1.497	1.938	2.527	-
R5	272	200	1.742	2.232	2.625	3.017	3.620
R2	297	240	-	1.390	2.250	3.303	4.258
R2	282	~282	1.128	1.521	1.962	2.305	2.747
R4	343	~343	1.334	2.031	2.453	2.963	3.561
R6	305	261	0.942	1.246	1.854	2.766	3.806

N.B.: Thn. for thickness; In for initial; Fin. for final.

Curve fit equation: $T = 0.002514516N + 0.00007714N2$

$\pm$ 0.669 Nmm

at 95% confidence level.

Table A6.2(b) Calculated 95% confidence interval of the mean Torque values in table A6.2(a)

Parameters	100 rpm	125 rpm	150 rpm	175 rpm	200 rpm
Mean $\bar{T}$	1.161	1.521	2.101	2.777	3.588
n	10	13	13	13	11
S_{n-1}	0.261	0.331	0.296	0.345	0.445
B	0.590	0.726	0.649	0.757	0.996
B_{mean}	0.187	0.201	0.180	0.210	0.300
$\bar{T} + B_{mean}$	1.348	1.722	2.281	2.987	3.888
$\bar{T} - B_{mean}$	0.974	1.320	1.921	2.567	3.288

N.B.: Torque in Nmm were calculated as T = (measured values in g x 1/1000) kg x shaft radius (10 mm) x 9.81 m/s^2.

S_{n-1} = sample standard deviation

$$= \sqrt{\frac{(T - \bar{T})^2}{n-1}}$$

n = number of sample

$B = t.S_{n-1}$

$B_{mean} = \pm B/\sqrt{n}$ (i.e. 95% confidence interval of a sample mean)

(Cleland *et al*, 1989)

Standard error of curve fit $= \sqrt{\frac{\Sigma(T_o - T_c)^2}{n-1}}$

(Holman, 1978)

where T_o is the observed torque, and
T_c is the computed torque.

A6.3 TORQUE ON SMOOTH SURFACE OF BIOREACTOR

Theoretical formula, $T = 4\pi\mu\, h\Omega R^2 \frac{k^2}{(1 - k^2)}$ (Appendix 1)

Average R for Bioreactor = 55.3 mm

Average kR for bioreactor ~ 50 mm

h, height ofwetted surface = 100 mm

$\therefore$ k = 0.904

$\therefore$ Torque = 0.000013694 Ω Nm

at Ω = 200 rpm (20.944 rad/s),

Torque = 0.000013694 x 20.944

= 0.0002868 Nm (or ~ 0.29 Nmm)

N.B. μ at 30 ^{o}C = 797 μ Pa.s (or 797 x 10^{-6} Ns/m^2)

(Cooper and Le Fevre, 1969)

APPENDIX 7

DATA OF NET BIOFILM ACCUMULATION ON BIOREACTOR SURFACE

Table A7.1 RAW DATA : Rise in liquid height, Δh mm, representing cummulative increase in cell quantity (volume) attached on bioreactor surface at different days of growth

Data Set No. 1

Time (day)	R6 @ 30 rpm	R1 @ 35 rpm	R5 @ 125 rpm
4	2.0	2.25	3.50
6	3.10	3.0	5.0
8	3.75	3.25	6.75
10	4.75	4.50	9.0
12	5.0	5.50	-
14	6.0	6.25	-
16	7.0	6.75	-
18	7.25	7.50	-
20	8.0	8.50	-

Data Set No. 2

Time (day)	R1 @ 80 rpm (a)	R6 @ 150 rpm	R5 @ 175 rpm
3	1.50	3.0	3.5
5	3.50	4.50	7.50
7	6.75	7.25	10.25
9	8.50	9.0	-
11	9.75	-	-

cont...

Data Set No. 3

Time (day)	R1 @ 80 rpm (b)	R5 @ 200 rpm
2	1.50	2.25
4	3.0	5.50
6	5.25	10.0
8	6.0	12.50
10	6.75	-

Data Set No. 4

Time (day)	R5 @ 250 rpm	R1 @ 300 rpm
2	3.25	3.25
4	10.75	9.75
6	15.25	14.0
7	19.50	18.75

Data Set No. 5

Time (day)	R5 @ 350 rpm	R1 @ 400 rpm
2	7.50	9.0
3	11.50	12.0
4	14.50	14.50
5	17.0	16.50

cont...

Data Set No. 6

Time (day)	R5 @ 500 rpm	R1 @ 550 rpm
1	0.50	1.0
2	5.0	3.5
3	9.0	-
4	-	9.0

N.B.: R for reactor number.

Table A7.2 Calculated net biofilm accumulation (growth) in terms of thickness, z and volumetric quantity at various days of growth

Data Set No. 1

Time	R6 @ 30 rpm		R1 @ 35 rpm		R1 @ 80 rpm (a)	
day	z mm	vol. mm^3	z mm	vol. mm^3	z mm	vol. mm^3
0	0	0	0	0	0	0
3	-	-	-	-	0.086	2716
4	0.116	3645	0.129	4073	-	-
5	-	-	-	-	0.201	6336
6	0.179	5649	0.172	5431	-	-
7	-	-	-	-	0.387	12220
8	0.217	6834	0.187	5884	-	-
9	-	-	-	-	0.487	15388
10	0.275	8656	0.258	8147	-	-
11	-	-	-	-	0.558	17651
12	0.289	9112	0.316	9957	-	-
14	0.347	10934	0.359	11315	-	-
16	0.404	12757	0.387	12220	-	-
18	0.418	13213	0.430	13578	-	-
20	0.462	14579	0.487	15388	-	-

cont...

Data Set No. 2

Time	R5 @ 125 rpm		R6 @ 150 rpm		R5 @ 175 rpm	
day	z mm	vol. mm^3	z mm	vol. mm^3	z mm	vol. mm^3
0	0	0	0	0	0	0
3	-	-	0.174	5467	0.200	6301
4	0.200	6301	-	-	-	-
5	-	-	0.260	8201	0.428	13501
6	0.286	9001	-	-	-	-
7	-	-	0.418	13213	0.584	18452
8	0.385	12151	-	-	-	-
9	-	-	0.519	16402	-	-
10	0.513	16202	-	-	-	-

Data Set No. 3

Time	R1 @ 80 rpm (b)		R5 @ 200 rpm		R5 @ 250 rpm	
day	z mm	vol. mm^3	z mm	vol. mm^3	z mm	vol. mm^3
0	0	0	0	0	0	0
2	0.086	2716	0.129	4050	0.186	5851
4	0.172	5431	0.314	9901	0.613	19352
6	0.301	9505	0.570	18002	0.867	27453
7	-	-	-	-	-	35103
8	0.344	10862	0.712	22502	-	-
10	0.387	12220	-	-	-	-

cont...

Data Set No. 4

Time	R1 @ 300 rpm		R5 @ 350 rpm		R1 @ 400 rpm	
day	z mm	vol. mm^3	z mm	vol. mm^3	z mm	vol. mm^3
0	0	0	0	0	0	0
2	0.187	5884	0.428	13501	0.515	16294
3	-	-	0.655	20702	0.686	21725
4	0.558	17652	0.824	26103	0.828	26251
5	-	-	-	30603	-	29872
6	0.800	25346	-	-	-	-
7	-	33945	-	-	-	-

Data Set No. 5

Time	R5 @ 500 rpm		R1 @ 550 rpm	
day	z mm	vol. mm^3	z mm	vol. mm^3
0	0	0	0	0
1	0.029	900	0.058	1810
2	0.286	9001	0.201	6336
3	0.513	16202	-	-
4	-	-	0.515	16294

N.B.: The values of thickness, z and volume are calculated from the raw data in Table A7.1 using their relationship with h established in Appendix 4.
The biofilm quantity as dry mass (g) can be computed by multiplying the volume (mm^3) by the dry density of 0.022 mg/mm^3 x 10^{-3}.

Filename: grseel m*x

Curve fit for net growth rate at 30 r

*** Stopping after 3 iterations

Coefficents after last iteration :

Chi Square	M
4.516000266E+05	771.908854
E format	7.71908854E+02
Std devs	17.1467324630
%	2.2213
Dependencies	0.0000

Correlation Coefficients
1.00000

Degrees of Freedom : 9
Finial Lamda : 0.00000100

Data and fitted values

i	x(i)	y(i)	Pred Y	Residual	Z Resi
1	0.00000000	0.00000000	0.00000000	0.00000000	0.0000
2	4.00000000	3645.00000000	3087.63541660	557.36458340	0.8293
3	6.00000000	5649.00000000	4631.45312490	1017.54687510	1.5141
4	8.00000000	6804.00000000	6175.27083320	628.72916680	0.9802
5	10.00000000	8656.00000000	7719.08854150	936.91145851	1.3941
6	12.00000000	9112.00000000	9262.90624980	-150.90624979	-0.2245
7	14.00000000	10934.00000000	10806.72395800	127.27604191	0.1893
8	16.00000000	12757.00000000	12350.54166600	406.45833360	0.6048
9	18.00000000	13213.00000000	13894.35937500	-681.35937470	-1.0139
10	20.00000000	14579.00000000	15438.17708300	-859.17708300	-1.2785

ANOVA

Source of variation	df.	SS	MS	F
Model	1	0186257912.66000000	186257912.66000000	412.43999486
Residual	9	4064400.23960000	451600.02662000	
Total	10	9190322312.90000000		

R-sq. 97.86%
adjusted for df. 97.86%

Filename: grsee2 mfx

Curve fit for net growth rat at 35 rpm

*** Stopping after 3 iterations

Coefficents after last iteration :

Chi Square	M
2.82447826lE+05	783.201823
E format	7.832018236E+02
Std devs	13.5604315940
%	1.7314
Dependencies	0.0000

Correlation Coefficients
1.00000

Degrees of Freedom : 9
Finial Lamda : 0.00000100

Data and fitted values

i	x(i)	y(i)	Pred Y	Residual	Z Resid
1	0.00000000	0.00000000	0.00000000	0.00000000	0.00000
2	4.00000000	4073.00000000	3132.80729150	940.19270851	1.76908
3	6.00000000	5431.00000000	4699.21093720	731.78906278	1.37694
4	8.00000000	5884.00000000	6265.61458300	-381.61458297	-0.71805
5	10.00000000	8147.00000000	7832.01822870	314.98177129	0.59267
6	12.00000000	9957.00000000	9398.42187440	558.57812555	1.05102
7	14.00000000	11315.00000000	10964.82552000	350.17447981	0.65889
8	16.00000000	12220.00000000	12531.22916600	-311.22916594	-0.58561
9	18.00000000	13578.00000000	14097.63281200	-519.63281168	-0.97774
10	20.00000000	15388.00000000	15664.03645700	-276.03645742	-0.51939

ANOVA

Source of variation	df.	SS	MS	F
Model	1	9202710621.67000000	9202710621.67000000	717.69227069
Residual	9	92542030.43490000	10282447.82610000	
Total	10	9205252652.10000000		

R-sq.	98.76%
adjusted for df.	98.76%

Filename: grsee3 m*x

Curve fit for net growth rate at 80 rp

*** Stopping after 3 iterations (a

Coefficents after last iteration :

Chi Square	M
1.823353126E+06	1607.091228
E format	1.60709123E+03
Std devs	79.9858130320
%	4.9771
Dependencies	0.0000

Correlation Coefficients
1.00000

Degrees of Freedom : 5
Finial Lamda : 0.00000100

Data and fitted values

i	x(i)	y(i)	Pred Y	Residual	Z Resid
1	0.00000000	0.00000000	0.00000000	0.00000000	0.00000
2	3.00000000	2716.00000000	4821.27368420	-2105.27368420	-1.55909
3	5.00000000	6336.00000000	8035.45614030	-1699.45614030	-1.25856
4	7.00000000	12220.00000000	11249.63859600	970.36140352	0.71861
5	9.00000000	15388.00000000	14463.82105300	924.17894739	0.68441
6	11.00000000	17651.00000000	17678.00350900	-27.00350875	-0.01999

ANOVA

Source of variation	df.	SS	MS	F
Model	1	0244467411.21000000	244467411.21000000	134.07573540
Residual	5	9116765.62800000	1823353.12560000	
Total	6	5253584176.83000000		

R-sq. 96.40%
adjusted for df. 96.40%

Filename: grsee3x m*x

Curve fit for net growth rate at 80 rpm

(b)

*** Stopping after 3 iterations

Coefficents after last iteration :

Chi Square	M
7.109303600E+05	1333.100000
E format	1.33310000E+03
Std devs	56.84629986460
%	4.2642
Dependencies	0.0000

Correlation Coefficients
1.00000

Degrees of Freedom : 5
Finial Lamda : 0.00001000

Data and fitted values

t	x(t)	y(t)	Pred Y	Residual	Z Residu
1	0.00000000	0.00000000	0.00000000	0.00000000	0.000000
2	2.00000000	2716.00000000	2666.20000030	49.79999972	0.059065
3	4.00000000	5431.00000000	5332.40000060	98.59999944	0.116940
4	6.00000000	9505.00000000	7998.60000080	1506.39999920	1.786597
5	8.00000000	10862.00000000	10664.80000100	197.19999887	0.233880
6	10.00000000	12220.00000000	13331.00000100	-1111.00000140	-1.317651

ANOVA

Source of Variation	df.	SS	MS	F
Model	1	114431108.20000000	114431108.20000000	160.95965883
Residual	5	3554651.80000000	710930.36000000	
Total	6	117985760.00000000		

R-sq. 96.99%
adjusted for df. 96.99%

Filename: grsee4 m*x

Curve fit for net growth rate at 125 rj

*** Stopping after 3 iterations

Coefficents after last iteration :

Chi Square	M
1.492834120E+05	1566.842593
E format	1.56684259E+03
Std devs	26.2010931650
X	1.6722
Dependencies	0.0000

Correlation Coefficients
1.00000

Degrees of Freedom : 4
Finial Lamda : 0.00000100

Data and fitted values

i	x(i)	y(i)	Pred Y	Residual	Z Resid
1	0.00000000	0.00000000	0.00000000	0.00000000	0.00000
2	4.00000000	6301.00000000	6267.37037030	33.62962969	0.08703
3	6.00000000	9001.00000000	9401.05555540	-400.05555546	-1.03890
4	8.00000000	12151.00000000	12534.74074100	-383.74074063	-0.99650
5	10.00000000	16202.00000000	15668.42592600	533.57407422	1.38563

ANOVA

Source of variation	df.	SS	MS	F
Model	1	4149127268.35000000	4149127268.35000000	1005.69083420
Residual	4	593133.64815000	148283.41204000	
Total		4149720402.00000000		

R-sq. 99.60%
adjusted for df. 99.60%

Filename: grsee5 m*x

Curve fit for net growth rate at 150 rpm

*** Stopping after 3 iterations

Coefficients after last iteration :

Chi Square	M
2.566961997E+05	1814.115854
E format	1.81411585E+03
Std devs	39.5628707380
%	2.1808
Dependencies	-0.0000

Correlation Coefficients:

1.00000

Degrees of Freedom : 4

Finial Lamda : 0.00001000

Data and fitted values

i	x(i)	y(i)	Pred Y	Residual	Z Resi
1	0.00000000	0.00000000	0.00000000	0.00000000	0.0000
2	3.00000000	5467.00000000	5442.34756140	24.65243862	0.0486
3	5.00000000	8201.00000000	9070.57926900	-869.57926898	-1.7163
4	7.00000000	13213.00000000	12698.81097700	514.18902343	1.0148
5	9.00000000	16402.00000000	16327.04268400	74.95731586	0.1479

ANOVA

Source of variation	df.	SS	MS	F
Model	1	1650430 60.40000000	1650430 60.40000000	642.95093031
Residual	4	1026784.79880000	256696.19970000	
Total	5	4166069845.20000000		

R-sq. 99.38%

adjusted for df. 99.38%

Filename: grsee6 m*<

Curve fit for net growth rate at 175 rpm

*** Stopping after 3 iterations

Coefficents after last iteration :

Chi Square	M
8.536265622E+05	2597.253012
E format	2.59725301E+03
Std devs	101.41300098 00
%	3.9046
Dependencies	0.0000

Correlation Coefficients
1.00000

Degrees of Freedom : 3
Finial Lamda : 0.00000100

Data and fitted values

i	x(i)	y(i)	Pred Y	Residual	Z Resid
1	0.00000000	0.00000000	0.00000000	0.00000000	0.00000
2	3.00000000	6301.00000000	7791.75903570	-1490.75903570	-1.61351
3	5.00000000	13501.00000000	12986.26506000	514.73494042	0.55712
4	7.00000000	18452.00000000	18180.77108300	271.22891661	0.29356

ANOVA

Source of variation	df.	SS	MS	F
Model	0194052897.31000000	194052897.31000000		227.32762299
Residual	32560879.68670000	853626.56225000		
Total	31966137 77.00000000			

R-sq. 98.70%
adjusted for df. 98.70%

Filename: grsee7 m*x

*** Stopping after 9 iterations

Curve fit for net growth rate at 200 rp

Coefficents after last iteration :

Chi Square	M
1.38612761?E+06	2797.76666?
E format	2.79776667E+03
Std devs	107.47587389??
%	3.8415
Dependencies	0.0000

Correlation Coefficients
1.00000

Degrees of Freedom : 4
Finial Lamda : 0.00001000

Data and fitted values

i	X(i)	Y(i)	Pred Y	Residual	Z Resid
1	0.00000000	0.00000000	0.00000000	0.00000000	0.000000
2	2.00000000	4050.00000000	5595.53333390	-1545.53333390	-1.312734
3	4.00000000	9901.00000000	11191.06666800	-1290.06666770	-1.095747
4	6.00000000	18002.00000000	16786.60000200	1215.39999840	1.032327
5	8.00000000	22502.00000000	22382.13333800	119.86666453	0.101811

ANOVA

Source of variation	df.	SS	MS	F
Model	1	0346230393.53000000	346230393.53000000	249.78247989
Residual		45544510.46670000	1386127.61670000	
Total		4351774904.00000000		

R-sq.	98.42%
adjusted for df.	98.42%

Filename: grsee8 m/s

Curve fit for net growth rate at 250 rpm

*** Stopping after 3 iterations

Coefficents after last iteration :

Chi Square	M
4.49200E112E+06	4757.601906
E format	4.75760191E+03
Std devs	206.8357112600
%	4.3478
Dependencies	0.0000

Correlation Coefficients
1.00000

Degrees of Freedom : 4
Finial Lamda : 0.00001000

Data and fitted values

i	x(i)	y(i)	Pred y	Residual	% Residu
1	0.00000000	0.00000000	0.00000000	0.00000000	0.000000
2	2.00000000	5850.60000000	9515.20381110	-3664.60381110	-1.729047
3	4.00000000	19351.90000000	19030.40762200	321.49237773	0.151687
4	6.00000000	27452.60000000	28545.61143300	-1093.01143340	-0.515708
5	7.00000000	35103.40000000	33303.21333900	1800.18666110	0.849370

ANOVA

Source of variation	df.	SS	MS	F
Model	0	836340603.39000000	836340603.39000000	186.18420867
Residual	4	17968024.450000004	4492006.11240000	
Total		4854308627.83000000		

R-sq. 97.90%
adjusted for df. 97.90%

Filename: grseey m*x

Curve fit for net growth rate at 300 rpm

*** Stopping after 3 iterations

Coefficents after last iteration :

Chi Square	M
4.63651436 1E+06	4495.849524
E format	4.49584952E+03
Std devs	210.1363387700
%	4.6740
Dependencies	0.0000

Correlation Coefficients
1.00000

Degrees of Freedom : 4
Final Lamda : 0.00001000

Data and fitted values

i	Y(i)	Y(i)	Pred Y	Residual	Z Residua
1	0.00000000	0.00000000	0.00000000	0.00000000	0.00000000
2	2.00000000	5883.80000000	8991.69904760	-3107.89904760	-1.4433481
3	4.00000000	17691.50000000	17983.39809500	-291.89809522	-0.1541377
4	6.00000000	25345.70000000	26975.09714300	-1629.39714280	-0.7567129
5	7.00000000	33945.20000000	31470.94666700	2474.25333340	1.1490749

ANOVA

Source of variation	df.	SS	MS	F
Model	0750293727.49000000	750293727.49000000		161.82279815
Residual	418546057.44300000	4636514.36060000		
Total	4768839784.93000000			

R-sq. 97.59%
adjusted for df. 97.59%

Filename: grseell m*x

Curve fit for net growth rate at 350 rpm

*** Stopping after 3 iterations

Coefficents after last iteration :

Chi Square	M
1.234024182E+06	6417.279629
E Format	6.41727963E+03
Std devs	151.169771260
%	2.3557
Dependencies	0.0000

Correlation Coefficients
1.00000

Degrees of Freedom : 4
Final Lamda : 0.00000100

Data and fitted values

I	x(i)	y(i)	Pred Y	Residual	Z Residu
1	0.00000000	0.00000000	0.00000000	0.00000000	0.000000
2	2.00000000	13501.30000000	12834.55935800	666.74074200	0.600198
3	3.00000000	20702.00000000	19251.83888700	1450.16111300	1.305432
4	4.00000000	26102.50000000	25669.11851600	433.38148400	0.390129
5	5.00000000	30602.90000000	32086.39814500	-1483.49814500	-1.335442

ANOVA

Source of variation	df.	SS	MS	F
Model	05	70921456.49000000	570921456.49000000	462.65013672
Residual	4	4936096.72770000	1234024.18190000	
Total		4575857553.21000000		

R-sq.	99.14%
adjusted for df.	99.14%

Filename: grseel0 m*x

Curve fit for net growth rate at 400 rpm

*** Stopping after 3 iterations

Coefficents after last iteration :

Chi Square	M
5.68653680SE+06	6520.818519
E format	6.52081852E+03
Std devs	324.5092273100
%	4.9765
Dependencies	0.0000

Correlation Coefficients
1.00000

Degrees of Freedom : 4
Finial Lamda : 0.00000100

Data and fitted values

i	x(i)	y(i)	Pred Y	Residual	Z Residu
1	0.00000000	0.00000000	0.00000000	0.00000000	0.0000000
2	2.00000000	16293.70000000	13041.63703700	3252.06296300	1.3637509
3	4.00000000	21714.30000000	19562.48555600	2151.81444440	0.9068199
4	4.00000000	26250.30000000	26083.27407400	167.02592593	0.0702978
5	5.00000000	29871.70000000	32604.09259300	-2732.39259250	-1.1458827

ANOVA

Source of variation	df.	SS	MS	F
Model	1	0523624896.69000000	523624896.690000000	92.08151017
Residual	422746147.22100000	5686536.80530000		
Total	4546371043.91000000			

R-sq.	95.84%
adjusted for df.	95.84%

Filename: grseel3 m*x

Curve fit for net growth rate at 500 rpm

*** Stopping after 3 iterations

Coefficents after last iteration :

Chi Square	M
6.26906148 6E+06	4821.907143
E format	4.82190714E+03
Std devs	669.1712098000
%	12.877
Dependancies	0.0000

Correlation Coefficients
1.00000

Degrees of Freedom : 3
Finial Lamda : 0.00000100

Data and fitted values

i	x(i)	y(i)	Pred y	Residual	Z Residual
1	0.00000000	0.00000000	0.00000000	0.00000000	0.00000000
2	1.00000000	900.10000000	4821.90714280	-3921.80714280	-1.56670614
3	2.00000000	9000.90000000	9643.81428570	-642.91428570	-0.25677446
4	3.00000000	16201.60000000	14465.72142900	1735.87857140	0.69329501

ANOVA

Source of variation	df.	SS	MS	F
Model	1	155174607.23000000	155174607.23000000	24.75244621
Residual	3	18807184.45900000	6269061.48640000	
Total	4	3173981791.69000000		

R-sq.	89.19%
adjusted for df.	89.19%

Filename: grceel2 m*x

Curve fit for net growth rate at 550 rpm

*** Stopping after 3 iterations

Coefficents after last iteration :

Chi Square	M
2.250137540E+06	3793.238095
E format	3.79323810E+03
Std devs	327.3068422600
	8.6295
Dependencies	0.0000

Correlation Coefficients
1.00000

Degrees of Freedom : 3
Finial Lamda : 0.00000100

Data and fitted values

i	x(i)	y(i)	Pred Y	Residual	Z Residu
1	0.00000000	0.00000000	0.00000000	0.00000000	0.000000
2	1.00000000	1810.40000000	3793.23809520	-1982.83809520	-1.321851
3	2.00000000	6336.40000000	7586.47619050	-1250.07619050	-0.833058
4	4.00000000	16293.70000000	15172.95238100	1120.74761900	0.747142

ANOVA

Source of Variation	df.	SS	MS	F
Model	1	152827250.13000000	152827250.13000000	67.91907047
Residual	2	36750412.61950000	2250137.53980000	
Total	3	3159577662.75000000		

R-sq. 95.77%
adjusted for df. 95.77%

Table A7.3 Computed biofilm net attached growth rate at various speeds (rpm) and shear stresses

Speed N rpm	Linear Velocity v m/s	Shear Stress σ N/m^2	Net Growth Rate G_n g/d
30	0.158	0.091	0.017
35	0.184	0.115	0.017
80(a)	0.421	0.438	0.035
80(b)	0.421	0.438	0.029
125	0.658	0.958	0.034
150	0.789	1.332	0.040
175	0.921	1.766	0.057
200	1.052	2.262	0.062
250	1.316	3.435	0.105
300	1.579	4.851	0.099
350	1.842	6.511	0.141
400	2.105	8.413	0.143
500	2.631	12.948	0.106
550	2.894	15.580	0.083

N.B.: The following relationships are used for calculating the values in the above Table:

i) v m/s $= \omega \overline{kR}$ where $\overline{kR}$ is 0.05025 m on average, with biofilm growth on the reactor surface, and ω is in rad/s.

ii) σ N/m^2 $= \dfrac{(T \text{ Nmm}) \times 10^{-3}}{2(kR)^2(0.100\text{m})}$

where T is as defined in Appendix 6, section A6.2.

iii) G_n is as determined by curve fit.

Curve fit for net growth rate Vs. shear stress

Filename: netgsee A+B*X+C*(X^2) Quadratic

*** Stopping after 3 iterations

Coefficients after last iteration :

Chi Square	Con	X	X^2
8.428036785E-05	0.014283	0.027533	-0.001509
E format	1.428283059E-02	2.753297738E-02	-1.508541UE-03
Std devs	0.004078447 5	0.001834576	0.0001229595
%	28.5549	6.6639	-8.1509
Dependencies	0.6938	0.9628	0.9501

Correlation Coefficients

```
 1.00000
-0.72129 1.00000
 0.59659-0.96014 1.00000
```

Degrees of Freedom : 11
Final Lamda : 0.00000100

Data and fitted values

I	x(I)	y(I)	Pred Y	Residual	Z Residual
1	0.09100000	0.01700000	0.01677581	0.00022419	0.02441992
2	0.11500000	0.01700000	0.01742915	-0.00042915	-0.04674591
3	0.43800000	0.03500000	0.02605285	0.00894715	0.97458951
4	0.43800000	0.02900000	0.02605285	0.00294715	0.32102563
5	0.95800000	0.03400000	0.03927491	-0.00527491	-0.57458215
6	1.33200000	0.04000000	0.04828024	-0.00828024	-0.90194450
7	1.76600000	0.05700000	0.05820127	-0.00120127	-0.13085137
8	2.26200000	0.06200000	0.06884373	-0.00684373	-0.74546945
9	3.43500000	0.10500000	0.09105897	0.01394103	1.51855917
10	4.85100000	0.09900000	0.11234599	-0.01334599	-1.45374260
11	6.51100000	0.14100000	0.12959826	0.01140174	1.24196105
12	8.41300000	0.14300000	0.13914537	0.00885463	0.41987465
13	12.94800000	0.10600000	0.11787183	-0.01187183	-1.29316656
14	15.58000000	0.08300000	0.07706877	0.00593123	0.64607258

ANUVA

Source of variation	df.	SS	MS	F
Model	2	0.02391663	0.01195832	141.88731521
Residual	11	0.00092708	0.00008428	
Total	13	0.02484371		

R-sq. 96.27%
adjusted for df. 95.59%

APPENDIX 8

DATA OF SUBSTRATE CONCENTRATION IN BIOREACTOR DURING GROWTH

Table A8.1 RAW DATA: Absorbance at 279 nm representing substrate (phenol) concentration in the bioreactor at different days of growth for various constant rotational speeds (rpm)

Data Set No. 1

Time (day)	R6 @ 30 rpm	R1 @ 35 rpm	R5 @ 125 rpm
0	1.20	1.20	1.20
1	0.82	0.85	0.80
5	0.75	0.77	0.64
6	0.68	0.64	0.52
9	0.94	0.94	0.64
10	0.82	0.80	0.475
12	0.95	0.90	0.71
15	0.92	0.91	0.69
16	0.93	0.91	0.67
19	0.90	0.90	0.66
20	0.91	0.72	0.48

cont...

Data Set No. 2

Time (day)	R1 @ 80 rpm (a)	R6 @ 150 rpm	R5 @ 175 rpm
0	1.20	1.20	1.20
2	0.55	0.405	0.22
3	0.68	0.52	0.31
4	0.78	0.475	0.225
5	0.79	0.48	0.165
6	0.61	0.485	0.34
7	0.85	0.43	0.54
9	0.85	0.445	0.53
11	0.64	-	0.25

Data Set No. 3

Time (day)	R1 @ 80 rpm (b)	R5 @ 200 rpm
0	1.20	1.20
1	0.74	0.31
2	0.75	0.24
3	0.79	0.31
4	0.78	0.27
6	0.70	0.225
7	0.70	0.255
8	0.75	0.38
10	0.71	-

cont...

Data Set No. 4

Time (day)	R5 @ 250 rpm	R1 @ 300 rpm
0	1.20	1.20
1	0.095	0.08
2	0.235	0.16
4	0.19	0.12
6	0.06	0.08
7	0.10	0.085

Data Set No. 5

Time (day)	R5 @ 350 rpm	R1 @ 400 rpm
0	1.20	1.20
1	0.10	0.10
2	0.137	0.145
3	0.085	0.08
4	0.07	0.077
5	0.07	0.07

cont...

Data Set No. 6

Time (day)	R5 @ 500 rpm	R1 @ 550 rpm
0	1.20	1.20
1	0.045	0.065
2	0.05	0.06
3	0.083	0.065
4	0.07	0.085

Table A8.2 Calculated substrate (phenol) consumption or removal in bioreactor during growth at various film thickness for different constant rotational speeds (rpm)

Data Set No. 1

Time	R6 @ 30 rpm		R1 @ 35 rpm		R1 @ 80 rpm (a)	
(day)	z mm	S g/l	z mm	S g/l	z mm	S g/l
0	0	0.150	0	0.150	0	0.150
1	0.025	0.103	0.025	0.106	-	-
2	-	-	-	-	0.102	0.069
3	-	-	-	-	0.153	0.085
4	-	-	-	-	0.204	0.098
5	0.123	0.094	0.124	0.096	0.255	0.099
6	0.147	0.085	0.149	0.080	0.306	0.076
7	-	-	-	-	0.357	0.106
9	0.221	0.118	0.224	0.118	0.459	0.106
10	0.246	0.103	0.249	0.100	-	-
11	-	-	-	-	0.561	0.080
12	0.295	0.119	0.299	0.113	-	-
15	0.369	0.115	0.373	0.114	-	-
16	0.393	0.116	0.398	0.114	-	-
19	0.467	0.113	0.473	0.113	-	-
20	0.491	0.114	0.498	0.090	-	-

cont...

Data Set No. 2

Time	R5 @ 125 rpm		R6 @ 150 rpm		R5 @ 175 rpm	
(day)	z mm	S g/l	z mm	S g/l	z mm	S g/l
0	0	0.150	0	0.150	0	0.150
1	0.050	0.100	-	-	-	-
2	-	-	0.115	0.051	0.165	0.028
3	-	-	0.173	0.065	0.248	0.039
4	-	-	0.231	0.059	0.331	0.028
5	0.249	0.080	0.289	0.060	0.413	0.021
6	0.299	0.065	0.346	0.061	0.496	0.043
7	-	-	0.404	0.054	0.579	0.068
9	0.449	0.080	0.520	0.056	0.744	0.066
10	0.499	0.060	-	-	-	-
11	-	-	-	-	0.909	0.031
12	0.598	0.089	-	-	-	-
15	0.748	0.086	-	-	-	-
16	0.798	0.084	-	-	-	-
19	0.948	0.083	-	-	-	-
20	0.997	0.060	-	-	-	-

cont...

Data Set NO. 3

Time	R1 @ 80 rpm (b)		R5 @ 200 rpm		R5 @ 250 rpm	
(day)	z mm	S g/l	z mm	S g/l	z mm	S g/l
0	0	0.150	0	0.150	0	0.150
1	0.042	0.093	0.089	0.039	0.151	0.012
2	0.085	0.094	0.178	0.030	0.303	0.029
3	0.127	0.099	0.267	0.039	-	-
4	0.169	0.098	0.356	0.034	0.606	0.024
6	0.254	0.088	0.534	0.028	0.909	0.008
7	0.296	0.088	0.623	0.032	1.060	0.013
8	0.339	0.094	0.712	0.048	-	-
10	0.423	0.089	-	-	-	-

Data Set No. 4

Time	R1 @ 300 rpm		R5 @ 350 rpm		R1 @ 400 rpm	
(day)	z mm	S g/l	z mm	S g/l	Z mm	S g/l
0	0	0.150	0	0.150	0	0.150
1	0.143	0.010	0.204	0.013	0.207	0.013
2	0.286	0.020	0.409	0.017	0.414	0.018
3	-	-	0.613	0.011	0.621	0.010
4	0.571	0.015	0.817	0.009	0.828	0.010
5	-	-	1.021	0.009	1.036	0.009
6	0.857	0.010	-	-	-	-
7	1.000	0.011	-	-	-	-

cont...

Data Set No. 5

Time	R5 @ 500 rpm		R1 @ 550 rpm	
(day)	z mm	S g/l	z mm	S g/l
0	0	0.150	0	0.150
1	0.153	0.006	0.120	0.008
2	0.307	0.006	0.241	0.008
3	0.460	0.010	0.361	0.008
4	0.614	0.009	0.482	0.011

N.B.: The values of biofilm thickness, z are computed from the established net growth rates for the various constant speed as derived from best straight line fit by Curve Fit in Appendix 7 and the equations in Appendix 4 (section A4.2).

Table A8.3 Steady-state substrate (phenol) consumption or removal in bioreactor at different rotational speeds and shear stresses

N (rpm)	Shear Stress, σ N/m^2	S_o-S_e (g/l)
30	0.091	0.042
35	0.115	0.046
80(a)	0.438	0.060
80(b)	0.438	0.057
125	0.958	0.071
150	1.332	0.097
175	1.766	0.110
200	2.262	0.114
250	3.435	0.133
300	4.851	0.137
350	6.511	0.138
400	8.413	0.138
500	12.948	0.142
550	15.580	0.141

N.B.: S_o-S_e is the substrate consumed or removed where S_e, the effluent substrate concentration is equal to $\bar{S}$, the substrate concentration in the reactor.

Curve fit for steady-state substrate removal Vs. shear stress

Filename: subsee A+B*exp(C*X) Exponential

*** Stopping after 5 iterations

Coefficents after last iteration :

Chi Square	A	B	C
1.9323752106E-05	0.141528	-0.106572	-0.607845
E format	1.41528104E-01	-1.0657241E-01	-6.0784462E-01
Std devs	0.0021826515	0.0034102350	0.0508038894
%	1.5422	-3.1999	-8.3580
Dependencies	0.7548	0.6146	0.6964

Correlation Coefficients

```
 1.00000
-0.46024 1.00000
 0.61750 0.16579 1.00000
```

Degrees of Freedom : 11
Final Lamda : 0.00000001

Data and fitted values

i	x(i)	y(i)	Pred Y	Residual	Z Residual
1	0.09100000	0.04200000	0.04069055	0.00130945	0.29788121
2	0.11500000	0.04600000	0.04215092	0.00384908	0.87561151
3	0.43800000	0.06000000	0.05986611	0.00013389	0.03045912
4	0.43800000	0.05700000	0.05986611	-0.00286611	-0.65199824
5	0.95800000	0.07100000	0.08199637	-0.01099637	-2.50151731
6	1.33200000	0.09700000	0.09410186	0.00289814	0.65928485
7	1.76600000	0.11000000	0.10509889	0.00490111	1.11493346
8	2.26200000	0.11400000	0.11458088	-0.00058088	-0.13214263
9	3.43500000	0.13300000	0.12831937	0.00468063	1.06477728
10	4.85100000	0.13700000	0.13594262	0.00105738	0.24058811
11	6.51100000	0.13800000	0.13949178	-0.00149178	-0.33935776
12	8.41300000	0.13800000	0.14088726	-0.00288726	-0.65681105
13	12.94800000	0.14200000	0.14148740	0.00051260	0.11660810
14	15.58000000	0.14100000	0.14151989	-0.00051989	-0.11826663

ANOVA

Source of variation	df.	SS	MS	F
Model	2	0.01940515	0.00970258	502.10623989
Residual	11	0.00021256	0.00001932	
Total	13	0.01961771		

R-sq. 98.92%
adjusted for df. 98.72%

APPENDIX 9

DATA OF BIOFILM TOTAL GROWTH AND LOSS RATES DURING GROWTH PHASE

Table A9 Calculated total growth and loss rates at different shear stresses

Speed (rpm)	Shear Stress (N/m^2)	S_o-S_e (g/l)	$Q(S_o-S_e)Y_t$ (g/d)	G_n* (g/d)	R_s (g/d)
30	0.091	0.042	0.126	0.017	0.109
35	0.115	0.046	0.137	0.017	0.120
80(a)	0.438	0.060	0.179	0.035	0.144
80(b)	0.438	0.057	0.170	0.029	0.141
125	0.958	0.071	0.212	0.034	0.178
150	1.332	0.097	0.290	0.040	0.250
175	1.766	0.110	0.329	0.057	0.272
200	2.262	0.114	0.341	0.062	0.279
250	3.435	0.133	0.397	0.105	0.292
300	4.851	0.137	0.409	0.099	0.310
350	6.511	0.138	0.412	0.141	0.271
400	8.413	0.138	0.412	0.143	0.269
500	12.948	0.142	0.424	0.106	0.318
550	15.580	0.141	0.421	0.083	0.338

N.B.: The values of S_o-S_e are at steady-state only.

Y_t, the true yield taken as 0.92 g/g (Rao, 1985).

* Values are taken from Table A7.3, Appendix 7.

Total Growth Rate, $G_t = Q(S_o-S_e)Y_t$.

Curve fit for total growth rate Vs. shear stress

Filename: grtol A+B*exp(C*X) Exponential

*** Stopping after 4 iterations

Coefficents after last iteration :

Chi Square	A	B	C
1.739841747E-04	0.422524	-0.318249	-0.609556
E format	4.22524291E-01	-3.18249949E-01	-6.09556634E-01
Std devs	0.0065424143	0.0102366552	0.0511857980
%	1.5484	-3.2166	-8.3972
Dependencies	0.7543	0.6143	0.6962

Correlation Coefficients

```
 1.00000
-0.46243  1.00000
 0.61705  0.16696  1.00000
```

Degrees of Freedom : 11
Finial Lamda : 0.00000010

Data and fitted values

i	x(i)	y(i)	Pred Y	Residual	Z Residual
1	0.09100000	0.12600000	0.12144730	0.00455270	0.34515488
2	0.11500000	0.13700000	0.12581980	0.01118020	0.84760721
3	0.43800000	0.17900000	0.17884574	0.00015426	0.01169530
4	0.43800000	0.17000000	0.17884574	-0.00884574	-0.67062397
5	0.95800000	0.21200000	0.24504026	-0.03304026	-2.50488921
6	1.33200000	0.29000000	0.28122128	0.00877872	0.66554326
7	1.76600000	0.32900000	0.31406671	0.01493329	1.13214131
8	2.26200000	0.34100000	0.34236473	-0.00136473	-0.10346431
9	3.43500000	0.39700000	0.38331124	0.01368876	1.03778931
10	4.85100000	0.40900000	0.40598270	0.00301730	0.22875126
11	6.51100000	0.41200000	0.41651075	-0.00451075	-0.34197439
12	8.41300000	0.41200000	0.42063795	-0.00863795	-0.65487121
13	12.94800000	0.42400000	0.42240542	0.00159458	0.12089043
14	15.58000000	0.42100000	0.42250040	-0.00150040	-0.11374986

ANOVA

Source of variation	df.	SS	MS	F
Model	2	0.17298453	0.08649227	497.12720008
Residual	11	0.00191383	0.00017398	
Total	13	0.17489836		

R-sq. 98.91%
adjusted for df. 98.71%

APPENDIX 10

SHEAR TEST DATA

BIOFILM LOSS AT SHEAR STRESS GREATER THAN THE STRESS (0.115 N/m2) ADAPTED DURING GROWTH PHASE

Table A10.1 RAW DATA: Absorbance representing cell concentration in reactor due to shear loss at various rotational speeds (growth at 35 rpm)

100 rpm

Reactor, R2; Reactor liquid volume, 190 ml; Δh, 1.5 mm

Time (mins.)	0	1	3	6	11	16	26
Abs. @ 620nm	0.013	0.015	0.017	0.020	0.020	0.026	0.025

Reactor, R5; Reactor liquid volume, 199 ml; Δh, 3 mm

Time (mins.)	0	2	4	7	10	15	20	30
Abs.@ 620 nm	0.02	0.025	0.025	0.027	0.03	0.032	0.032	0.035

Reactor, R4; Reactor liquid volume, 180 ml; Δh, 4 mm

Time (mins.)	0	3	8	18	33	53
Abs. @ 620 nm	0.130	0.140	0.150	0.155	0.155	0.155

125 rpm

Reactor, R2; Reactor liquid volume, 200 ml; Δh, 1.4 mm

Time (mins.)	0	1	3	6	11	16	21	26
Abs. @ 620nm	0.010	0.015	0.015	0.018	0.018	0.02	0.02	0.019

Reactor, R2; Reactor liquid volume, 199 ml; Δh, 3 mm

Time (mins.)	0	1	2	4	7	10	15	20
Abs.@ 620nm	0.007	0.016	0.025	0.04	0.045	0.05	0.05	0.055

cont...

Reactor, R6; Reactor liquid volume, 185 ml; Δh, 4.75 mm

Time (mins.)	0	1	2	4	9	19	29
Abs. @ 620 nm	0.010	0.025	0.030	0.035	0.035	0.042	0.041

Reactor, R5; Reactor liquid volume, 176.6 ml, Δh, 5.5 mm

Time (mins.)	0	1	2	4	9	19	29	39
Abs.@ 620nm	0.013	0.03	0.035	0.036	0.068	0.068	0.075	0.073

Reactor, R5; Reactor liquid volume, 190 ml; Δh, 6 mm

Time (mins.)	0	1	2	4	7	10	15	20
Abs. @ 620 nm	0.03	0.045	0.047	0.05	0.055	0.06	0.06	0.07

150 rpm

Reactor, R1; Reactor liquid volume, 187 ml; Δh, 2.25 mm

Time (mins.)	0	1	2	4	7	10	15	20
Abs.@ 620nm	0.004	0.045	0.05	0.051	0.052	0.06	0.057	0.056

Reactor, R5; Reactor liquid volume, 195 ml; Δh, 4 mm

Time (mins.)	0	2	4	7	10	15	20	30
Abs.@ 620 nm	0.015	0.125	0.135	0.16	0.17	0.18	0.178	0.178

Reactor, R6; Reactor liquid volume, 180 ml; Δh, 4 mm

Time (mins.)	0	2	5	10	20	35	55
Abs. @ 620 nm	0.06	0.14	0.205	0.235	0.243	0.25	0.243

Reactor, R5; Reactor liquid volume, 179 ml; Δh, 5.25 mm

Time (mins.)	0	3	8	18	33	53
Abs. @ 620 nm	0.005	0.180	0.180	0.195	0.210	0.220

cont...

175 rpm

Reactor, R2; Reactor liquid volume, 190 ml; Δh, 1.5 mm

Time (mins.)	0	1	3	6	11	16	26
Abs. @ 620nm	0.025	0.03	0.034	0.0365	0.0375	0.0385	0.0385

Reactor, R4; Reactor liquid volume, 197 ml, Δh, 2 mm

Time (mins.)	0	1	2	4	7	10	15	20
Abs.@ 620nm	0.008	0.03	0.03	0.035	0.045	0.055	0.05	0.057

Reactor, R2; Reactor liquid volume, 190 ml; Δh, 5.25 mm

Time (mins.)	0	1	2	4	7	10	15	20
Abs.@ 620nm	0.015	0.035	0.065	0.055	0.07	0.07	0.0685	0.073

Reactor, R2; Reactor liquid volume, 183 ml; Δh, 6 mm

Time (mins.)	0	2	4	7	10	15	20
Abs.@ 620nm	0.005	0.1425	0.23	0.28	0.265	0.3	0.2875

Reactor, R5; Reactor liquid volume, 174 ml; Δh, 7.75 mm

Time (mins.)	0	2	4	7	10	15	20
Abs. @ 620 nm	0.005	0.1275	0.15	0.1475	0.18	0.18	0.1825

200 rpm

Reactor, R5; Reactor liquid volume, 194 ml; Δh, 2.2 mm

Time (mins.)	0	1	2	4	7	10	15
Abs. @ 620nm	0.02	0.04	0.055	0.0625	0.07	0.075	0.08

Reactor, R2; Reactor liquid volume, 183 ml; Δh, 3 mm

Time (mins.)	0	1	2	4	7	10	13	16
Abs. @ 620nm	0.05	0.42	0.5	0.58	0.69	0.68	0.71	0.7

cont...

Reactor, R4; Reactor liquid volume, 195 ml; Δh, 5.1 mm

Time (mins.)	0	1	2	4	7	10	15
Abs. @ 620 nm	0.03	0.455	0.4	0.5	0.495	0.5	0.51

Reactor, R6; Reactor liquid volume, 177.6 ml; Δh, 5.5 mm

Time (mins.)	0	1	2	4	7	10	15
Abs. @ 620 nm	0.0225	0.575	0.75	0.82	0.88	0.86	0.87

N.B.: The reactor cell concentration at time, 0 min. was the initial concentration before shearing started.

Table A10.2 Calculated biofilm shear loss at rotational speeds higher than the speed (35 rpm) adapted during growth

100 rpm

Film thickness: 0.085 mm

Time (mins.)	0	1	3	6	11	16	26
Loss (mg)	0	0.22	0.44	0.77	0.77	1.38	1.32

Film thickness: 0.172 mm

Time (mins.)	0	2	4	7	10	15	20	30
Loss (mg)	0	0.58	0.58	0.81	1.16	1.39	1.39	1.73

Film thickness: 0.229 mm

Time (mins.)	0	3	8	19	33	53
Loss (mg)	0	1.04	2.08	2.61	2.61	2.61

cont...

125 rpm

Film thickness: 0.079 mm

Time (mins.)	0	1	3	6	11	16	21	26
Loss (mg)	0	0.58	0.58	0.87	0.87	1.16	1.16	1.01

Film thickness: 0.170 mm

Time (mins.)	0	1	2	4	7	10	15	20	30	40
Loss (mg)	0	1.04	2.07	3.8	4.38	4.95	4.95	5.53	5.2	5.2

Film thickness: 0.275 mm

Time (mins.)	0	1	2	4	9	19	29
Loss (mg)	0	1.61	2.14	2.68	2.68	3.40	3.32

Film thickness: 0.315 mm

Time (mins.)	0	1	2	4	9	19	29	39
Loss (mg)	0	1.74	2.25	2.35	5.57	5.57	6.34	6.08

Film thickness: 0.343 mm

Time (mins.)	0	1	2	4	7	10	15	20	30	40
Loss (mg)	0	1.65	1.87	2.2	2.75	3.3	3.3	4.4	4.4	3.85

150 rpm

Film thickness: 0.129 mm

Time (mins.)	0	1	2	4	7	10	15	20	30
Loss (mg)	0	4.44	4.98	5.09	5.20	6.06	5.74	5.63	6.06

Film thickness: 0.230 mm

Time (mins.)	0	2	4	7	10	15	20	30
Loss (mg)	0	12.42	13.55	16.37	17.50	18.63	18.35	18.35

cont...

Film thickness: 0.232 mm

Time (mins.)	0	2	5	10	20	35	55
Loss (mg)	0	8.34	15.11	18.24	19.02	19.80	19.02

Film thickness: 0.300 mm

Time (mins.)	0	3	8	18	33	53
Loss (mg)	0	18.14	18.14	19.69	21.25	22.28

175 rpm

Film thickness: 0.085 mm

Time (mins.)	0	1	3	6	11	16	26
Loss (mg)	0	0.55	0.99	1.27	1.38	1.49	1.49

Film thickness: 0.114 mm

Time (mins.)	0	1	2	4	7	10	15	20	30
Loss (mg)	0	2.51	2.51	3.08	4.22	5.36	4.79	5.59	5.76

Film thickness: 0.296 mm

Time (mins.)	0	1	2	4	7	10	15	20
Loss (mg)	0	2.20	5.50	4.40	6.05	6.05	5.89	6.33

Film thickness: 0.339 mm

Time (mins.)	0	2	4	7	10	15	20	25
Loss (mg)	0	14.57	23.84	29.14	27.55	31.26	29.93	29.93

Film thickness: 0.443 mm

Time (mins.)	0	2	4	7	10	15	20
Loss (mg)	0	12.34	14.61	14.36	17.63	17.63	17.88

cont...

200 rpm

Film thickness: 0.126 mm

Time (mins.)	0	1	2	4	7	10	15
Loss (mg)	0	2.25	3.93	4.77	5.62	6.18	6.74

Film thickness: 0.170 mm

Time (mins.)	0	1	2	4	7	10	13	16
Loss (mg)	0	39.21	47.68	56.16	67.82	66.76	69.94	68.88

Film thickness: 0.291 mm

Time (mins.)	0	1	2	4	7	10	15
Loss (mg)	0	47.98	41.78	53.07	52.50	53.07	54.20

Film thickness: 0.319 mm

Time (mins.)	0	1	2	4	7	10	15
Loss (mg)	0	56.82	74.81	82.01	88.18	86.13	87.15

Curve fit for initial loss rate Vs. film thickness at 125 rpm

```
Filename: irseer2       m*x

*** Stopping after 3 iterations

Coefficients after last iteration :
Chi Square              M
-------------------------------
1.730612798E-02         5.341515
  E format        5.341515086E+00
-------------------------------
    Std devs        0.229827237
      %                 4.3027
Dependencies            0.0000


Correlation Coefficients
 1.00000


Degrees of Freedom :    4
Final Lamda        : 0.00000100

Data and fitted values
----------------------
```

i	x(i)	y(i)	Pred Y	Residual	Z Residual
1	0.07900000	0.41700000	0.42197969	-0.00497969	-0.03785319
2	0.17000000	0.96000000	0.90805756	0.05194244	0.39484111
3	0.27500000	1.31600000	1.46891665	-0.15291665	-1.16239788
4	0.31500000	1.58800000	1.68257725	-0.09457725	-0.71893019
5	0.34300000	2.01700000	1.83213967	0.18486033	1.40521820

ANOVA

Source of variation	df.	SS	MS	F
Model	1	1.41519269	1.41519269	81.77407967
Residual	4	0.06922451	0.01730613	
Total	4	1.48441720		

```
R-sq.                   95.34%
adjusted for df.        95.34%
```

Curve fit for initial loss rate Vs. film thickness at 150 rpm

Filename: irseef3 m*x

*** Stopping after 3 iterations

Coefficents after last iteration :

Chi Square	M
2.0109757388E-01	18.792539
E format	1.8792539B6E+01
Std devs	0.97082696?1
%	5.1660
Dependencies	0.0000

Correlation Coefficients
1.00000

Degrees of Freedom : 3
Finial Lamda : 0.00000100

Data and fitted values

I	X(I)	Y(I)	Pred Y	Residual	Z Residua
1	0.12900000	3.05600000	2.42423748	0.631?6252	1.4088035
2	0.23000000	4.57100000	4.32228388	0.24871612	0.5546263
3	0.23200000	4.06300000	4.35986896	-0.29686896	-0.6620051
4	0.30000000	5.40500000	5.63776158	-0.23276158	-0.5190484

ANUVA

Source of variation	df.	SS	MS	F
Model	0	2.29212203	2.29212203	11.39805909
Residual	3	0.60329272	0.20109757	
Total	3	2.89541475		

R-sq. 79.16%
adjusted for df. 79.16%

Curve fit for initial loss rate Vs. film thickness at 175 rpm

```
Filename: irseer4      m*x

*** Stopping after 3 iterations

Coefficents after last iteration :
Chi Square              M
-----------------------------
1.04896368E+00       22.19773
  E format       2.21977318E+01
-----------------------------
     Std devs       1.58222991102
       %                 7.1279
Dependencies             0.0000


Correlation Coefficients
 1.00000


Degrees of Freedom :    4
Finial Lamda       : 0.00000100

Data and fitted values
----------------------
```

i	x(i)	y(i)	Pred Y	Residual	Z Residual
1	0.08500000	0.76900000	1.88680720	-1.11780720	-1.09140686
2	0.11400000	2.35300000	2.53054142	-0.17754142	-0.17334825
3	0.29600000	5.26300000	6.57052861	-1.30752861	-1.27664744
4	0.33900000	8.57100000	7.52503107	1.04596893	1.02126526
5	0.44300000	10.16700000	9.83359518	0.33340482	0.32553048

ANUVA

Source of variation	df.	SS	MS	F
Model	0	59.32978848	59.32978848	56.56038388
Residual	4	4.19585472	1.04896368	
Total	4	63.52564320		

```
R-sq.                  93.40%
adjusted for df.       93.40%
```

Curve fit for initial loss rate Vs. film thickness at 200 rpm

```
Filename: irseer5      m*x

*** Stopping after 3 iterations

Coefficents after last iteration :
Chi Square              M
-------------------------------
8.34055756E+01      130.462576
  E format        1.30462576E+02
-------------------------------
     Std devs      18.9927006290
       %              14.2307
Dependencies           0.0000


Correlation Coefficients
 1.00000


Degrees of Freedom :    3
Finial Lamda       : 0.00000100

Data and fitted values
----------------------
```

i	x(i)	y(i)	Pred Y	Residual	Z Residual
1	0.12600000	3.50000000	16.81628463	-13.31628463	-1.45809402
2	0.17000000	28.00000000	22.68863800	5.31136200	0.58157852
3	0.29100000	35.29000000	38.83760975	-3.54760975	-0.38845284
4	0.31900000	48.24000000	42.57456189	5.66543811	0.62034882

ANUVA

Source of variation	df.	SS	MS	F
Model	1	810.53974833	810.53974833	9.71805234
Residual	3	250.21672667	83.40557556	
Total	3	1060.75647500		

```
R-sq.                  76.41%
adjusted for df.       76.41%
```

Table A10.3 Calculated shear loss rate at various rotational speeds and film thicknesses

Speed (rpm)	Shear stress (N/m^2)	Film thickness z (mm)	Initial loss rate (mg/min.)
100	0.645	0.085	0.152
		0.172	0.208
		0.229	0.381
125	0.958	0.079	0.417
		0.170	0.960
		0.275	1.316
		0.315	1.588
		0.343	2.017
150	1.332	0.129	3.056
		0.230	4.571
		0.232	4.063
		0.300	5.405
175	1.766	0.085	0.769
		0.114	2.353
		0.296	5.263
		0.339	8.571
		0.443	10.167
200	2.262	0.126	3.50
		0.170	28.00
		0.291	35.29
		0.319	48.24

Curve fit for initial loss rate per unit film thickness Vs. shear stress

Filename: irseer A + B*X Linear

*** Stopping after 3 iterations

Coefficents after last iteration :

Chi Square	Con	X
1.06762446E+01	-11.629216	20.074828
E format	-1.1629216E+01	2.0074827E+01
Std devs	4.8659452065	3.9000110200
%	-41.8424	19.4274
Dependencies	0.9248	0.9248

Correlation Coefficients

1.00000
-0.94195 1.00000

Degrees of Freedom : 2
Final Lamda : 0.00000100

Data and fitted values

I	x(I)	y(I)	Pred Y	Residual	Z Residual
1	0.64500000	1.52320000	1.31904764	0.20415236	0.06248059
2	0.95800000	5.34150000	7.60246870	-2.26096870	-0.69196685
3	1.33200000	18.79250000	15.11045424	3.68204576	1.12688584
4	1.76600000	22.19770000	23.82292944	-1.62522944	-0.49739959

ANUVA

Source of variation	df.	SS	MS	F
Model	1	282.87234917	282.87234917	26.49549141
Residual	2	21.35248935	10.67624468	
Total	3	304.22483853		

R-sq. 92.98%
adjusted for df. 89.47%

APPENDIX 11

DATA FOR BIOFILM DRY DENSITY DETERMINATION

Table A11.1 RAW DATA: Dry mass and wet volume for biofilm density measurement

Reactor	Δh(mm)	Dry wt.* without biofilm (g)	Dry wt.* with biofilm (g)
R5 @ 44 rpm	11.75	24.7038	1) 25.1739 2) 25.1433 3) 25.1390
R2 @ 30 rpm	5.5	27.6202	1) 27.9257 2) 27.9229 3) 27.9264
R4 @ 30 rpm	7.75	32.1136	1) 32.4228 2) 32.4196 3) 32.4244
R5 @ 125 rpm	18.0	47.9903	1) 48.4081 2) 48.4034 3) 48.4024
R1 @ 35 rpm	8.5	27.6200	1) 27.9090 2) 27.9063 3) 27.9066
R6 @ 30 rpm	8.5	32.0443	1) 32.3368 2) 32.3359 3) 32.3316
R1 @ 80 rpm	9.75	24.4921	2) 24.7438 3) 24.7487
R6 @ 150 rpm	11.25	27.5564	1) 27.8707 2) 27.8730
R5 @ 175 rpm	14	23.8631	1) 24.3608 2) 24.3658
R5 @ 200 rpm	12.5	23.7718	1) 24.0624 2) 24.0633

N.B.: * These are total dry weight of watch glass and filters; (1) for after 1 day; (2) for after 2 days; and (3) for after 3 days.

Table A11.2 Calculated biofilm dry density, wet volume and thickness from bioreactor operating at various speeds

Reactor	Wet volume (mm^3)	Thickness (mm)	Dry density (mg/mm^3)
R5 @ 44rpm	21152.033	0.672	0.021
R2 @ 30rpm	9792.640	0.311	0.031
R4 @ 30rpm	13937.662	0.443	0.022
R5 @ 125rpm	32403.114	1.00	0.013
R1 @ 35rpm	15388.477	0.488	0.019
R6 @ 30rpm	15490.528	0.493	0.019
R1 @ 80rpm	17651.488	0.560	0.014
R6 @ 150rpm	20502.169	0.652	0.015
R5 @ 175rpm	25202.422	0.800	0.020
R5 @ 200rpm	22502.163	0.715	0.013

N.B.: The average dry density for film thickness up to 0.488 mm is 0.022 mg/mm^3, i.e. the value used for computing the biofilm mass in this study.